



BIOSYNTHESIS OF 5-PHOSPHORIBOSYL-1-PYROPHOSPHATE IN PLANTS: A REVIEW

Hiroshi Ashihara^{[a]*}

Keywords: 5-phosphoribosyl-1-pyrophosphate (PRPP), nucleotide biosynthesis, PRPP synthetase, metabolite, enzyme, plant, *PRS* gene.

5-Phosphoribosyl-1-pyrophosphate (PRPP) is an essential substrate for biosynthesis of nucleotides, tryptophan and histidine, functioning as the phosphoribosyl donor. PRPP is synthesised from ribose-5-phosphate and ATP by PRPP synthetase (ribose phosphate pyrophosphokinase, EC 2.7.6.1). In the present review, the occurrence and biosynthesis of PRPP in plant cells and tissues are summarized, and then the properties of two types of plant PRPP synthetases are described. In addition to the inorganic phosphate (Pi)-dependent PRPP synthetases (class I) which have similar properties to mammalian enzymes, plant specific Pi-independent PRPP synthetases (class II) have been discovered in plants. Finally, reports which show fluctuation of the PRPP synthetase activity accompanied by various physiological phenomena in plants and the transgenic plants which enhanced PRPP synthetase activity and relation to biotechnology are introduced.

* Corresponding Author

Fax: +81-3-5700-4225

E-Mail: ashihara.hiroshi@ocha.ac.jp

[a] Department of Biology, Ochanomizu University, Tokyo, Japan

of PRPP determination is based on the release of ¹⁴CO₂ from [carboxyl-¹⁴C]orotic acid by the consecutive action of purified orotate phosphoribosyltransferase and orotidine-5'-monophosphate decarboxylase. The levels of PRPP in plant cells and tissues are summarized in table 2.

Introduction

5-Phosphoribosyl-1-pyrophosphate (PRPP) is an essential substrate for several pathways including *de novo* and salvage biosynthesis of purine, pyrimidine and pyridine nucleotides as well as tryptophan and histidine biosynthesis.¹ The enzyme reactions which utilize PRPP as substrate are summarised in table 1. In plants, some natural products, such as caffeine and nicotine, are derived from nucleotides,^{2,3} therefore, PRPP is also an important metabolite for the biosynthesis of these secondary metabolites. Nevertheless, compared with bacteria and animals, little attention has been given to PRPP in plants and research has been carried out by only a few groups. From 1970s, a group led by Ashihara at Ochanomizu University in Tokyo studied PRPP-related topics and showed the occurrence of PRPP and a partial characterization of PRPP synthetase.⁴⁻⁶ They reported that PRPP synthetase activity is Pi-independent and this properties were different from the enzymes obtained from other organisms.⁵⁻⁸ Cloning and characterization of plant PRPP synthetase genes started by Hove-Jensen's group at the University of Copenhagen in 1999.⁹ Their excellent studies revealed that plants have two classes of PRPP synthetase, mammalian-like Pi-dependent PRPP synthetase and plant specific Pi-independent PRPP synthetase.¹⁰ In the present review, the current status of research on PRPP synthesis in plants are described. The synthesis of PRPP in humans has been reviewed by Becker.¹¹

Occurrence of PRPP in plant tissue and cells

There are several methods for the measurement of PRPP, but up to now only radiochemical methods are reliable for plant materials. The most sensitive and easy assay method

The PRPP levels in plant tissue were first reported by Ross and Murray¹² with germinating pea seeds using this radiochemical method. PRPP was undetectable in dry seeds, but the level in cotyledons increased rapidly during imbibition and attained a maximum (23 nmoles per a pair of cotyledons) 12 h after imbibition. Similar results were also reported with germinating seeds of black gram (*Phaseolus mungo*) using essentially the same radiochemical method of Ashihara and Kameyama.¹³ The level of PRPP was extremely low in dry seeds (<0.03 nmol per a seed), but increased rapidly in cotyledons after imbibition, attaining maximum level (0.53 nmol per a pair of cotyledons) at 24 h after which it decreased. In contrast, the level in the embryonic axes increased with growth. At 96 h after imbibition, the level was 0.78 nmol per an axis. These results suggest that dry seeds contain very limited amounts of PRPP but it is synthesized during germination.

More detailed studies on PRPP and "PRPP availability" have been reported in cultured cells of *Catharanthus roseus* by Hirose and Ashihara.⁴ In culture, four growth phases, (i) the lag phase (day 0-1), (ii) the cell division phase (day 1-4), (iii) the cell expansion phase (day 4-7) and (iv) the stationary phase (day 7-10), were recognized from several growth parameters.^{14,15} The PRPP level varied between 0.41-2.2 nmol g⁻¹ of fresh weight (FW) during culture and these values corresponded to 0.24-1.4 nmol per 10⁷ cells. On both a cell number and a fresh weight basis, the PRPP content curve was seen to rise sharply during the first day, and, after a fall at day 2, increasing again to its maximum level at day 3, following which it then fell away for the remainder of the period.

In addition to the measurement of PRPP levels, cellular "availability of PRPP" was measured using intact *Catharanthus roseus* cells.

Table 1. PRPP-utilizing enzymes in plants.

Enzyme	EC number	Reaction
Purine nucleotide biosynthesis		
Phosphoribosylamine synthetase	2.4.2.14	Glutamine + PRPP → Phosphoribosylamine + PPi
Adenine phosphoribosyltransferase	2.4.2.7	Adenine + PRPP → AMP + PPi
Hypoxanthine-guanine phosphoribosyltransferase	2.4.2.8	Hypoxanthine + PRPP → IMP + PPi
Xanthine phosphoribosyltransferase	2.2.2.22	Guanine + PRPP → GMP + PPi Xanthine + PRPP → XMP + PPi
Pyrimidine nucleotide biosynthesis		
Orotate phosphoribosyltransferase	2.4.2.10	Orotate + PRPP → OMP + PPi
Uracil phosphoribosyltransferase	2.4.2.9	Uracil + PRPP → UMP + PPi
Pyridine nucleotide biosynthesis		
Quinolate phosphoribosyltransferase	2.4.2.19	Quinolate + PRPP → Nicotinate mononucleotide + PPi + CO ₂
Nicotinate phosphoribosyltransferase	2.4.2.11	Nicotinate + PRPP → Nicotinate mononucleotide + PPi
Nicotinamide phosphoribosyltransferase*	2.4.2.12	Nicotinamide + PRPP → Nicotinamide mononucleotide + PPi
Tryptophan biosynthesis		
Anthranilate phosphoribosyltransferase	2.4.2.18	Anthranilate + PRPP → Phosphoribosylanthranilate + PPi
Histidine biosynthesis		
ATP phosphoribosyltransferase	2.4.2.17	ATP + PRPP → Phosphoribosyl-ATP + PPi

The “availability” was estimated from the rate of incorporation of exogenously supplied [8-¹⁴C]adenine into nucleotides and nucleic acids in the cells.⁴ This estimation method was essentially the same used for Ehrlich ascites tumour cells by Henderson and Khoo,¹⁶ although these investigators measured only incorporation of [8-¹⁴C]adenine into nucleotides and did not include the incorporation into nucleic acids.

Table 2. PRPP levels in plant cell and tissue.

Sample	Content (nmol)	Method	Ref. No.
Pea (germinating seeds)	0–23 cotyledon ⁻¹	RI	12
Black gram (germinating seeds)	0.03–0.5 cotyledon ⁻¹ 0.08–0.8 embryonic axis ⁻¹	RI	13
<i>Catharanthus roseus</i> (cultured cells)	0.4–2.2 g ⁻¹ FW	RI	4, 8
Maize (endosperm)	Not detectable	SP	17
<i>Arum maculatum</i> (club)	Not detectable	SP	17
<i>Arabidopsis thaliana</i>	Not detectable	SP	18

RI: radioisotopic analysis; SP: spectrophotometrical analysis

The rates of “PRPP availability” were 33–125 nmol h⁻¹ g⁻¹ FW, values corresponding to 20–68 nmol h⁻¹ 10⁷ cells⁻¹. The “PRPP availability” for nucleotide synthesis increased rapidly during the lag phase of cell culture, decreased at the early cell division phase (day 2) and then gradually increased accompanied by cell development until day 7 and then decreased. The lowest rate was observed in the cells at the stationary phase (day 10). The “PRPP availability”, i.e.,

rate of adenine nucleotide formation from adenine was always much higher than the PRPP content during the entire culture period.⁴ These results suggest that the cellular pool size of PRPP is small, but its turnover PRPP in plant cells is rapid.

In connection to a study on concentration of inorganic pyrophosphate (PPi) in plant cells, Dancer and Rees¹⁷ attempted to measure PRPP level in clubs of the spadices of *Arum maculatum* and the developing endosperm of *Zea mays*, but they could not find detectable amounts of the enzyme. It is obvious that the level of PPi (30–60 nmol g⁻¹ FW) seems to be much higher than that of PRPP, therefore, PPi content released from PRPP during extraction is negligible. However, the difficulties of measuring PRPP in this study may be due to the use of spectrometric assay with a relatively low sensitivity. The limit of detection corresponded to a value of 3 nmol g⁻¹ FW.¹⁷ Koslowsky et al.¹⁸ also mentioned that several attempts were made to measure PRPP contents in seedlings of *Arabidopsis thaliana* and *Nicotiana tabacum* cultures. However, no reliable results were obtained. This appears to be also due to the limited sensitivity of the non-radiochemical assay. The radiochemical methods used by Ross and Murray¹² and Hirose and Ashihara⁴ have also been used with animal cells and in various clinical investigations.^{19,20}

PRPP biosynthesis in plants

PRPP is synthesized from ribose-5-phosphate and ATP by PRPP synthetase (EC 2.7.6.1, ATP: D-ribose-5-phosphate diphosphotransferase) (Figure 1). In plants, ribose-5-phosphate, a substrate of PRPP synthetase, is an intermediate of the photosynthetic carbon reduction cycle (Calvin-Benson-Bassham cycle) as well as the oxidative pentose phosphate (PP) pathway.²¹ Therefore, ribose-5-phosphate is generated both in chloroplasts and in cytosol of plant cells.

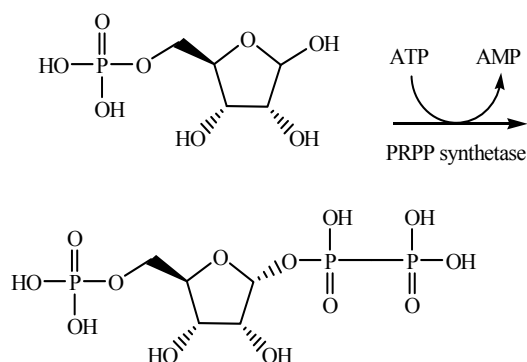


Figure 1. Reaction of the 5-phosphoribosyl-1-pyrophosphate (PRPP) synthetase.

The relationship between the PP pathway and PRPP biosynthesis has been reported in non-photosynthetic plant tissues and cells where the function of the photosynthetic carbon reduction cycle is negligible. In these tissues, carbohydrate metabolism starts from sucrose or starch and after conversion to hexose phosphate, namely glucose-6-phosphate or fructose-6-phosphate, they are metabolised in the PP pathway and ribose-5-phosphate is formed (Figure 2).

There are two distinct branches in the PP pathway; one is the oxidative branch in which NADPH is generated by two dehydrogenases and these steps are physiologically irreversible (steps 1–2 in Figure 2). The second is a non-oxidative branch catalysed by transketolase, transaldolase, ribose-5-phosphate isomerase and ribulose-5-phosphate epimerase. These reactions are reversible.²² Ribose-5-phosphate is produced from both the oxidative (steps 1–3 in Figure 2) and/or the non-oxidative branches (steps 5–6 in Figure 2).

Levels of PRPP and intermediates of the PP pathway has been measured in hypocotyls of etiolated black gram seedlings²² and cultured *Catharanthus roseus* cells^{4,23} (Table 3). As shown in table 3, the pool size of PRPP was smaller than any metabolites of the PP pathway. PRPP content (2 nmol g⁻¹ FW) was 15 times lower than the content of ribose-5-phosphate (30 nmol g⁻¹ FW) and more than 100 times lower than that of glucose-6-phosphate (276 nmol g⁻¹ FW). Similarly, the PRPP content of *Catharanthus roseus* cells (1 nmol g⁻¹ FW) is more than 300 times lower than the level of glucose-6-phosphate content (337 nmol g⁻¹ FW).

Profiles of activity of enzymes involved in the PP pathway and the PRPP synthetase have been investigated in the hypocotyls of etiolated black gram seedlings representing different stages of differentiation (Table 4). Compared with the enzyme activity of the PP pathway, PRPP synthetase activity (1–22 pkat g⁻¹ FW) was extremely low. The activities of the enzymes of the PP pathway and PRPP synthetase were higher in the immature part (Part I), but the relative amounts of the enzymes were fairly constant in more differentiated tissues (Parts III and V). The enzyme profile data suggested that activity of the enzymes of non-oxidative branch of the pathway, namely, transketolase and transaldolase, was lower than those of oxidative branch.

However, activity of the oxidative branch enzyme, glucose-6-phosphate dehydrogenase and 6-phosphogluconate dehydrogenase, is regulated by the NADPH/NADP⁺ ratio and other effectors strictly in *planta*.^{24–26}

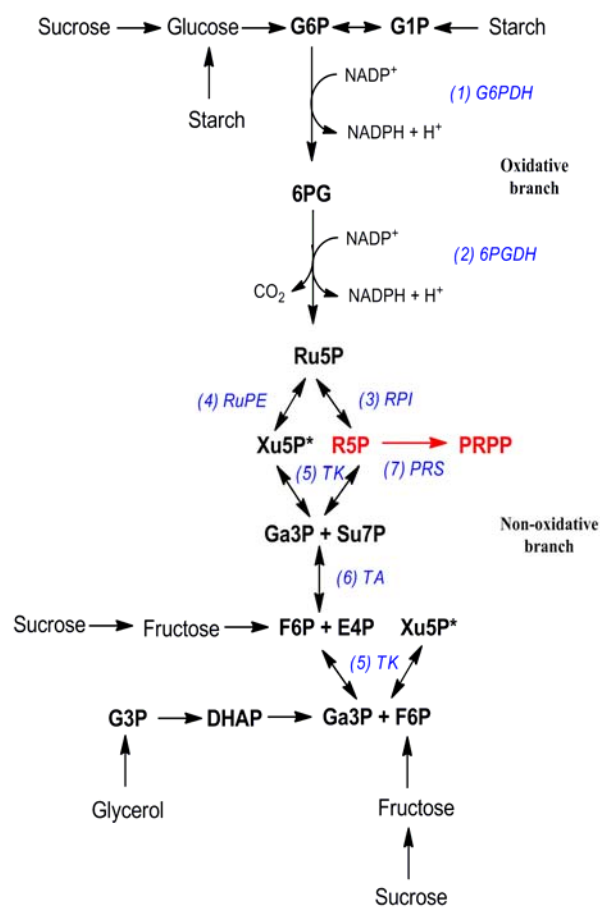


Figure 2. The oxidative pentose phosphate (PP) pathway and 5-phosphoribosyl-1-pyrophosphate (PRPP) synthesis. Enzymes and the EC numbers are as follows: (1) glucose-6-phosphate dehydrogenase (G6PDH) [EC:1.1.1.49]; (2) 6-phosphogluconate dehydrogenase (6PGDH) [EC:1.1.1.44]; (3) ribose-5-phosphate isomerase (RPI) [EC:5.3.1.6]; (4) ribulose-5-phosphate 3-epimerase (RuPE) [EC:5.1.3.1]; (5) transketolase (TK) [EC:2.2.1.1]; (6) transaldolase (TA) [EC:2.2.1.2]; (7) PRPP synthetase (PRS) [EC:2.7.6.1]. Abbreviations of metabolites: DHAP, dihydroxyacetone phosphate; E4P, erythrose-4-phosphate; F6P, fructose-6-phosphate; G1P, glucose-1-phosphate; G3P, glyceraldehyde-3-phosphate; G6P, glucose-6-phosphate; Ga3P, glyceraldehyde-3-phosphate; R5P, ribose-5-phosphate; Ru5P, ribulose-5-phosphate; Su7P, sedoheptulose-7-phosphate; Xu5P, xylulose-5-phosphate

Interrelationship between the PP pathway and PRPP synthesis has been investigated in cultured cells of *Catharanthus roseus*.²⁷ Theoretically, ribose 5-phosphate for PRPP synthesis is supplied both from the oxidative and the non-oxidative branch of the PP pathway. The relative contribution of these branches to ribose 5-phosphate synthesis for PRPP production has been estimated by monitoring exogenous adenine induced increases in AMP synthesis. Exogenously supplied 0.1 mM adenine stimulated 15–31 fold AMP synthesis which was used to produce PRPP in the cultured cells.

However, $^{14}\text{CO}_2$ released from $[1-^{14}\text{C}]$ glucose at 6-phosphogluconate dehydrogenase step (step 2 in figure 2) and incorporation of $[6-^{14}\text{C}]$ glucose into nucleotides were not accelerated by the adenine treatment. In contrast, incorporation of $[2-^{14}\text{C}]$ glycerol into nucleotides via PRPP increased with the adenine treatment (see Figure 2). No significant increase in nucleotide synthesis was caused by methylene blue, a stimulator of the oxidative branch of the PP pathway (steps 1 and 2 in Figure 2).²⁷ From these results it has been concluded that the oxidative branch of the PP pathway is not an essential contributor in the supply of ribose 5-phosphate for PRPP synthesis in plant cells.

Table 3. Comparison of the levels of PRPP and metabolites involved in the pentose phosphate pathway in plants.

Metabolites (nmol g ⁻¹ FW)	Black gram hypocotyls ^a	<i>Catharanthus roseus</i> cells ^b
PRPP	2	1
Glucose-6-phosphate	276	337
6-Phosphogluconate	3	–
Ribulose-5-phosphate	4	–
Xylulose-5-phosphate	3	–
Ribose-5-phosphate	30	–
Erythrose-4-phosphate	12	–
Sedohepturase-7-phosphate	30	–
Fructose-6-phosphate	61	58
Glyceraldehyde-3-phosphate	5	10
Dihydroxyacetone-phosphate	5	20
Fructose-1,6-bisphosphate	8	32
ATP	54	160
Pi	–	5680

^aPart III of hypocotyl (the segment 15–25 mm from the hypocotyl tip); ^bFour-day-old (cell-division phase) cultured cells. The data were taken from Ashihara and Komamine²² and from Kubota and Ashihara.²³

Table 4. Comparison of the activity of PRPP synthetase and enzymes involved in the PP pathway in different parts of black gram hypocotyls.

Enzyme activity (nkat g ⁻¹ FW)	Parts of hypocotyls ^a		
	Part I	Part III	Part V
PRPP synthetase	0.022	0.004	0.001
Glucose-6-phosphate dehydrogenase	5.2	1.1	1.1
6-Phosphogluconate dehydrogenase	4.3	1.0	0.9
Ribose-5-phosphate isomerase	74.0	22.3	21.1
Ribulose-5-phosphate epimerase	1.5	0.2	0.2
Transketolase	0.4	0.1	0.1
Transaldolase	0.3	0.1	0.2
Glucose-6-phosphate isomerase	20.6	2.7	1.6

^aPart I, apical 5 mm of a hypocotyl including a hook, Part III, the segment 15–25 mm from the tip, and Part V, the segment 45–55 mm from the tip. Based on data from Ashihara and Komamine.²²

In plants, the main functions of the PP pathway are (i) supply of NADPH for the biosynthesis as a reducing power and (ii) supply of sugar substrates for biosynthesis. If the tissues needs high reducing power, the oxidative branch of the PP pathway is stimulated and ribose-5-phosphate is supplied. In contrast, no marked regulatory mechanism is present in the non-oxidative branch of the PP pathway.²²

Properties of PRPP synthetase from plants

Plant PRPP synthetase has been characterised using native enzymes since 1970s and it has been shown that the Pi-independent properties are distinct from bacterial and mammalian PRPP synthetase for which Pi is essential for their activity.^{11,28} Recent recombinant enzyme studies revealed that both Pi-dependent (class I) and Pi-independent PRPP synthetase (class II) occur in plants. In this review, the properties of native enzymes are summarized first, and then discussed in the context of the recently revealed isozymes of plant PRPP synthetase from recombinant enzymes (Table 5).

Properties of native PRPP synthetase from plants

There are four reports on native PRPP synthetase from plant sources (Table 5). Ashihara and Komamine⁷ first examined the kinetic and regulatory properties using crude enzyme preparation (35–50 % ammonium sulphate participating fraction) of etiolated black gram hypocotyls using an assay method based on Kornberg et al.²⁹ The apparent Km for ATP and R5P were, respectively, 180 μM and 14 μM. Mg²⁺ was essential for the enzyme activity. About 50 % inhibition of the activity was caused by 1 mM of ADP, GDP or AMP. In contrast to enzymes from other sources, such as human erythrocytes, inhibition of the plant enzyme by NADP⁺ and NADPH was negligible. Pi was not necessary for the activity of black gram PRPP synthetase, and Pi inhibited the activity at concentrations >5 mM.

Ashihara⁵ partially purified PRPP synthetase from spinach leaves by fractionation with ammonium sulphate, DEAE-cellulose column chromatography, and ultrafiltration. Spinach PRPP synthetase required divalent cations for activity. The highest activity was found with Mg²⁺. While Mn²⁺ or Co²⁺ can replace Mg²⁺ to a limited extent. As with black gram PRPP synthetase,⁷ Pi was not required for the activity but serves as an inhibitor. Among the various nucleoside triphosphate tested, ATP was the best pyrophosphoryl donor for the reaction, but inosine 5'-triphosphate (ITP) could also act as a donor although the rate was about one-third of that with ATP. The pH optimum of the enzyme was 7.6. The Km values for ATP, ribose-5-P and Mg²⁺ at the optimal pH were 36 μM, 10 μM, and 1.0 mM, respectively. The subcellular distribution of spinach PRPP synthetase was also investigated. A homogenate of spinach leaves was fractionated by differential centrifugation into four fractions containing chiefly nuclei (600 g pellet), chloroplasts (1200 g pellet), mitochondria (12,000 g pellet), and soluble supernatant. More than 95 % of the activity was found in the supernatant fraction and the specific activity in this fraction was more than ten times higher than in the other fractions. The results suggest that the bulk of the PRPP synthetase activity is located in the cytosol.

Using the partially purified spinach PRPP synthetase, the regulation of the activity of this enzyme, especially the effect of the “energy charge”, was investigated.⁶ The concept of “energy charge” has been proposed by Atkinson.³⁰ “Adenylate energy charge”, which is calculated by the relative concentrations of ATP, ADP and AMP, i.e., $([ATP]+1/2 [ADP]) / ([ATP]+[ADP]+[AMP])$ is an index used to measure the energy status of cells.

Enzymes of ATP-generating, catabolic pathways are inhibited by a high energy charge. On the other hand, anabolic enzymes utilizing ATP for biosynthetic purposes are less active at a low energy charge values and are more active at a high energy charge values.³⁰

By using partially purified enzymes from *Escherichia coli*, Atkinson and Fall³¹ and Klungsøyr et al.³² showed that the activity of PRPP synthetase was dependent upon the “adenylate energy charge” in the assay mixture as predicted for an anabolic enzyme.

The activity of spinach PRPP synthetase appears to be dependent upon the “adenylate energy charge” as shown with the enzyme from *Escherichia coli*. However, the response curve of the spinach PRPP synthetase reaction to the “energy charge” is less steep than that obtained from *E. coli* enzyme. The curve is linear at high “energy charge” values. This suggests that the “energy charge” control of spinach PRPP synthetase is weaker compared to that of *E. coli* enzyme.⁶

Table 5. Properties of the native and recombinant PRPP synthases from plants.

Enzyme source	Iso-zyme	Purification	Molecular mass (kDa)	Pi-requirement (Class)	K_m (μ M)		Inhibitor	Localization	Ref. No.
					R5P	ATP			
Black gram hypocotyls ^a		crude		No (Class II)	14	180	Pi, ADP, GDP	cytosol	7
Spinach leaves ^a		10-fold		No (Class II)	10	36	Pi NMP, NDP	cytosol	5,6
Rubber tree latex ^a		380-fold	200 (57 x 4)	Dependent on ribose-5-P conc.	40	200	no effect	cytosol	33
<i>Bryopsis sp.</i> ^a		crude		No (Class II?)			Pi	cytosol chloroplasts	36
<i>Arabidopsis thaliana</i> ^b	PRS1		38	Yes (Class I)					9
	PRS2		34	Yes (Class I)					
	PRS3		36	No (Class II)					
	PRS4		38	No (Class II)					
Spinach ^b	PRS1		37	Yes (Class I)			ADP ^c	chloroplasts	10
	PRS2		43	Yes (Class I)			ADP ^c	chloroplasts	10
	PRS3	homogeneity	45	No (Class II)	110	170	ADP ^d , GDP ^d	mitochondria	10,34
	PRS4	homogeneity	~110 (35 x 3)	No (Class II)	48	77	ADP ^d	cytosol	10,35
Sugarcane ^b	PRS4			No (Class II)			Pi		40

^anative enzyme; ^brecombinant enzyme; ^callosteric inhibitor; ^dcompetitive inhibitor. Abbreviations: NMP, nucleoside triphosphates; NDP, nucleoside monophosphate.

The activity of spinach PRPP synthetase was inhibited by nucleoside 5'-monophosphates and nucleoside 5'-diphosphates examined. ~50 % inhibition was found at 1 mM.⁶ The enzymes are also inhibited by nucleoside 5'-triphosphates, but the rate of inhibition is slight. Similar inhibition was also detected in PRPP synthetase from black gram seeds and a moss, *Atrichum undulatum*.⁵⁻⁷ The activity of the enzyme is not influenced by plant growth regulators, such as indole-3-acetic acid, 2,4-dichlorophenoxyacetic acid, gibberellic acid, kinetin and 3',5'-cyclic AMP.⁶

PRPP synthetase from latex of the rubber tree (*Hevea brasiliensis*) was purified to apparent homogeneity by sodium dodecyl sulfatepolyacrylamide gel electrophoresis (SDS-PAGE) by Gallois et al.³³ The apparent molecular weight of non-denatured protein estimated by gel filtration was ~200,000. A single band corresponding to a molecular weight ~57,000 was detected after SDS-PAGE. The enzyme seemed to be present as a homo-tetramer. The K_m values for ribose-5-phosphate and ATP are 40 μ M and 200 μ M, respectively. Mg^{2+} is essential for the activity and optimum pH is 7.5. In contrast to spinach PRPP synthetase,^{5,6} ITP did not act as a pyrophosphate group donor and nucleoside mono- and diphosphates had no notable effect on the rubber

latex PRPP synthetase.³³ Effect of Pi on the activity of the latex PRPP synthetase was influenced by the concentration of ribose-5-phosphate; in the presence of a low concentration (20 μ M), Pi strongly inhibits the activity, while of a high concentration of ribose-5-phosphate (1 mM), Pi acts as a positive allosteric effector of this enzyme (Hill's coefficient, 2.3).

Genes and recombinant enzymes of plant PRPP synthetase

Hove-Jensen and co-workers performed the cloning and sequencing of four *Arabidopsis thaliana* PRPP synthase-encoding cDNAs which they expressed in *Escherichia coli*.⁹ The four cDNAs were designated *PRS1*, *PRS2*, *PRS3* and *PRS4* and their gene products PRPP synthetase isozymes PRS1, PRS2, PRS3 and PRS4, respectively (Table 5). In addition, the *Arabidopsis thaliana* genome sequencing project has revealed a fifth member of this new gene family designated *PRS5*. The deduced amino acid sequences of PRPP synthetase isozymes, PRS1 and PRS2 are 96 % similar, whereas the similarity of the gene product of *PRS5* with PRS1 and PRS2 is 81 % and 88 %, respectively. The

deduced amino acid sequences of isozymes PRS3 and PRS4 are 71 % similar. In contrast, the similarity of PRS1, PRS2 or the gene product of *PRS5* with PRS 3 or PRS4 is only 21 % to 26 %. Pi is required for the maximum activity of PRS1 and PRS2. In contrast, the activity of PRS3 and PRS4 is Pi-independent. PRPP synthase isozymes, PRS1 and PRS2 resemble the PRPP synthetase obtained from *Escherichia coli*, *Salmonella typhimurium*, *Bacillus subtilis* and mammalian organisms (class I). In contrast, isozymes, PRS3 and PRS4 appeared to be a novel “plant-specific” enzymes (class II). This is based on both their low sequence similarity and apparent phylogenetic divergence from the bacterial and mammalian PRPP synthetases.

Comparison of class I and class II PRPP synthetase

Subcellular localization of four isozymes and characterization of class II PRPP synthetase was investigated in spinach by Krath and Hove-Jensen.^{10,34,35} The distinction between the two types is based on their enzymatic properties i.e., dependence on Pi for activity, allosteric regulation, and specificity for pyrophosphoryl donor. Thus, the activity and stability of type I PRPP synthetases is dependent on Pi, whereas class II PRPP synthetases are independent of Pi (Figure 3A). Enzymes of type I are inhibited allosterically by purine ribonucleoside diphosphates, whereas class II enzymes are not (Figure 3B). Finally, class I enzymes use ATP or, in some instances, dATP, whereas class II enzymes have much broader specificity, accepting dATP, GTP, CTP, or UTP in addition to ATP.

Subcellular localization of PRPP synthetase

PRPP synthase isozymes, PRS2 and PRS3 contained 76 and 87-amino acid extensions, respectively, at their N-terminal ends in comparison with other PRS. PRS2 was synthesized *in vitro* and shown to be imported and processed by pea chloroplasts. Amino acid sequence analysis indicated that PRS3 may be transported to mitochondria and that PRS4 may be located in the cytosol (Table 5).

Occurrence of PRPP synthetase activity in the different compartments have been already demonstrated by the traditional biochemical subcellular fractionation. It has been reported that PRPP synthetase occurred mainly in cytosol (>96 % of total activity) of spinach leaves⁵ and in chloroplasts (45 % of total activity) and cytosol (54 % of total activity) of fronds of *Bryopsis sp.*³⁶ The latter material was chosen because subcellular components of *Bryopsis sp.* were easily squeezed out from the algal fronds without any requirement for homogenization, thus, it is suitable for isolating intact organelles.³⁷ The occurrence of PRPP synthetase activity in mitochondria (27 % of total activity) and cytosol (59 % of total activity) has been reported in heterotrophically grown *Catharanthus roseus* cells.³⁸ Le Floch and Lafleurie³⁹ also reported the presence of PRPP synthetase in mitochondria in Jerusalem artichoke tubers and suggested that adenine is recycled for the synthesis of purine nucleotides within mitochondria.

Characterization of plant specific class II PRPP synthetase

Detailed characterization of Pi-independent class II PRPP synthetase, namely PRS3 and PRS4, has been reported in spinach by Krath and Hove-Jensen.^{34,35} A recombinant form of PRS3 resembling the presumed mature enzyme has been synthesized in an *Escherichia coli* strain in which the endogenous PRPP synthase gene was deleted, and has been purified to near homogeneity. The activity of PRS3 is independent of Pi, and the enzyme is inhibited by nucleoside 5'-diphosphates in a purely competitive manner, which indicates a lack of allosteric inhibition by these compounds. The spinach PRS 3 shows an unusual low specificity toward pyrophosphoryl donors by accepting dATP, GTP, CTP, and UTP in addition to ATP. The kinetic mechanism of the enzyme is an ordered steady state Bi Bi mechanism with Km values for ATP and ribose-5-phosphate are 170 and 110 μM , respectively. The enzyme has an absolute requirement for Mg^{2+} , and maximal activity is obtained at pH 7.6.³⁴

Recombinant spinach PRS 4 was also synthesized in *Escherichia coli* and purified to near homogeneity.³⁵ Similar to PRS3, the activity of the enzyme is independent of Pi; it is inhibited by ADP in a competitive manner, indicating a lack of an allosteric site; and it accepts ATP, dATP, GTP, CTP, and UTP as pyrophosphoryl donors. Km values for ATP and R5P are 77 and 48 μM , respectively. Gel filtration reveals a molecular mass of the enzyme of ~ 110 kD, which is consistent with a homotrimer. The properties of isozyme 4 is similar to those of isozyme 3, but some differences are present. Isozyme 3 shows substrate inhibition with GTP and hyperbolic saturation kinetics with UTP, a similar result to that observed with the PRS4. Although both isozymes were inhibited in a competitive manner by ADP, only the PRS3 was inhibited by GDP.

Purification, crystallization and preliminary crystallographic analysis of the sugar cane recombinant PRPP synthetase has been performed by Napolitano et al.⁴⁰ The recombinant enzyme contains 328 amino acids with a molecular mass of 36.6 kDa. Sculaccio et al.⁴¹ characterized a sugarcane *prs* gene from the Sugar Cane Expressed Sequence Tag Genome Project. This gene contains a 984-bp open reading frame encoding a 328-amino acid protein. The predicted amino acid sequence has 77 % and 78 % amino acid sequence identity to *Arabidopsis thaliana* and spinach PRS4, respectively. The assignment of sugarcane PRS as a class II PRPP synthetase is verified following enzyme assay and phylogenetic reconstruction of PRS homologues. The results indicate that the maximum activity is achieved in the absence of Pi, and a linear decrease in activity is observed with higher concentrations of Pi. Contrast to from spinach PRS4,¹⁰ Pi inhibits the catalytic reaction.

The reported properties of native PRPP synthetases in etiolated hypocotyls of black gram,⁷ heterotrophically cultured *Catharanthus roseus* cells,⁸ spinach leaves,⁵ *Bryopsis* fronds³⁶ and rubber tree latex³³ are similar to PRS4 of spinach recombinant enzyme. These enzymes are mainly located in the cytosol and possess Pi-independent activity. Except for *Bryopsis* fronds and spinach leaves, materials used in these previous studies have no distinct chloroplasts. Therefore, chloroplast-type isozymes of PRPP synthetase appeared to be missing. The PRPP synthetase activity in the

Bryopsis chloroplast extracts was inhibited ~50 % by 25 mM Pi, thus this is not the class I enzyme shown in spinach chloroplasts. This discrepancy might be due to the difference in plant species, i.e., *Bryopsis* (green algae) and spinach (vascular plant).

In the case of native spinach enzyme, the existence of chloroplast PRS1 and PRS2 might have been overlooked probably because of their low activity and/or the low stability of chloroplast isozymes in extracts.⁵ In fact, in contrast to spinach leaves, Yin and Ashihara⁴² found that Pi (20 mM) stimulated PRPP synthetase activity in *Arabidopsis thaliana* cells cultured in the light. Consequently, both Pi-dependent and Pi-independent isoenzymes are present in the extracts from higher plant cells. The estimated molecular mass of the subunit of rubber tree latex enzyme (57 k Da) [33] is different from PRS3 and PRS4 (35 kDa) in molecular size (Table 5). Therefore, PRPP synthetase molecules in the latex seems to be different from the enzyme in plant cells and tissues.

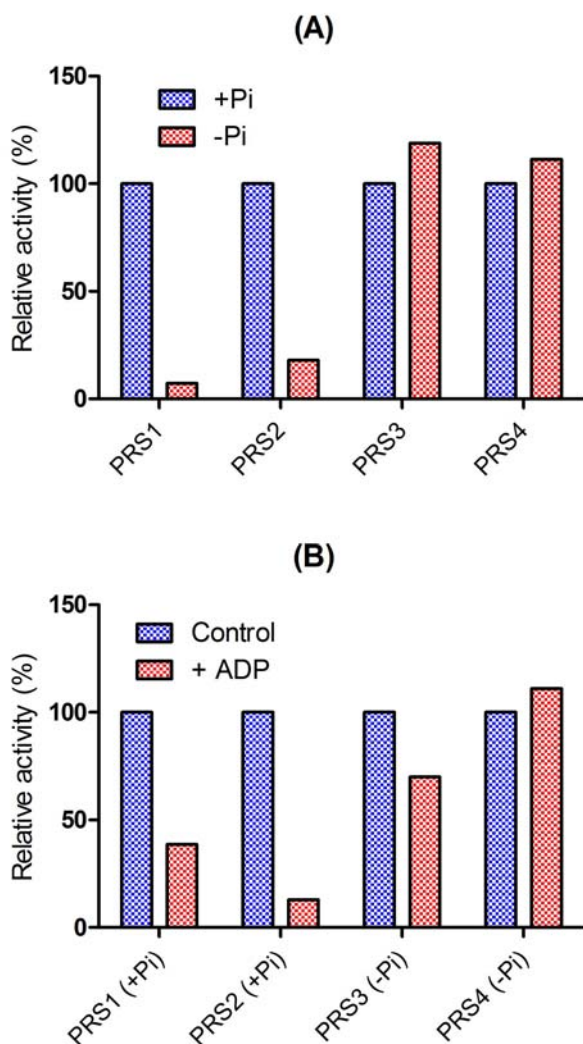


Figure 3. Comparison of relative activity of isozymes of spinach recombinant PRPP synthetase. (A) Effect of presence or absence of 50 mM Pi; (B) Effect of 1 mM ADP. PRPP synthetase activity was determined in the presence of 5 mM ribose-5-phosphate, 5 mM MgCl₂ and 3 mM (A) or 1 mM (B) ATP. The relative activity is expressed as % of the velocity in the presence of 50 mM Pi (A) or % of these in the absence of 1 mM ADP (B). Based on original data of Krath and Hove-Jensen.¹⁰

Fluctuation of level of PRPP synthetase activity in plant cells and organs

It has been reported that PRPP synthetase activity fluctuated in parallel with various physiological events of plants. Dry seeds of black gram possessed a significant level of PRPP synthetase activity and its level was maintained during early phase of seed germination and then decreased.¹³ A similar pattern of fluctuation was found in the PRPP utilised enzymes, orotate phosphoribosyltransferase and uracil phosphoribosyltransferase, which, respectively, participate in the *de novo* and the salvage pathways of pyrimidine biosynthesis.¹³ Ashihara and Kameyama¹³ suggested that PRPP synthetase and PRPP utilizing enzymes that participate in the pyrimidine nucleotide biosynthesis are present at adequate levels in cotyledons of dry seeds and become functional after hydration of the enzyme proteins by imbibition.

The activity of PRPP synthetase has been investigated in connection with purine alkaloid biosynthesis. Biosynthesis of caffeine was found in the young leaves of tea (*Camellia sinensis*) harvested in the spring. The highest level of PRPP synthetase activity was found in young leaves in April accompanied by the highest activity of *N*-methyltransferases which participates in caffeine biosynthesis. The level of PRPP synthetase activity declined significantly to ~6 % of the maximum in June when caffeine biosynthesis had ended.⁴³ Since the purine skeletons of caffeine are supplied mainly by the *de novo* purine biosynthesis in young tea leaves,⁴⁴ supply of large amounts of PRPP seems to be required in young tea leaves. In addition to young leaves, caffeine biosynthesis occurs in stamens and petals of tea flower buds.⁴⁵ Relatively high activity of PRPP synthetase was also observed in these organs.⁴⁶

The level of PRPP synthetase activity was measured in a study on pyrimidine metabolism during senescence of tobacco leaves.⁴⁷ The highest activity of PRPP synthetase was found in fully-expanded dark-green mature leaves. The level of PRPP synthetase activity was 76 % of the mature leaves in an intermediate stage of senescence (50 % of chlorophyll content was reduced), and then decreased markedly in fully senescent stage where >90 % chlorophyll was degraded. The activity of uracil phosphoribosyltransferase activity was also reduced significantly in this stage.

Marked changes in respiration and some enzyme activities including PRPP synthetase in the early stage of callus formation in a root tissue culture of carrot (*Daucus carota*) has been reported.⁴⁸ The respiratory rate increased in two phases during early stages of callus formation. In the first phase, active RNA synthesis occurred accompanied by increase in PRPP synthetase activity. The increase was inhibited by cycloheximide, indicating that *de novo* synthesis of the enzyme may occur immediately after culture. In the second phase, the activities of some respiratory enzymes, i.e., glucose-6-phosphate isomerase, ATP-dependent phosphofructokinase and succinate dehydrogenase increased. The results indicated initial synthesis of PRPP synthetase is important for initiation of callus formation from carrot-root slices.

Changes in activity of PRPP synthetase during growth of cultured plant cells have been reported in some plant species. Kanamori et al.¹⁴ reported that PRPP synthetase activity increased during the lag phase and operated actively during cell division of *Catharanthus roseus* cells. The activity of the uracil salvage using PRPP for RNA synthesis increases during the lag phase. The activity then decreases at the later cell division phase. In contrast, the *de novo* pathway of pyrimidine nucleotide synthesis for RNA is developed at the cell division phase. The activity of PRPP synthetase and *de novo* and salvage pathways of pyrimidine nucleotide biosynthesis declined during the cell expansion and stationary phase. These results suggest that the activity of PRPP synthetase is closely linked to the nucleic acid synthesis. Essentially the same fluctuation of the activity of PRPP synthetase has been also observed during the growth of cultured cells of *Arabidopsis thaliana*⁴³ and white spruce (*Picea glauca*).⁴⁹

PRPP synthetase activity was determined during an investigation of somatic embryogenesis of carrot cells.⁵⁰ The activity of PRPP synthetase in the embryogenic cells was higher than in the non-embryogenic cells. Simultaneously, activity of orotate phosphoribosyltransferase, a PRPP utilizing enzyme which participated in the *de novo* pyrimidine biosynthesis, was three times higher in the embryogenic cells. In contrast, no difference in the activity of uracil phosphoribosyltransferase which participated in uracil salvage was found in both cells. Therefore, PRPP in the embryogenic cells may be preferentially utilized for increased activity of *de novo* pyrimidine biosynthesis during embryogenesis of carrot cells.

PRPP synthetase activity was determined at various stages of somatic embryo development of white spruce cells.⁵¹ White spruce somatic embryogenesis was divided into four distinct stages designated as stages I to IV characterized by a different developmental stage of the embryos. The embryogenic tissues were maintained with 2,4-dichlorophenoxyacetic acid (stage I). Embryogenic tissue was transferred into hormone-free medium for 7 days (stage II) and then into a liquid maturation medium containing abscisic acid for 7 days (stage III). After that, the embryogenic tissues were placed on a solid maturation medium with abscisic acid (stage IV). Mature somatic embryos characterised by developed cotyledons were obtained after 40 days of incubation in the dark. The activity of PRPP synthetase increased sharply at stage II. The activity decreased at the stage III to the first week of the stage IV, before declining at the late stage of embryo development (stage IV). Orotate phosphoribosyltransferase activity was high during the initial phases of embryo development, after which it gradually declined. Low activity of uracil phosphoribosyltransferase was detected throughout the developmental period. These results indicate that the fluctuation pattern of PRPP synthetase activity was different from those of PRPP utilizing enzymes involved in pyrimidine biosynthesis during embryo development of white spruce.

Desiccation is a natural process occurring during the late stages of seed maturation. Although desiccation is absent during the late developmental stages of somatic embryogenesis, a drying period followed by rehydration has been found to stimulate germination of somatic embryos of several species including white spruce.⁵² The imposition of a

partial drying treatment on mature white spruce somatic embryos is a necessary step for germination and embryo conversion into plantlets. Stasolla et al.⁵³ reported that the activity of PRPP synthetase almost doubled during this treatment. The activity of adenine phosphoribosyltransferase, an enzyme responsible for the salvage of adenine to adenine nucleotides also increased in dried embryos. In contrast, the activity of orotate phosphoribosyltransferase and uracil phosphoribosyltransferase did not significantly change as the embryos dried. The increased PRPP synthetase activity may contribute to the rapid turnover of adenine nucleotide synthesis during the drying process.

Germination of white spruce embryos was achieved by transferring the partially dried embryos mentioned above onto the germination medium. Germination occurred under light. Pyrimidine nucleotide metabolism was investigated during the initial stages of somatic embryo. The activity of PRPP synthetase and orotate phosphoribosyltransferase increased with the onset of germination, whereas activity of uracil phosphoribosyltransferase was low and remained almost constant during germination.⁵⁴

Brassinolide-improved development of *Brassica napus* microspore-derived embryos is associated with increased activities of purine and pyrimidine salvage pathways. However, no marked fluctuations in the activity of PRPP synthetase was observed in embryos cultured under control conditions and in the presence of brassinolide or brassinazole.⁵⁵

Effect of phosphate on the biosynthesis of PRPP

Pi is one of the major nutrients essential for plant growth. There are several reports which indicate that Pi is the most important nutrient which influences the growth and metabolism of cultured plant cells. Ashihara and co-workers reported that the intracellular level of ATP was increased by addition of Pi to cultures of *Catharanthus roseus*.^{56,57} Ukaji and Ashihara⁸ reported that the intracellular level of PRPP and the "availability of PRPP" increased markedly in the Pi-deficient cultures of *C. roseus* during the 24 h after the addition of Pi. The activity of Pi-independent PRPP synthetase increased ~20 % in this period.

In mammalian cells, there are several lines of evidence which indicated that Pi causes an increase in the net biosynthesis of nucleotides as a result of activation of Pi-dependent PRPP synthetase by Pi.^{1,58,59} In contrast to mammalian cells, Pi seems to be not directly connected to the activation of PRPP synthesis in plant cells, because plant PRPP synthetase activity is not Pi-dependent. The most plausible mechanism of rapid PRPP synthesis in *Catharanthus roseus* caused by Pi involves increments in the availability of ATP, a substrate of PRPP synthetase, which is increased by increases in the rate of turnover of ATP by Pi. The high ratio of ATP/ADP also influences the activity of PRPP synthetase, because *Catharanthus* PRPP synthetase is inhibited by ADP.⁸

In photosynthetic plant cells, both Pi-dependent PRPP synthetase (class I) and Pi-independent PRPP synthetase (class II) are present. Yin and Ashihara⁴² investigated the effect of Pi level on the two classes of PRPP synthetase. They first estimated the cellular phosphate level using ³³Pi

in suspension-cultured *Arabidopsis thaliana* cells. ^{33}P i in the culture medium was taken up by the cells, and the concentration of Pi in cells increased up to $5.5 \mu\text{mol g}^{-1}$ fresh weight within 24 h once the cells were transferred to the fresh medium; its concentration then fell because of the conversion of Pi to organic compounds. In vitro activity of PRPP synthetase increased after inoculation and maintained a high activity until the early exponential phase of growth. The transcript levels of *PRS1* and *PRS2* encoding class I PRPP synthetase and *PRS3* encoding class II enzymes increased rapidly after the cells were transferred to fresh Pi-containing culture medium and then remained almost constant during the early exponential growth phase. In contrast, constitutive expression of *PRS4* encoding cytosolic class II enzyme was observed during culture. During long-term Pi-starvation the transcript levels of *PRS1* and *PRS2* were reduced, but *PRS3* and *PRS4* were expressed continually during the Pi starvation. Pi-dependent PRPP synthetase activity was simultaneously reduced, but Pi-independent activity did not change. Expression of *PRS1* and *PRS2* and the activity of Pi-dependent enzyme grew to normal rates by 24 h after supply of Pi.

Hewitt et al.⁶⁰ reported effects of Pi limitation on expression of genes involved in pyrimidine biosynthesis in seedlings of *Arabidopsis thaliana*. The expression of genes encoding Pi-transporter and enzymes involved in the *de novo* and the salvage pyrimidine biosynthesis increased from 2 to 10-fold in response to Pi-starvation in shoots. Pi-limitation resulted in induction of *PRS2* encoding Pi-dependent PRPP synthetase 2 (*PRS2*). However, they suggest that the potential contribution of an increase in *PRS2* enzyme activity to overall PRPP synthesis may be minimal at low intracellular concentrations of Pi and ATP. In contrast, *PRS3* encoding Pi-independent PRPP synthetase 3 (*PRS3*) constitutively expressed in root and shoot tissues. They concluded that *PRS3* may play a novel role in providing PRPP to cellular metabolism under low P availability.

The expression profile of *PRS2* observed in the Pi-deficient *Arabidopsis thaliana* seedlings by Hewitt et al.⁶⁰ differs from that reported in cultured cells by Yin and Ashihara,⁴² but the discrepancy may be due to the materials used. Constitutively expressed Pi-independent class II PRPP synthetase, *PRS4*, in the cultured cells and *PRS3* in root and shoot tissues of *A. thaliana*, may be an adaptation to severe environments, including Pi deficiency.

Transgenic plants

Koslowsky et al.¹⁸ reported that a higher biomass accumulation was achieved by increasing PRPP synthetase activity in transgenic *Arabidopsis thaliana* and *Nicotiana tabacum* plants. The filamentous fungus, *Ashbya gossypii* genes coding for either PRPP synthetase (*PRS* class I) or a mutated variant of the same gene which resembles a protein of *PRS* class II activity, were over-expressed under the control of a constitutive promoter. It was shown that increased PRPP synthetase activity in *A. thaliana* or *N. tabacum* leads to a substantial increase in fresh weight (1.1–1.3 fold) under standardized growth conditions. Growth enhancement was accompanied by changes in the amount of some sugars and other metabolites. The decreased sucrose content and the increased hexose-to-sucrose ratio

correlated well with the increased *PRS* activity in both *A. thaliana* and *N. tabacum* expressing either the wild-type or mutant *PRS* gene.

The results obtained from these transgenic plants provide evidence that the supply of PRPP co-limits the growth rates. It is postulated that increased PRPP synthetase activity increases PRPP accessibility in the cytosol, which promotes nucleotide availability by enhancing nucleotide salvage processes. This study has implications for biotechnological strategies aiming to increase plant biomass as an alternative renewable energy source. Further studies are needed to confirm these results under field conditions and to investigate the impact on the total seed yield.

Concluding Remarks

PRPP is an essential phosphoribosyl donor for the biosynthesis of purine, pyrimidine and pyridine nucleotides, tryptophan, histidine and some secondary metabolites derived from these primary metabolites. Although cellular pool size of PRPP is very small, active PRPP synthesis has been demonstrated in plant cells.⁴ Plants have unique Pi-independent PRPP synthetase activity which was predicted in crude enzyme extracts more than 40 years ago.⁷ Recent molecular genetic studies have identified at least four PRPP synthetase isozymes which are classified as class I (Pi-dependent) and class II (Pi-independent) enzymes.¹⁰ In this article on the current status of PRPP related topics in plant cells has been comprehensively reviewed, however it is obvious that numbers of citable references are limited and more in depth studies are needed to reveal the detailed mechanism underlying the biosynthesis and utilization of PRPP in plants. The presence of plant specific Pi-independent PRPP synthetase appears to be adapted to plant specific physiological and environmental conditions, and as a consequence this topic is potentially an attractive area of future plant biology research. In addition, transgenic crop plants which enhanced PRPP synthetase activity and have increased yields represent an interesting area for biotechnological strategies.

Acknowledgement

The author is grateful to Professor Alan Crozier (University of California, Davis) for his kind help to prepare the manuscript.

Reference

- ¹Becker, M. A., Raivio, K. O., Seegmiller, J. E., *Adv. Enzymol. Relat. Areas Mol. Biol.* **1979**, *49*, 281–306.
- ²Ashihara, H., Ogita, S., Crozier, A., *Plant Metabolism and Biotechnology*, John Wiley & Sons, New York, **2011**, 163–189.
- ³Shoji, T., Hashimoto, T., *Plant Metabolism and Biotechnology*, John Wiley & Sons, New York, **2011**, 191–216.
- ⁴Hirose, F., Ashihara, H., *Z. Pflanzenphysiol.*, **1983**, *110*, 183–190.
- ⁵Ashihara, H., *Z. Pflanzenphysiol.*, **1977**, *83*, 379–392.

- ⁶Ashihara, H., Z., *Pflanzenphysiol.*, **1977**, *85*, 383–392.
- ⁷Ashihara, H., Komamine, A., *Plant Sci. Lett.*, **1974**, *2*, 119–123.
- ⁸Ukaji, T., Ashihara, H., *Int. J. Biochem.*, **1987**, *19*, 1127–1131.
- ⁹Krath, B. N., Eriksen, T. A., Poulsen, T. S., Hove-Jensen, B., *Biochim. Biophys. Acta*, **1999**, *1430*, 403–408.
- ¹⁰Krath, B. N., Hove-Jensen, B., *Plant Physiol.*, **1999**, *119*, 497–505.
- ¹¹Becker, M. A., *Prog. Nucl. Acid Res. Mol. Biol.*, **2001**, 115–148.
- ¹²Ross, C., Murray, M. G., *Plant Physiol.*, **1971**, *48*, 626–630.
- ¹³Ashihara, H., Kameyama, Y., *Curr. Sci.*, **1989**, *58*, 889–891.
- ¹⁴Kanamori, I., Ashihara, H., Komamine, A., *Z. Pflanzenphysiol.*, **1979**, *93*, 437–448.
- ¹⁵Kanamori-Fukuda, I., Ashihara, H., Komamine, A., *J. Exp. Bot.*, **1981**, *32*, 69–78.
- ¹⁶Henderson, J. F., Khoo, M. K. Y., *J. Biol. Chem.*, **1965**, *240*, 2358–2362.
- ¹⁷Dancer, J. E., Rees, T., *Planta*, **1989**, *177*, 261–264.
- ¹⁸Koslowsky, S., Riegler, H., Iler, E., Zrenner, R., *Plant Biotechnol. J.*, **2008**, *6*, 281–294.
- ¹⁹Tax, W. J. M., Veerkamp, J. H., *Clin. Chim. Acta*, **1977**, *78*, 209–216.
- ²⁰Tax, W. J. M., Veerkamp, J. H., *Comp. Biochem. Physiol.*, **1978**, *59B*, 219–222.
- ²¹Ashihara, H., Kato, M., *Thirty Lectures on Metabolism and Biosynthesis*, Asakura Shoten, **2011**.
- ²²Ashihara, H., Komamine, A., *Plant Sci. Lett.*, **1974**, *2*, 331–337.
- ²³Kubota, K., Ashihara, H., *Biochim. Biophys. Acta*, **1990**, *1036*, 138–142.
- ²⁴Ashihara, H., Komamine, A., *Physiol. Plant.*, **1976**, *36*, 52–59.
- ²⁵Ashihara, H., Komamine, A., *Int. J. Biochem.*, **1975**, *6*, 667–673.
- ²⁶Ashihara, H., Fowler, M. W., *Int. J. Biochem.*, **1979**, *10*, 675–681.
- ²⁷Hirose, F., Ashihara, H., *Plant Sci. Lett.*, **1984**, *35*, 123–126.
- ²⁸Jensen, K. F., *Metabolism of Nucleotides, Nucleosides and Nucleobases in Microorganisms*, Academic Press, **1983**, 1–20.
- ²⁹Kornberg, A., Lieberman, I. and Simms, E.S., *J. Biol. Chem.*, **1955**, *215*, 389–402.
- ³⁰Atkinson, D. E., *Cellular Energy Metabolism and its Regulation*, Academic Press, **1977**.
- ³¹Atkinson, D. E., Fall, L., *J. Biol. Chem.*, **1967**, *242*, 3241–3242.
- ³²Klungsoeyr, L., Hagemen, J. H., Fall, L., Atkinson, D. E., *Biochemistry*, **1968**, *7*, 4035–4040.
- ³³Gallois, R., Prevot, J. C., Clement, A., Jacob, J. L., *Plant Physiol.*, **1997**, *115*, 847–852.
- ³⁴Krath, B. N., Hove-Jensen, B., *J. Biol. Chem.*, **2001**, *276*, 17851–17856.
- ³⁵Krath, B. N., Hove-Jensen, B., *Protein Sci.*, **2001**, *10*, 2317–2324.
- ³⁶Ashihara, H., *Curr. Sci.*, **1989**, *59*, 939–941.
- ³⁷Misonou, T., Ishihara, J., Pak, J. Y., Nitta, T., *Phycologia*, **1989**, *28*, 422–428.
- ³⁸Kanamori, I., Ashihara, H., Komamine, A., *Z. Pflanzenphysiol.*, **1980**, *96*, 7–16.
- ³⁹Le Floch, F., Lafleurriel, J., *Z. Pflanzenphysiol.*, **1983**, *113*, 61–71.
- ⁴⁰Napolitano, H. B., Sculaccio, S. A., Thiemann, O. H., Oliva, G., *Acta Crystallogr. Sect. F*, **2005**, *61*, 49–51.
- ⁴¹Sculaccio, S. A., Napolitano, H. B., Beltramini, L. M., Oliva, G., Carrilho, E., Thiemann, O. H., *Plant Mol. Biol. Rep.*, **2008**, *26*, 301–315.
- ⁴²Yin, Y., Ashihara, H., *Phytochem. Lett.*, **2009**, *2*, 126–129.
- ⁴³Fujimori, N., Suzuki, T., Ashihara, H., *Phytochemistry*, **1991**, *30*, 2245–2248.
- ⁴⁴Ito, E., Ashihara, H., *J. Plant Physiol.*, **1999**, *254*, 145–151.
- ⁴⁵Fujimori, N., Ashihara, H., *Phytochemistry*, **1990**, *29*, 3513–3516.
- ⁴⁶Fujimori, N., Ashihara, H., *Ann. Bot.*, **1993**, *71*, 279–284.
- ⁴⁷Ashihara, H., *Acta Physiol. Plant.*, **1981**, *3*, 77–84.
- ⁴⁸Komamine, A., Shimizu, T., *Physiol. Plant.*, **1975**, *33*, 47–52.
- ⁴⁹Ashihara, H., Stasolla, C., Loukanina, N., Thorpe, T. A., *Physiol. Plant.*, **2000**, *108*, 25–33.
- ⁵⁰Ashihara, H., Fujimura, T., Komamine, A., *Z. Pflanzenphysiol.*, **1981**, *104*, 129–137.
- ⁵¹Ashihara, H., Loukanina, N., Stasolla, C., Thorpe, T. A., *J. Plant Physiol.*, **2001**, *158*, 613–621.
- ⁵²Kong, L., Yeung, E. C., *Physiol. Plant.*, **1995**, *93*, 298–304.
- ⁵³Stasolla, C., Loukanina, N., Ashihara, H., Yeung, E. C., Thorpe, T. A., *Physiol. Plant.*, **2001**, *111*, 93–101.
- ⁵⁴Stasolla, C., Loukanina, N., Ashihara, H., Yeung, E. C., Thorpe, T. A., *In Vitro-Plant*, **2001**, *37*, 285–292.
- ⁵⁵Belmonte, M., Elhiti, M., Ashihara, H., Stasolla, C., *Planta*, **2011**, *233*, 95–107.
- ⁵⁶Ashihara, H., Ukaji, T., *J. Plant Physiol.*, **1986**, *124*, 77–85.
- ⁵⁷Ashihara, H., Li, X. N., Ukaji, T., *Ann. Bot.*, **1988**, *61*, 225–232.
- ⁵⁸Boer, P., Lipstein, B., De Vries, A., Sperling, O., *Biochim. Biophys. Acta*, **1976**, *432*, 10–17.
- ⁵⁹Raivio, K. O., Lazar, C. S., Becker, M. A., *Biochim. Biophys. Acta* **1981**, *678*, 58–64.
- ⁶⁰Hewitt, M. M., Carr, J. M., Williamson, C. L., Slocum, R. D., *Plant Physiol. Biochem.*, **2005**, *43*, 91–99.

Received: 31.08.2016.

Accepted: 19.09.2016.



KINETICS AND MECHANISM OF OXIDATION OF SECONDARY ALCOHOLS BY MORPHOLINIUM FLUOROCHROMATE

Vinita Purohit^[a] and Pallavi Mishra^{[a]*}

Keywords: Alcohols, correlation analysis, halochromate, kinetics, mechanism, oxidation.

Oxidation of several secondary alcohols by morpholinium fluorochromate (MFC) in DMSO leads to the formation of corresponding ketones. The reaction is first order each in MFC and acidity. The reaction exhibited Michaelis-Menten kinetics with respect to alcohols. The oxidation of 2-propanol-*d*₂ (MeCDOHMe) exhibited a substantial primary kinetic isotope effect ($k_{\text{H}}/k_{\text{D}} = 5.16$ at 298 K). The oxidation of 2-propanol has been studied in nineteen different organic solvents. The solvent effect has been analysed using Taft's and Swain's multiparametric equations. The reaction was subject to both polar and steric effects of the substituents. A mechanism involving transfer of hydride ion from alcohol to the oxidant, via a chromate ester, has been proposed.

* Corresponding Authors

Phone : +91 9829198772

E-Mail: pallavianuk@gmail.com

[a] Department of Chemistry, J.N.V. University, Jodhpur 342 005, India

INTRODUCTION

Chromium (VI) is a versatile oxidant but is a rather drastic and non-selective oxidant. To improve the selectivity of Cr (VI), a number of organic halochromates have been synthesized used as mild and selective oxidizing reagents in synthetic organic chemistry.¹⁻⁵ Morpholinium fluorochromate (MFC) is one such compound used for the oxidation of aryl alcohols.⁶ Some reports on the kinetic aspects of oxidation by MFC, including that on the oxidation of primary alcohols, has appeared recently,⁷ however, there seems to be no report on the oxidation of secondary alcohols by MFC. It is known, however, that primary and secondary organic compounds sometimes follow different mechanistic pathways.⁸ We now report the kinetics and mechanism of oxidation of ten secondary alcohols by MFC in DMSO as a solvent. The mechanistic aspects have been discussed.

EXPERIMENTAL

Materials

All the alcohols were commercial products (Fluka) and the liquid alcohols were dried over anhydrous magnesium sulphate and then fractionated. Benzhydrol was recrystallised from ethanol. MFC was prepared by the reported method⁶ and its purity was checked by an iodometric method. 2-Propanol-2*d*₁ (MeCDOHMe, D-2-Pr), of 98 % atom D, was obtained from Sigma-Aldrich. Due to the non-aqueous nature of the solvents, p-toluenesulphonic acid (TsOH) was used as a source of hydrogen ions. Solvents were purified by the usual methods.⁹

Product Analysis

The product analysis was carried out under kinetic conditions, i.e., with an excess of the alcohol over MFC. In a typical experiment, 2-propanol (0.05 mol), TsOH (0.005 mol) and MFC (2.07 g, 0.01 mol) were made up to 100 mL in DMSO and the reaction mixture was kept in dark for ≈ 10 h to ensure completion of the reaction. The solution was then treated with excess (200 mL) of a saturated solution of 2,4-dinitrophenylhydrazine in 2 mol dm⁻³ HCl and kept overnight in a refrigerator. The precipitated 2,4-dinitrophenylhydrazone (DNP) was filtered off, dried, weighed, recrystallized from ethanol, and weighed again. The yields of DNP before and after recrystallization were 2.16 g (91 %) and 2.05 g (86 %) respectively, based on the consumption of MFC. The DNP was found to be identical (m.p. and mixed m.p.) with the DNP of acetone.

In similar experiments, with other alcohols, the yield of the DNP was in the range of 77-87 % after recrystallization. The oxidation state of chromium in completely reduced reaction mixture, determined by iodometric titrations, was 3.90 ± 0.15 .

Kinetic Measurements

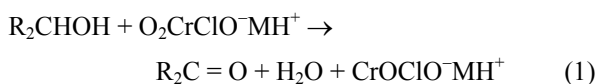
Reactions were carried out under pseudo-first-order conditions by keeping an excess ($\times 15$ or greater) of the alcohol over MFC. The solvent was DMSO, unless mentioned otherwise. All reactions were carried out in flasks blackened from the outside to prevent any photochemical reactions.

The reactions were carried out at constant temperature (± 0.1 K) and were followed up to 80 % of the extent of reaction, by monitoring the decrease in the concentration MFC spectrophotometrically at 356 nm. The pseudo-first-order rate constant, k_{obs} , was computed from the linear least-squares plot of $\log [\text{MFC}]$ versus time. Duplicate runs showed that the rate constants were reproducible to within ± 3 %.

RESULTS

The kinetic and other data were obtained for all the alcohols under study. As the results are similar, only representative data are reproduced here.

The oxidation of alcohols by MFC leads to the formation of corresponding ketones. The overall reaction may be written as eqn. 1 (here M = morpholine).



MFC undergoes a two-electron change. This is accord with the earlier observations with other halochromates. It has already been shown that both pyridinium chlorochromate¹⁰ and pyridinium fluorochromate (PFC)¹¹ act as two-electron oxidants and are reduced to chromium (IV) species. The oxidation state of the spent chromium species is shown to be four by determining its oxidation state by magnetic susceptibility, ESR and IR studies.^{10,11}

Rate Laws

The reactions are of first order with respect to MFC. Further, the pseudo-first-order rate constant, k_{obs} , is independent of the initial concentration of MFC. The reaction rate increases linearly with an increase in the acidity of the solution (Table 1). The reaction rate increases with increase in the concentration of the alcohol but not linearly (Table 1). A plot of $1/k_{\text{obs}}$ against $1/[\text{alcohol}]$ is linear ($r > 0.995$) with an intercept on the rate-ordinate. Thus, Michaelis-Menten type kinetics are observed with respect to the alcohol. This leads to the postulation of following overall mechanism (2) and (3) and rate law (4).



$$\text{Rate} = k_2 K [\text{alcohol}] [\text{MFC}] / (1 + K [\text{alcohol}]) \quad (4)$$

The dependence of reaction rate on the reductant concentration was studied at different temperatures and the values of K and k_2 were evaluated from the double reciprocal plots. The thermodynamic parameters of the complex formation and activation parameters of the decomposition of the complexes were calculated from the values of K and k_2 respectively at different temperatures (Tables 2 and 3).

Test for Free Radicals

The oxidation of alcohols, in an atmosphere of nitrogen, failed to induce polymerisation of acrylonitrile. Further, the addition of acrylonitrile did not affect the rate (Table 1). To further confirm the absence of free radicals in the reaction

pathway, the reaction was carried out in the presence of 0.05 mol dm⁻³ of 2,6-di-*t*-butyl-4-methylphenol (butylated hydroxytoluene or BHT). It was observed that BHT was recovered unchanged, almost quantitatively. This indicates that a one-electron oxidation, giving rise to free radicals, is highly unlikely in the present reaction.

Kinetic Isotope Effect

Table 1. Rate constants for the oxidation of 2-propanol by MFC at 298 K.

$10^3[\text{MFC}]$ mol dm ⁻¹	[Alcohol] mol dm ⁻³	[H ⁺] mol dm ⁻³	$10^4 k_{\text{obs}}$ s ⁻¹
1.0	0.02	0.1	2.01
1.0	0.03	0.1	2.90
1.0	0.04	0.1	3.81
1.0	0.08	0.1	6.96
1.0	0.12	0.1	9.62
1.0	0.20	0.1	13.7
1.0	0.25	0.1	16.1
2.0	0.20	0.1	13.3
3.0	0.20	0.1	13.9
5.0	0.20	0.1	13.6
8.0	0.20	0.1	13.5
1.0	0.20	0.2	27.0
1.0	0.20	0.3	41.1
1.0	0.20	0.5	68.6
1.0	0.20	0.7	95.2
1.0	0.20	1.0	135
1.0	0.20	0.1	13.8*

*contained 0.001 mol dm⁻¹ acrylonitrile

To ascertain the importance of the cleavage of α -C-H bond in the rate-determining step, the oxidation of 2-propanol-2-*d*₁ (MeCDOHMe, D-2-Pr) was studied. The oxidation of D-2-Pr showed that the formation constant, K , is not appreciably affected by isotopic substitution but the rate constant of the decomposition of the intermediate, k_2 , exhibited a substantial primary kinetic isotope effect (Tables 2 and 3).

Effect of Solvents

The oxidation of 2-propanol was studied in 19 different organic solvents. The choice of solvents was limited due to the solubility of MFC and its reaction with primary and secondary alcohols. There was no reaction with the solvents chosen. The kinetics was similar in all the solvents. The values K and k_2 at 308 K are recorded in Table 4.

DISCUSSION

The correlation between activation enthalpies and entropies of the oxidation of the ten secondary alcohols is not satisfactory ($r^2 = 0.9122$), indicating that the compensation effect in this reaction is not operative in this reaction.¹² It is known, however, that the correlations between the activation enthalpies and entropies are often vitiated by the experimental errors inherent in their values. However, the oxidation of the ten secondary alcohols exhibited a good correlation in terms of Exner's equation

Table 2. Formation constants and thermodynamic parameters of the formation of MFC-alcohol (RCHOHMe) intermediate.

R	K				ΔH kJ mol ⁻¹	ΔS J mol ⁻¹ K ⁻¹	ΔG kJ mol ⁻¹
	288 K	298 K	308 K	318 K			
Me	3.24	2.52	1.94	1.56	-21.2±0.2	-56±1	-4.77±0.6
Et	5.01	3.95	3.10	2.41	-21.0±0.4	-51±2	-4.87±0.3
Pr	5.49	4.18	3.70	2.62	-20.3±0.7	-48±3	-6.12±0.6
i-Pr	5.55	4.41	3.40	2.60	-21.8±0.6	-53±2	-6.12±0.6
i-Bu	2.13	1.66	1.32	1.03	-21.0±0.2	-58±1	-3.74±0.2
Bu	2.66	1.99	1.60	1.25	-21.4±0.4	-58±2	-4.25±0.3
ClCH ₂	3.02	2.30	1.74	1.35	-23.0±0.3	-62±2	-4.53±0.2
MeOCH ₂	2.95	2.19	1.75	1.40	-21.3±0.4	-57±2	-4.50±0.3
Ph	5.95	4.56	3.56	2.81	-21.5±0.4	-52±1	-6.25±0.3
Benzhydrol	3.02	2.25	1.67	1.20	-27.3±0.6	-77±3	-4.45±0.6
D-2-Pr	3.29	2.48	2.00	1.45	-22.8±0.6	-61±3	-4.77±0.6

Table 3. Rate constants and activation parameters of the decomposition of the MFC-alcohol (RCHOHMe) intermediate.

R	10 ⁴ k ₂ s ⁻¹				ΔH^\ddagger kJ mol ⁻¹	ΔS^\ddagger J mol ⁻¹ K ⁻¹	ΔG^\ddagger kJ mol ⁻¹
	288 K	298 K	308 K	318 K			
Me	19.7	41.1	85.7	178	53.3±0.7	-112±3	86.6±0.6
Et	33.4	68.7	143	277	51.4±0.4	-114±2	85.3±0.4
Pr	58.3	108	223	400	47.0±0.7	-125±3	84.1±0.6
i-Pr	94.5	170	331	567	43.5±0.8	-133±3	83.0±0.6
i-Bu	155	262	467	749	37.9±0.6	-149±2	82.0±0.5
Bu	65.5	125	241	530	55.1±0.8	-113±3	83.8±0.7
ClCH ₂	0.40	1.10	2.57	5.94	65.6±0.7	-101±2	95.7±0.5
MeOCH ₂	3.34	7.36	16.7	36.3	58.2±0.8	-110±3	90.1±0.6
Ph	151	292	530	970	44.5±0.4	-126±1	81.8±0.3
Benzhydrol	160	300	540	970	43.1±0.5	-130±2	81.7±0.3
D-2-Pr	3.42	7.95	18.0	40.9	58.0±0.4	-109±3	90.4±0.4
k _H /k _D	5.76	5.16	4.76	4.35			

Table 4. Effect of solvents on the oxidation of 2-propanol by MFC at 308 K.

Solvent	K	10 ⁴ k ₂ , s ⁻¹	Solvent	K	10 ⁴ k ₂ , s ⁻¹
Chloroform	2.04	33.6	Acetic acid	2.13	18.1
1,2-Dichloroethane	1.98	32.1	Cyclohexane	1.68	1.27
Dichloromethane	1.86	33.0	Toluene	1.89	8.21
DMSO	1.94	85.7	MeCOPh	2.11	34.6
Acetone	2.03	27.6	THF	1.83	13.4
DMF	2.12	46.4	t-Butyl alcohol	2.04	17.5
Butanone	2.09	20.5	1,4-Dioxane	2.15	14.0
Nitrobenzene	1.92	36.0	1,2-Dimethoxyethane	1.89	8.92
Benzene	1.97	9.84	Carbon disulfide	2.04	4.35
Ethyl acetate	2.03	12.3			

of isokinetic relation.¹³ An Exner's plot between log k₂ at 288 K and at 318 K was linear (r² = 0.9990). The value of isokinetic temperature evaluated from the Exner's plot is 730±73 K. The linear isokinetic correlation implies that all the alcohols are oxidized by the same mechanism and the changes in rate are governed by the changes in both the enthalpy and entropy of the activation.

The formation constant, K, does not show any substantial variation with the nature of the solvent (Table 4), however, the rate constant of the decomposition, k₂, of the intermediate vary with the solvent. The rate constants of the

decomposition, k₂, was therefore subjected to correlation analysis.

The rate constant, k₂, in eighteen solvents (CS₂ was not considered, as the complete range of solvent parameters was not available) were correlated in terms of the linear solvation energy relationship (LESR) of Kamlet and Taft (eqn. 5).¹⁴

$$\log k_2 = \rho\pi^* + b\beta + \alpha\alpha + A_0 \quad (5)$$

In this equation, π^* represents the solvent polarity, β the hydrogen bond acceptor basicities and α is the hydrogen bond donor acidity. A_0 is the intercept term. It may be mentioned here that out of the 18 solvents, 12 have a value of zero for α . The results of correlation analyses in terms of eqn. (5), a biparametric equation involving π^* and β , and separately with π^* and β are given below as equations (6) - (9). Here n is the number of data points and ψ the Exner's statistical parameter.¹⁵

$$\log k_2 = 1.56(\pm 0.16) \pi^* + 0.13(\pm 0.13) \beta + 0.29(\pm 0.12) \alpha - 3.83 \quad (6)$$

$$R^2 = 0.8898, sd = 0.15, n = 18, \psi = 0.36$$

$$\log k_2 = 1.45 (\pm 0.17) \pi^* + 0.23 (\pm 0.40) \beta - 3.76 \quad (7)$$

$$R^2 = 0.8466, sd = 0.17, n = 18, \psi = 0.42$$

$$\log k_2 = 1.51 (\pm 0.18) \pi^* - 3.72 \quad (8)$$

$$r^2 = 0.8207, sd = 0.17, n = 18, \psi = 0.44$$

$$\log k_2 = 0.49 (\pm 0.32) \beta - 2.91 \quad (9)$$

$$r^2 = 0.1258, sd = 0.38, n = 18, \psi = 1.09$$

Kamlet's¹⁴ LESR explains *ca.* 89 % of the effect of solvent on the oxidation. However, by Exner's criterion¹⁵ the correlation is not even satisfactory (cf. eqn. 6). The major contribution is of solvent polarity. It alone accounted for *ca.* 82 % of the data. Both β and α play relatively minor roles.

The data on the solvent effect were analysed in terms of Swain's¹⁶ equation (10) of cation- and anion-solvation concept also.

$$\log k_2 = aA + bB + C \quad (10)$$

Here A represents the anion-solvating power of the solvent and B the cation-solvating power. C is the intercept term. ($A + B$) is postulated to represent the solvent polarity. The rates in different solvents were analysed in terms of eqn. (10), separately with A and B and with ($A + B$).

$$\log k_2 = 1.17 (\pm 0.02) A + 1.43 (\pm 0.01) B - 4.14 \quad (11)$$

$$R^2 = 0.9996, sd = 0.01, n = 19, \psi = 0.01$$

$$\log k_2 = 0.97 (\pm 0.47) A - 3.03 \quad (12)$$

$$r^2 = 0.2010, sd = 0.28, n = 19, \psi = 0.97$$

$$\log k_2 = 1.34 (\pm 0.20) B - 3.63 \quad (13)$$

$$r^2 = 0.7091, sd = 0.23, n = 19, \psi = 0.55$$

$$\log k_2 = 1.35 \pm 0.03 (A + B) - 4.01 \quad (14)$$

$$r^2 = 0.9899, sd = 0.04, n = 19, \psi = 0.10$$

The rates of oxidation of 2-propanol in different solvents showed an excellent correlation in Swain's equation (cf. eqn. 11) with cation- and anion-solvating powers playing the important roles, though the contribution of the cation-solvation is somewhat more. In fact, the cation-solvation alone account for *ca.* 71 % of the data. The correlation with the anion-solvating power alone was very poor. The solvent polarity, represented by ($A + B$), also accounted for *ca.* 99 % of the data. Since solvent polarity accounted for 99 % of the data, attempt was made to correlate the rate constant with relative permittivity (RM). However, correlation with the inverse of RM was poor (eqn. 15).

$$\log k_2 = 1.60 \pm 0.26(1/RM) - 2.40 \quad (15)$$

$$r^2 = 0.6139, sd = 0.61, n = 19, \psi = 0.84$$

Correlation analysis of reactivity

Since the formation constant, K , of the intermediate did not exhibit much variation with the structure of the alcohol, the rate constants k_2 of the 8 aliphatic secondary alcohols were analyzed in terms of Taft's¹⁷ substituent constants.

The rate constants of oxidation of alcohols failed to yield any significant correlation separately with Taft's σ^* and E_s values.¹⁷

$$\log k_2 = -1.78 (\pm 0.16) \Sigma \sigma^* - 2.16 \quad (16)$$

$$r^2 = 0.9510, sd = 0.19, n = 8, \psi = 0.24, T = 298 \text{ K}$$

$$\log k_2 = -1.36 (\pm 0.99) \Sigma E_s - 2.81 \quad (17)$$

$$r^2 = 0.2402, sd = 0.76, n = 8, \psi = 0.93, T = 298 \text{ K}$$

The rates were, therefore, correlated in terms of Pavelich-Taft's¹⁸ dual substituent -parameter equation (eqn. 18).

$$\log k_2 = \rho^* \Sigma \sigma^* + \delta \Sigma E_s + \log k_0 \quad (18)$$

The correlations are excellent; reaction constants being negative (Table 5). There is no significant co-linearity ($r^2 = 0.2322$) between σ^* and E_s of the eight substituents.

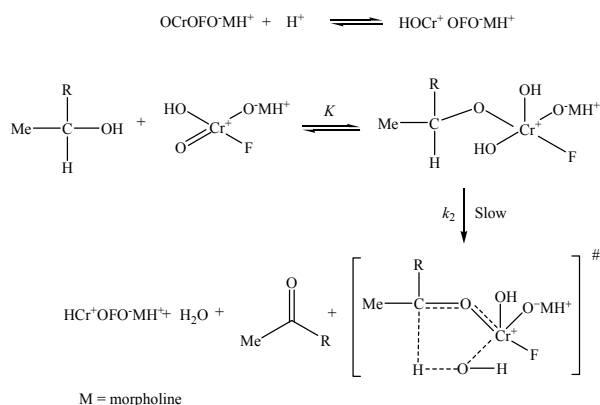
Table 5. Temperature dependence of the reaction constants.

Temp., K	ρ^*	δ	r^2	sd	ψ
288	-1.77±0.02	-0.72±0.02	0.9990	0.02	0.04
298	-1.65±0.03	-0.62±0.04	0.9985	0.03	0.05
308	-1.59±0.03	-0.57±0.04	0.9983	0.03	0.05
318	-1.53±0.03	-0.46±0.05	0.9981	0.04	0.05

The negative polar reaction constant indicates an electron-deficient carbon centre in the transition state of the rate-determining step. The negative steric reaction constants points to a steric acceleration of the reaction. This may be explained on the basis of the high ground state energy of the sterically crowded alcohols.

Since the crowding is relieved in the product, ketone, as well as in the transition state leading to it, the transition state energies of the crowded and un-crowded alcohols do not differ much and steric acceleration, therefore, results. The faster oxidation of 1-phenylethanol and benzhydrol may well be due to the stabilization of the electron-deficient carbon centre in the transition state by phenyl group through resonance.

MECHANISM



Scheme 1. Mechanism of the oxidation of secondary alcohols by MFC.

The presence of a substantial primary kinetic isotope effect confirms that the α -C-H bond is cleaved in the rate-determining step. The negative value of the polar reaction constant together with the substantial deuterium isotope effect indicates the presence of an electron-deficient carbon centre in the transition state. Hence, transfer of a hydride ion from the alcohol to the oxidant is suggested. The hydride ion transfer mechanism is also supported by major role of cation-solvating power of the solvents. The hydride-ion transfer may proceed by either an acyclic bimolecular reaction or may involve a cyclic symmetrical transition state via a chromate ester. Kwart and Nickle¹⁹ have shown that a study of the dependence of the kinetic isotope effect on temperature can be gainfully employed to resolve this problem. The data for protio- and deuterio-2-propanols, fitted to the familiar expression $k_{\text{H}}/k_{\text{D}} = A_{\text{H}}/A_{\text{D}} \exp(E_{\text{a}}/RT)$ show a direct correspondence with the properties of a symmetrical transition state^{20,21} in which the activation energy difference (E_{a}) for $k_{\text{H}}/k_{\text{D}}$ is equal to the zero-point energy difference for the respective C-H and C-D bonds (≈ 4.5 kJ/mol) and the frequency factors and the entropies of activation of the respective reactions are nearly equal. Bordwell²² has documented very cogent evidences against the occurrence of concerted one-step biomolecular processes by hydrogen transfer and it is evident that in the present studies also the hydrogen transfer does not occur by an acyclic biomolecular process. It is well-established that intrinsically concerted sigmatropic reactions, characterised by a transfer of hydrogen in a cyclic transition state, are the only truly symmetrical processes involving a linear hydrogen transfer.²³ Littler²⁴ has also shown that a cyclic hydride transfer, in the oxidation of alcohols by Cr(VI), involves six electrons and being a Huckel-type system is an allowed process. Thus, a transition state having a planar,

cyclic and symmetrical structure can be envisaged for the decomposition of the ester intermediate. The formation of an ester intermediate is supported by the kinetic studies also. Hence, the overall mechanism is proposed to involve the formation of a chromate ester in a fast pre-equilibrium step and then a decomposition of the ester in a subsequent slow step via a cyclic concerted symmetrical transition state leading to the product (Scheme 1). The observed negative value of entropy of activation also supports a polar transition state.

The solvent effect indicated that the transition state is more polarized than the reactant. Thus it is suggested the carbinol-carbon is positively polarized whereas the chromate-oxygen is negatively polarized. Similar observations have been recorded in the oxidation of organic sulphides by PFC²⁵ and methionine by pyridinium bromochromate²⁶ where a positively charged sulphur-centre and a negatively charged chromate-oxygen have been reported. In contrast, reactions involving free cations exhibited relatively much higher contribution of the cation-solvating power e.g., the oxidation of lower oxyacids of phosphorus by PFC²⁷ where the coefficient of cation-solvating power (B) is nearly five-times that the anion-solvating (A). In the oxidation of thioacids by quinolinium fluorochromate, where formation of a sulfenium cation in the rate-determining step has been suggested, the cation-solvating plays a relatively much bigger role.²⁸ The solvent effect also, thus, supports a hydride transfer reaction via a chromate ester.

ACKNOWLEDGEMENTS

Thanks are due to the Professor P. K. Sharma, Head, Department of Chemistry, J. N. V. University, Jodhpur, India for providing the facilities for carrying this work.

REFERENCES

- Corey, E.J., Suggs, W.J., *Tetrahedron Lett.*, **1975**, 2647.
- Guziec, F.S., Luzio, F.A., *Synthesis*, **1980**, 691.
- Bhattacharjee, M.N., Choudhuri, M.K., Dasgupta, H.S., Roy N., Khathing, D.T., *Synthesis*, **1982**, 588.
- Balasubramanian, K., Prathiba, V., *Indian J. Chem.*, **1986**, 25B, 326.
- Pandurangan A., Murugesan, V., Palamichamy, P., *J. Indian Chem. Soc.*, **1995**, 72, 479; Pandurangan, A., Murugesan, V., *J. Indian Chem. Soc.*, **1996**, 73, 484.
- Sayyed-Alangi, S. Z., Sajjadi-Ghotbabadi, H., Baei, M. T., Naderi, S., *E-J. Chem.*, **2011**, 8(2), 815.
- Vyas, N., Goswami, G., Choudhary, A., Prasadrao, P. T. S. R. K., Sharma, V., *Int. J. Chem.*, **2015**, 4(3), 215; Rao, A., Panwar, S., Prakash, O., Vyas, S., Sharma, P. K., *J. Chem. Bio. Phy. Sci., Sec. A*, **2016**, 6(3), 876; Alhaji, N. M. I., Mamani, R., Kaiyalvizhi, K., *Chem. Sci. Trans.*, **2016**, 5(1), 258; Rao, A., Purohit, T., Swami, P., Purohit, P., Sharma, P. K., *Eur. Chem. Bull.*, **2016**, 5(5), 189.
- March, J., *Advanced Organic Chemistry*, Academic Press, New York, **1977**, 181.
- Perrin, D. D., Armarego, L., Perrin, D. R., *Purification of Organic Compounds*, Pergamon, Oxford, **1966**.
- Bhattacharjee, M. N., Choudhary, M. K., Purukayastha, S., *Tetrahedron*, **1987**, 43, 5389.

- ¹¹Brown, H. C., Rao, G. C., Kulkarni, S. U., *J. Org. Chem.*, **1979**, *44*, 2809.
- ¹²Liu, L., Guo, W. E., *Chem. Review.*, **2001**, *101*, 673.
- ¹³Exner, O., *Collect. Czech. Chem. Commun.*, **1964**, *29*, 1094.
- ¹⁴Kamlet, M. J., Abboud, J. L. M., Abraham, M. H., Taft, R. W., *J. Org. Chem.*, **1983**, *48*, 2877.
- ¹⁵Exner, O., *Collect. Chem. Czech. Commun.*, **1966**, *31*, 3222.
- ¹⁶Swain, C. G., Swain, M. S., Powel, A. L., Alunni, S., *J. Am. Chem. Soc.*, **1983**, *105*, 502.
- ¹⁷Wiberg, K. B., *Physical Organic Chemistry*, Wiley, New York, **1963**, 416.
- ¹⁸Pevelich, W. A., Taft, R. W., *J. Am. Chem. Soc.*, **1957**, *79*, 1957.
- ¹⁹Kwart, H., Nickel, J. H., *J. Am. Chem. Soc.*, **1973**, *95*, 3394.
- ²⁰Kwart, H., Latimer, M. C., *J. Am. Chem. Soc.*, **1971**, *93*, 3770.
- ²¹Kwart, H., Slutsky, J., *J. Chem. Soc. Chem. Commun.*, **1972**, 1182.
- ²²Bordwell, F. G., *Acc. Chem. Res.*, **1974**, *5*, 374.
- ²³Woodward, R. W., Hoffmann, R., *Angew. Chem. Int. Ed. Eng.*, **1969**, *8*, 781.
- ²⁴Littler, J.S., *Tetrahedron*, **1971**, *27*, 81.
- ²⁵Banerji, K. K., *J. Chem. Soc. Perkin Trans. 2*, **1988**, 2065.
- ²⁶Sharma, V., Sharma, P. K., Banerji, K. K., *Indian J. Chem.*, **1997**, *36A*, 418.
- ²⁷Moondra, A., Mathur, A., Banerji, K. K., *J. Chem. Soc. Dalton Trans.*, **1990**, 2697.
- ²⁸Khurana, M., Sharma, P. K., Banerji, K. K., *Indian J. Chem.*, **1998**, *37A*, 1011.

Received: 30.08.2016.

Accepted: 24.09.2016.



SYNTHESIS AND ANTIMICROBIAL ACTIVITY OF SOME NEW *L*-LYSINE GLYCOSIDE DERIVATIVES

Yamina Chergui^[a] and Adil A. Othman^{[b]*}

Keywords: 1,3,4- oxadiazoles; 1,2,4- triazoles; glycosides ; *L*-lysine; antimicrobial activities.

Novel glycosides 2-(1,5-diaminopentyl)-*S*-fructosyl-1,3,4-oxadiazole-5-thione , 3-(1,5-diaminopentyl)-5-*S*-glucosyl-1,2,4-triazole-5-thiole and 3-(1,5-diaminopentyl)-4-amino-5-*S*- or 4-*N*-glucosyl-1,2,4-triazole-5-thiole are obtained by reacting the appropriate azoles with *D*-fructose and *D*-glucose. All intermediates and final products are characterized by IR, ¹H-NMR and ¹³C-NMR. The antimicrobial activities are assessed using the paper disk diffusion and broth dilution methods against *Acinetobacter*, *Pseudomonas aeruginosa*, *Bacillus cereus*, *Staphylococcus aureus* and *Spongopora subterranean*. Some of the synthesized compounds showed promising activity against microorganisms under test in comparison with commercially available antibiotics Polymixine and Oxytetracycline.

*Corresponding Authors:

E-Mail: delaliothman@gmail.com
Tel: +213 771537746

- [a] Ecole Doctorale d'chimie Moléculaire et Biomoléculaire, laboratoire de Synthèse Organique Appliquée Lsoa, Faculty of Science, University of Oran 1-Ahmed Benbella, Oran, Algeria
[b] Laboratory of Bioactive Organic Synthesis, Department of Industrial Organic Chemistry, Faculty of Chemistry, University of Science and Technology-Mohamed Boudiaf-Oran, Usto-MB, Oran, Algeria

In continuation of our investigations in this field to synthesize derivatives of 1,3,4-oxadiazylthione, 1,2,4-triazylthiol,⁷ and 4-amino-1,2,4-triazylthiol,⁸ and their respective glycosides,^{9,10,11} the synthesis of three azole-thiol derived from *L*-lysine and their antimicrobial effect is reported here.

Experimental

The IR-spectra, reported in wavenumber (ν , cm⁻¹), were recorded using KBr discs using a Jasco V-530 spectrophotometer. ¹H NMR and ¹³C NMR spectra were recorded on Bruker Avance AQS 300 MHz spectrometer at 300 and 75.5 respectively. Chemical shifts were measured in DMSO-*d*₆ as solvent to TMS as the internal standard.

The bacterial strains used for the experiment were collected as pure culture from Nekache El Sghir Hospital (Hopital El Mohgoun), Arzew, Oran. The Mueller Hinton medium was supplied by Difco.

All reactions were monitored by thin layer chromatographic analysis (silica gel supplied by Merck), and iodine used for visualization. The melting points were measured with a Büchi 540 melting point apparatus and were uncorrected.

Synthesis

Methyl *L*-lysinate (2).

Method (1): 5 ml H₂SO₄ was added dropwise with continuous stirring to *L*-lysine **1** (8.3 g, 0.06 mol) dissolved in methanol (200 mL) and the mixture was refluxed at 110 °C for 19 h. Excess of methanol was removed under vacuum at room temperature and aq. NaHCO₃ was added to neutralise the acid. The resulting solution was extracted with CH₂Cl₂, and dried over anhydrous MgSO₄, filtered and evaporated to dryness to give a solid substance which was recrystallized from ethanol to yield colorless crystalline methyl *L*-lysinate (**2**) (7.6 g, 83.4 %), m.p. 162 °C. IR, 3464 (broad, NH₂), 1725 (C=O).

Introduction

L-Lysine is a necessary building block for all proteins in the body. It also plays a major role in calcium absorption, building muscle protein, recovering from surgery or sports injuries and body's production of hormones, enzymes, and antibodies.¹ Some studies have found that lysine may be beneficial for those with herpes simplex infections.² *L*-lysine has a anxiolytic action through its effects on serotonin receptors in the intestinal tract, and is also hypothesized to reduce anxiety through serotonin regulation in the amygdala.^{3,4} There are lysine conjugates that show promise in the treatment of cancer, by causing cancerous cells to destroy themselves when the drug is combined with the use of phototherapy, while leaving non-cancerous cells unharmed.⁵ *L*-lysine is an important additive to animal feed because it is a limiting amino acid when optimizing the growth of certain animals such as chickens for the meat production.⁶

Several modifications to *L*-lysine concerning the two amino groups, substitution of hydrogen of five carbon chain and OH group of carboxylic acid residue have been reported.^{7,8}

Lysine can be modified through (acetyllysine) methylation (methyllysine), ubiquitination, sumoylation, neddylation, biotinylation, pupylation, and carboxylation, which tends to modify the function of the protein of which the modified lysine residue(s) are a part.⁹ To best of our knowledge, no modification of carboxylic group to azole rings with thione or thiol residue such as 1,3,4-oxadiazylthione, 1,2,4-triazylthiol and 4-amino-1,2,4-triazylthiol are reported.

Method (2): *L*-lysine **1** (2.0 gr, 0.014 mol), dissolved in methanol (75 ml), was treated with 5 ml chlorotrimethylsilane added dropwise with continuous stirring under N₂ atmosphere. The mixture was stirred further for 24 h. Volatiles were removed under vacuum to give a white solid which was recrystallized from ethanol to give colourless crystalline methyl *L*-lysinate (**2**) (1.95 g, 88.6 %). IR, 3469 (broad, NH₂), 1731 (C=O).

L-Lysine hydrazide (**3**).

20 mL hydrazine hydrate 64 % is added to methyl *L*-lysinate **2** (8.63 g, 0.05 mol) dissolved in ethanol (60 ml). The mixture is refluxed at 110 °C for 18 h, a white precipitate is formed during this period. The precipitate was filtered off and the filtrate is evaporated almost to dryness under vacuum at room temperature to give more solid which is combined with the previous one and recrystallized from water/ethanol to yield colorless crystalline *L*-lysine hydrazide **3** (6.25 g, 72 %), m.p. 187 °C. IR, 3446 (broad, NH₂), 1689 (N-C=O).

2-(1,5-Diaminopentyl)-1,3,4-oxadiazole-5-thione hydrochloride (**4**).

KOH (0.16 g, 0.004 mol) dissolved in ethanol (30 ml), was added to *L*-lysine hydrazide(**3**) (5.00 g, 0.03 mol) dissolved in ethanol (60 ml). Next, carbon disulphide (15 ml) is added and the mixture was refluxed at 110 °C for 13 h. The reaction mixture is then acidified to pH 5 by HCl (10 %). Excess ethanol was removed under vacuum, water was added and the aqueous mixture was then extracted by ethyl acetate, dried over anhydrous MgSO₄ and filtered. Volatiles were then removed under vacuum to give fine solid which was recrystallized from toluene/ethanol to colorless crystals (**4**) (4.18 g, 55.7 %), m.p. 173 °C. IR, 3426.3 (NH), 2655(S-H), 1644.93 (C=N), 1415.49(C=S), 1106.08(C-O-C). ¹H NMR (400 MHz) at 8.8 (HN-C=S), 4.3 (N=C-S-H) ppm of oxadiazole ring, 2.7-1.1 ppm for C-H side chain and ¹³C NMR 206.37(C=S), 172.00(N=C=SH), 154.00, 54.70, 31.10, 29.90, 26.60 and 16.20.

1,5-Diaminopentylthiosemicarbazide (**5**).

Ammonium thiocyanate (0.85 g, 0.2 mol) was added to *L*-lysine hydrazide (**3**) (1.00 g, 0.06 mol), dissolved in ethanol (80 ml). Next, HCl (20 ml) was added dropwise and the mixture was refluxed at 80 °C for 15 h. Excess of ethanol was then removed under vacuum to give white solid which was recrystallized from toluene/petroleum ether to yield 1,5-diaminopentylthiosemicarbazide (**5**) as white crystals (0.82 g, 84 %), m.p. 197 °C. IR, 3456, 3075(N-H?), 1686.3 (C=O), 1211.08 (C=S).

Potassium-1,5-diaminopentylthiosemicarbazinate (**6**).

KOH (1.86 g, 0.03 mol) was added to *L*-lysine hydrazide (**3**) (1.00 g, 0.06 mol) dissolved in ethanol (50 ml) at room temperature. CS₂ (5 ml) was next added drop by drop with stirring. Reaction mixture was allowed to stand for 18 h.

Excess of volatiles were evaporated under vacuum at room temperature. Diethylether (30 ml) was then added and the mixture was stirred for 1 h, filtered to give the solid (**6**) (1.32 g, 88 %), m.p. 193 °C. IR, 3380 (strong-NH₂), 2650(S-H), 1625(N-C=O) and 1590(N-C=S).

2-(1,5-Diaminopentyl)-1H-1,2,4-triazole-5-thiol (**7**).

1,5-Diaminopentylthiosemicarbazide (**5**) (2.0 g 0.01 mol) is dissolved in ethanol (200 ml), and an ethanolic KOH solution (KOH, 0.842 g in 20 ml of ethanol) was added and the mixture was refluxed for 13 h. Progress of the reaction was monitored by TLC. Careful neutralization was carried out with HCl. Volatiles were removed under vacuum, the reaction mixture was then extracted three times with ethyl acetate (50 ml), dried over MgSO₄, filtered and evaporated to dryness to give white solid (**7**) (1.10 g, 55 %), m.p. 203 °C. IR, 3342.5(N-H₂), 1526(C=N) and 1385.6 (S-H).

2-(1,5-Diaminopentyl)-1-amino-1H-1,2,4-triazole-5-thiol (**8**).

Potassium-1,5-diaminopentylthiosemicarbazinate (**6**) (1.23 g, 0.47 mmol) and hydrazine hydrate (64 %, 12 ml) were refluxed for 10 h. The progress of the reaction was monitored by TLC. Reaction mixture was cooled to 5 °C and acidified with HCl to pH 1 to yield a yellowish solid of **8.HCl** (2.05 g, 85 %), m.p. 190 °C. IR: 3456 (NH₂), 2640 (SH), 1456.9 (C=N). ¹H NMR, 9.71(d, 2H, NH₂), 3.38 (m, 4H, 2NH₂), 2.53 (s, 1H, SH), 1.86, 1.78, 1.50 (m, 9H, CH(CH₂)₄).

Synthesis of 2-(1,5-diaminopentyl)-5-*S*-*D*-fructosyl-1,3,4-oxadiazole (**9**), 2-(1,5-diaminopentyl)-5-*S*-*D*-fructosyl-1h-1,2,4-triazole (**10**), 2-(1,5-diaminopentyl)-1-amino-*N*-*D*-glucosyl-1H-1,2,4-triazole-5-thiol and 2-(1,5-diaminopentyl)-1-amino-5-*S*-*D*-glucosyl-1H-1,2,4-triazole (**11**).

Thiols (**4**), (**7**) and (**8**) were dissolved in DMF and few drops of HCl and an appropriate amount of *D*-fructose or *D*-glucose was added and the mixture was refluxed (see Table 2). The progress of the reactions was monitored with TLC. The mixtures were neutralized with solid NaHCO₃, and excess of solvent was removed by vacuum under moderate temperature. Residues were extracted with CH₂Cl₂ (50 ml), dried over MgSO₄, filtered and evaporated to dryness to give **9-11**. The yields were summarized in Table 1.

Antimicrobial test

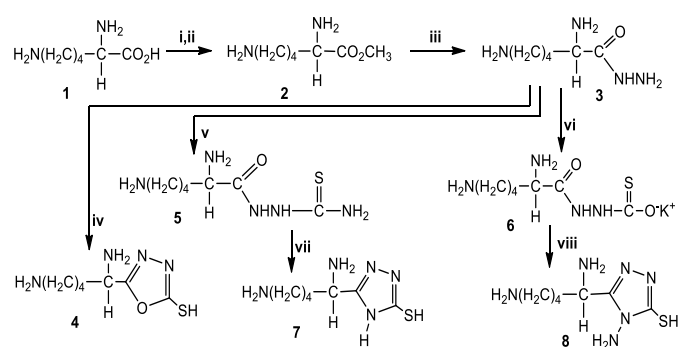
The test sample solutions containing the compounds were made by dissolving in calculated volumes of solvents separately and applied to sterile discs (6 mm diameter) at a concentration of 200 µg/disc and carefully dried to evaporate the residual solvents. Discs containing the test compound were placed on nutrient agar medium uniformly seeded with the test microorganisms. Standard antibiotics polymyxine and oxytetracycline (30 µg/disc) discs and blank discs (impregnated with solvents) were used as positive and negative controls, respectively. The antimicrobial activity of the test agent was determined by measuring the diameter of zone of inhibition expressed in millimeter. The experiments carried out in duplicates.

Table 1. Reaction conditions of the thiols **4**, **7** and **8** with sugars

Compound no.	Thiols (g mol ⁻¹)	<i>D</i> -Fructose (g mol ⁻¹)	<i>D</i> -Glucose (g mol ⁻¹)	Reflux time (h)	Result no.	Yield (%)	M.p. (°C)
4	0.35/0.002	1.8/ 0.01		12	9	68	231
7	02.3/0.010	1.8/ 0.01		08	10	40	253
8	0.105/0.0004		1.2/ 0.007	24	11	46	110

Results and discussion

The three nucleobases 1,3,4-oxadiazole-5-thione (**4**), 1,2,4-triazole-5-thiole (**7**) and 4-amino-1,2,4-triazole-5-thiole (**8**) derived from *L*-lysine via *L*-lysine hydrazide (**3**) (see Scheme 1).



i) CH₃OH, H₂SO₄; ii) CH₃OH, Si(CH₃)₃Cl; iii) NH₂NH₂·H₂O; iv) NaOH, CH₃OH; CS₂, NaOH; v) NH₄SCN; vi) NaOH; viii) NH₂NH₂.

Figure 1. General scheme for synthesis of azole-thiols (**4**), (**7**), and (**8**) from *L*-lysine

The oxadiazole thione (**4**) was obtained by refluxing hydrazide (**3**) with CS₂ in ethanol followed by acidification with HCl when the desired oxadiazole thion (**4**) was formed in 72 % yield, as a mixture of (thiol **4a** ⇌ thion **4b**) tautomers.¹¹

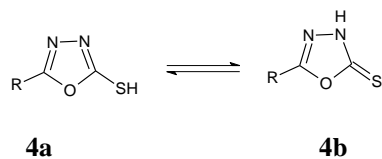


Figure 2. Enol-keto [**4a** ⇌ **4b**] tautomerism of oxadiazolethione (**4b**)

It was confirmed by IR spectroscopic measurements which showed bands at cm⁻¹ 2655 (SH) 1480 (oxadiazole ring) and 1415(C=S). ¹H NMR exhibited signals at 8.8 (HN-C=S), 4.3 (N=C-SH) ppm of oxadiazole ring, 2.7-1.1 ppm for C-H side chain and 206.37(C=S), 172(N=C-SH), 154,54.7, 31.1, 29.9,26.6 and 16.2 for ¹³C NMR.

1,5-Diaminopentylthiosemicarbazide (**5**) was obtained in good yield (84 %) by treating hydrazide (**3**) with ammonium thiocyanate as confirmed by TLC, IR and melting point.¹⁴

Refluxing (**5**) with ethanolic KOH solution yields 2-(1,5-diaminopentyl)-1H-1,2,4-triazole-5-thiol (**7**) which exhibits the characteristic IR bands of the 1,2,4-triazole ring at 1533 cm⁻¹.

Hydrazide (**3**) was treated with CS₂ in alkaline medium to yield potassium 1,5-diaminopentylthiosemicarbazinate (**6**) which was detected by TLC and IR and showed the following characteristic bands: 3380 (strong-NH₂), 2650(SH), 1625(N-C=O and 1590(N-C=S). The salt (**6**), without further purification was treated with hydrazine to give 2-(1,5-diaminopentyl)-1-amino-1H-1,2,4-triazole-5-thiol (**8**) which was confirmed with disappearance of IR bands at 1625 and 1590 and development of triazole bands at 1691, 1618, 1509 and 1402 attributed for C=N and C=S bonds. ¹H-NMR exhibited signals at 9.72 (1H, SH aromatic), 3.38(6H, 3NH₂), 2.54(1H, adjacent to NH₂ and triazole ring), and 1.86-1.5 (8H, 4CH₂).¹⁴

Oxadiazole (**4**) reacts as its thiol tautomer (**4a**) and triazole (**7**) are condensed with *D*-fructose while *N*-amino triazole (**8**) is condensed with *D*-glucose to give the corresponding *S*-glycosides (**9**), (**10**) and (**11**) (see Figure 3). Sugar carbonyl favors condensation with SH group than N-H group.

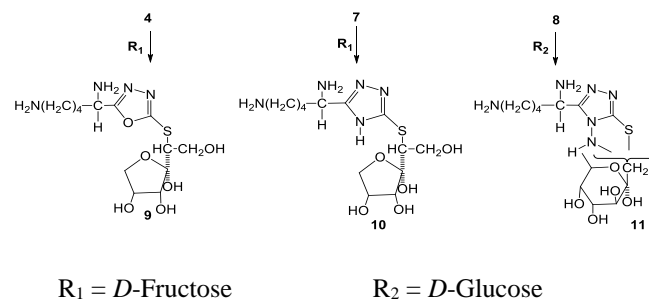


Figure 3. General synthesis scheme for glycosides (**9**), (**10**) and (**11**) from *L*-lysine

The acyclic thioglycoside supposed to be formed undergoes cyclization to give **9**, **10** and **11** via the proposed mechanism illustrated in Figure 4. The compound **11** shows acyclic-cyclic (furan- ⇌ pyrano-) equilibrium and quick trans *S*- to *N*-glycosidation.

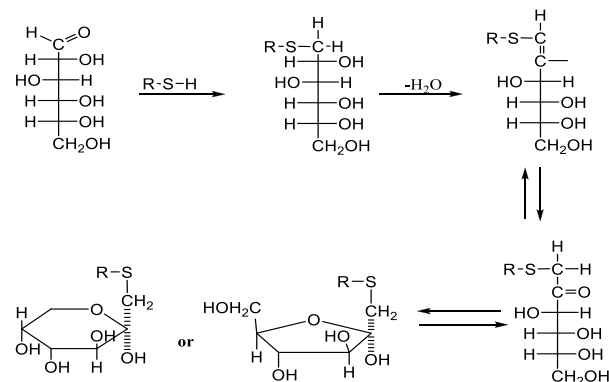


Figure 4. The proposed mechanism of acyclic-cyclic sugar *S*-glycoside tautomerism.

Antimicrobial screening

The antimicrobial activities of the tested compounds are evaluated in vitro using the paper disk diffusion method,¹⁵ against two gram-negative bacteria: *Acinetobacter*, *Pseudomonas aeruginosa*, gram-positive bacteria: *Bacillus cereus*, *Staphylococcus aureus* and one fungus *Spora subterranea*. DMSO known as bacterial static in the concentration of 2 µg ml⁻¹ is used as negative control and two standard disks (Mast Diagnostics, UK), saturated with known antibiotics polymixine and oxytetracycline (30 µg/disc) as positive control are applied.

Table 2. Antibacterial activity of the synthesized compounds

Compounds	Inhibition zone (mm)				Relative inhibition, %
	a	b	c	d	
<i>Acinetobacter</i>					
1	5	5	0	0	71.41
2	12	8	5	0	>100
3	7	0	0	0	100
4	10	10	5	0	>100
5	0	0	0	0	-
6	0	0	0	0	-
7	0	0	0	0	-
8	13	12	5	5	>100
9	7	7	6	6	58.30
10	11	11	9	4	91.66
11	10	8	0	0	71.80
DMSO	-	-	-	-	-
Polymixine	12				100
Oxytetracycline	7				100
<i>P. aeruginosa</i>					
1	12	7	5	0	60
2	0	0	0	0	-
3	7	7	5	5	35
4	12	12	7	0	60
5	8	8	8	0	40
6	8	0	0	0	33.33
7	10	7	4	0	41.66
8	8	0	0	0	60
9	9	9	8	0	35
10	8	6	0	0	40
11	8	5	3	0	60
DMSO	-	-	-	-	-
Polymixine	24				100
Oxytetracycline	20				100
<i>S. aureus</i>					
1	10	7	0		83.33
2	9	9	5	5	75
3	12	9	6		>100
4	11	9	6	0	91.66
5	12	8	0	0	>100
6	0	0	0	0	-
7	7	6	5	0	43.70
8	9	9	9	9	56
9	8	8	6	6	50
10	10	7	5	3	62.50
11	9	7	6	3	56
DMSO	-	-	-	-	-
Polymixine	12				100
Oxytetracycline					100

<i>B. cereus</i>					
1	16	10	8	6	100
2	17	13	7	7	>100
3	15	15	12	12	93.75
4	9	7	4	4	56.25
5	15	11	9	9	93.75
6	6	0	0	0	30
7	9	7	7	7	35
8	13	10	8	6	65
9	16	15	12	12	>100
10	21	11	9	9	>100
11	11	10	10	10	56.20
DMSO	-	-	-	-	-
Polymixine	20				100
Oxytetracycline	16				100
<i>S. subterranea</i>					
1	3	7	7	5	86.66
2	12	10	7	7	80
3	20	15	6	6	>100
4	12	10	10	9	80
5	13	13	13	13	86.66
6	8	5	0	0	53.33
7	10	10	9	9	66.66
8	8	8	8	7	53.33
9	12	10	9	7	80
10	4	0	0	0	26.66
11	7	7	0	0	46
DMSO	-	-	-	-	-
Polymixine	15				100
Oxytetracycline	15				100

Highly active = (inhibition zone > 20 mm), moderately active = (inhibition zone 11- 19 mm), slightly active = (inhibition zone 6 – 10 mm), Inactive = (inhibition zone < 6 mm); MIC a, b, c, d = (1, 1/2 , 1/4, 1/8) 2 µg mL⁻¹ ,*10 % , v/v= 1/1,

After incubation at 37 °C for 24 h, the zone of inhibition of growth around each disk is measured in mm and zone diameters are interpreted in accordance with clsi and nccls.¹⁶⁻¹⁸ The experiments are performed in duplicates and the average results are summarized in Table 2. Appreciable effects of compounds (2), (4), (7) and (10) were observed on *Acinetobacter* at concentration of 400 µg mL⁻¹ and certain extent at 200 µg mL⁻¹ but there was no any response in cases of compounds 5-7. *P. Aeruginosa* was affected by all compounds except ester (2) In c ases of both G-strains slight effect were observed G+bactria, *B. cereus* and *S. aureus* were affected by great extent by the studied compounds even at 50 µg mL⁻¹ concentration. The studied compounds also exhibited antifungal activity resembled by *S. subterranea*

Conclusion

We have presented synthesis and characterization of three new diazole derivatives (4), (7) and (8) and related S- and N-glycosides (9), (10) and (11). The structure of new compounds and their synthetic intermediates are confirmed by spectral data IR, ¹H and ¹³C-NMR. All compounds have been investigated for their antimicrobial activity against two gram-negative bacteria: *Acinetobacter*, *Pseudomonas aeruginosa*, and two gram-positive bacteria: *Bacillus cereus*, *Staphylococcus aureus* and one fungus: *Spora subterranea*.

The investigation of antibacterial and antifungal data showed that heterocyclic derivatives and their synthetic intermediates had variable effect, while all the glycosides (9)-(11) exhibited appreciable antimicrobial effect.

Acknowledgment

We are thankful to Professor A. Derdour, “Laboratoire de Synthèse Organique Appliquée Isoa”, Faculty of Science, University of Oran-1, ab., Oran. Thanks also are due to Miss Safia Salima Kerarma of Nekache el Sghir Hospital, Arzew, Oran for microbial tests.

References

- ¹Civitelli, R., Villareal, D. T., Agnusdei, D., Nardi, P., Avioli, L. V., Gennari, C., *Nutrition*, **1992**, 8, 400.
- ²Tomblin Jr, F. A., Lucas, K. H., *Am. J. Health syst. Pharm.*, **2001**, 58, 298.
- ³Smriga, M., Kameishi, M., Uneyama, H., Torii, K., *J. Nutr.*, **2002**, 132(12), 3744.
- ⁴Smriga, M., Ando, T., Akutsu, M., Furukawa, Y., Miwa, K., Morinaga Y., *Biomed Res.* **2007**, 28(2), 85.
- ⁵Chen, Y., Cao, W., Zhou, J., Pidhatika, B., Ziong, L., Huang, L., Tian, Q., Shu, Y., Wen, W., Hsing, I. M., Wu H., *ACS Appl Matter Interfaces.* **2015**, 7(4), 2919-2930. doi: 10.1021/am508399w.
- ⁶Aquilina, G., Bach, A., V.Bampidis, M. D. L., Bastos, L. G., Costa, G., Flachowsky, M.A., Gralak, C., Hogstrand, Leng, L., López-puente, S., Martelli, G., Mayo, B., Ramos, F., Renshaw, D., Rycken, G., Saarela, M., Sejrsen, K., Beelen, P.V., Wallace R. J., Westendorf, J., *Efsa J.*, **2015**;13(3), 4052.
- ⁷L-lysineDerivative, <http://www.ebi.ac.uk/chebi/searchid.do?Chebiid,2014,25095>.
- ⁸Kondo, M., Shimizu, Y., Murata, A., *Agric. Biol. Chem.*, **1982**, 46(4), 913917 doi:10.1080/00021369.1982.10865171
- ⁹Liu, Z., Wang, Y., Gao, T., Pan, Z., Cheng, H., Yang, Q., Cheng, Z., Guo, J., Ren, A., Xue, Y., *Nucl. Acids Res.*, **2013**, doi: 10.1093/nar/gkt1093
- ¹⁰Othman, A. A., Kihel, M., Amara, S., *Arab. J. Chem.*, in press, **2014**, doi: 10.1016/j.arabjc.2014.09.003..
- ¹¹Khiati, Z., Othman, A. A., Gussase, B., *S. Afr. J. Chem.*, **2007**, 60, 20.
- ¹²Mloston, G., Pieczonka, A. M., Wroblewska, A., Linden, A., Heimgartner, H., *Tetrahedron: Asymmetry*, **2012**, 23, 795-801.
- ¹³Pretsch, E., Buhlmann, P., Affolter, C.,. “Structure Determination of Organic Compounds – Tables of Spectral Data”, Springer. Berlin, **2000**, 259.
- ¹³Pretsch, E., Buhlmann, P., Affolter, C.,. “Structure Determination of Organic Compounds – Tables of Spectral Data”, Springer. Berlin, **2000**, p. 186 for ¹H-NMR and p. 104 for ¹³C-NMR.
- ¹⁵Caillier, L., de Givenchy, E. T., Levy, R., Vandenberghe, Y., Gèribaldi, S., Guittard, F., *Eur. J. Med. Chem.*, **2009**, 44, 3201.
- ¹⁶Dallal, M. M. S., Doyle, M. P., Rezadehbashi, M., Dabiri, H., Sanaei, M., Modarresi, R., Bakhtiari, K., Sharifiy, K., Taremi, M., Zali, M. R., Sharifi, Y. M. K., *Food Control*, **2010**, 21, 388-392.
- ¹⁷Clinical and Laboratory Standards Institute. *Performance Standards for Antimicrobial Susceptibility Testing*; Sixteenth International Supplements. **2006**, 26, 11.
- ¹⁸National Committee for Clinical and Laboratory Standards Villanova, Pa., *Methods for Dilution Antimicrobial Susceptibility Tests for Bacteria That Grow Aerobically*, 4/e, **1997**.

Received: 29.06.2016.

Accepted: 25.09.2016.



SYNTHESIS, CHARACTERIZATION AND ANTIMICROBIAL EVALUATION OF MIXED LIGAND COMPLEXES OF MANGANESE(II), COBALT(II), COPPER(II), NICKEL(II) AND MERCURY(II) WITH 1,10-PHENANTHROLINE AND A BIDENTATE SCHIFF BASE

Rehab K. Al-Shemary^{[a]*}, Ahmed T. Numan^[a] and Eman Mutar Atiyah^[a]

Keywords: 1,10-phenanthroline, Schiff base, mixed-ligand, transition metal (II) complexes.

A Schiff base (L, [2,2'-(1E,1'E)-(ethane-1,2-diylbis(azan-1-yl-1-ylidene))bis(methan-1-yl-1-ylidene)dibenzaldehyde]) has been synthesized by reacting *o*-phthaldehyde with ethylenediamine and characterized with spectral studies and elemental analysis. Mixed ligands complexes of Mn (II), Co (II), Cu (II), Ni (II) and Hg (II) with 1,10-phenanthroline and the Schiff base have been prepared and characterized. The results indicated tetrahedral and square planar structure for the complexes. Biological activity of the ligands and complexes against four selected bacteria viz. *Staphylococcus aureus*, *Bacillus cereus*, *Escherichia coli* and *Pseudomonas* were also examined. Some of the complexes exhibit good antibacterial activities.

* Corresponding Authors
E-Mail: drrehabalshemary@gmail.com

[a] Department of Chemistry, College of Education for Pure Sciences, Ibn -Al-Haitham, University of Baghdad, Baghdad, Iraq

Introduction

In recent years, there has been renewed interest in the synthesis and study of mixed ligand transition metal complexes. The utility aspects of these complexes have received their share of attention as these have found applications in diverse fields.¹ Chiral metal complexes are well known for their use as catalysts, especially in asymmetric synthesis.² Organic compound containing imino group have both salt forming and coordinating properties. The resulting imino complexes are generally insoluble in polar solvents and soluble in non-polar solvents and hence are very important from analytical point of view the studies of simple metal-imino complexes are available in the literature but a very little work has been done on their mixed ligand complexes.^{3,4}

Schiff bases derived from aromatic aldehydes and substituted aliphatic amines and have a large diversity of enforcements in many ranges, e.g. analytical,⁶ inorganic⁷ and biological chemistry.⁸ Schiff bases and their metal complexes are renowned to offer anticancer,⁹ antioxidant¹⁰ and anti-inflammatory activities.¹¹ Many transition metal complexes with oxygen and nitrogen donor Schiff bases possess unusual configuration, structural liability and are sensitive to the molecular environment.¹² Schiff bases are a significant class of ligand in coordination chemistry and find extensive utilities in different fields.¹³ Schiff bases derived from pyridoxal and amino acids are considered very important ligands from the biological point of view.¹⁴ Transition metal complexes of such ligands are important enzyme models.¹⁵ The rapid development of these ligands

resulted in an enhanced research activity in the field of coordination chemistry leading to very interesting conclusions.¹⁶ Mixed ligand complexes have been found to act as an active catalyst in reactions of industrial importance including hydrogenation, hydrogen formation, and oxidative hydrolysis of olefins and carboxylation of methanol.¹⁷ These complexes have also shown catalytic activity in various oxidation reactions of environmental and biological importance.¹⁸ Presently, we have been undertaken a study of mixed ligand complexes of some transition metal ions with 1,10-phenanthroline (phen) and a Schiff base (L) derived from *o*-phthaldehyde and ethylenediamine.

Experimental

Material

All materials applied in this research are of analytical reagent grade and were applied as received.

Methods

NMR spectra of the compounds were determined on "Bruker Spectrospin Ultrashield Magnets 300 MHz" instrument using TMS as an internal standard and DMSO-d₆ as a solvent at Sharif University of Technology in Iran. The shifts are expressed as δ ppm. FT-IR spectra were recorded on "SHIMADZU FTIR-8400 spectrophotometer" on KBr disc. The chloride content for complexes was determined using potentiometric titration method on 686-Titro Processor-665 Dosim A-Metrohm /Swiss. {Magnetic susceptibility} instrument measurements were recorded applying Bruker BM6 instrument at 298 K. Elemental analysis (C, H, and N) was put into Perkin Elmer 2400 series II CHN Analyzer. Melting points were determined by applying Digimelt kind start melting point instrument. The proposed molecular structures of the compounds were drawn by using chem. Office program, 3DX (2006).

Table 1. Some physical properties of the ligand (L) and its complexes.

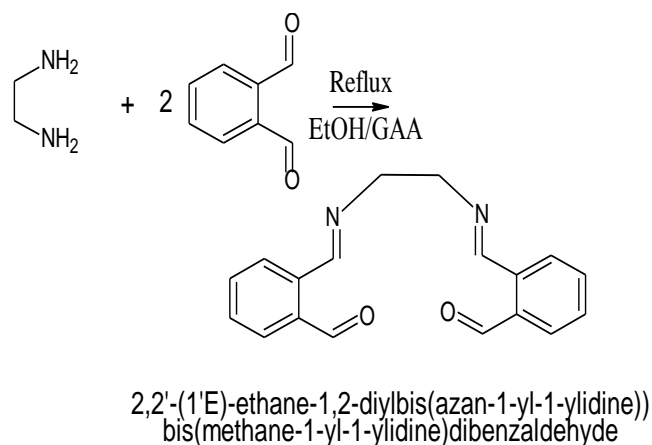
Compounds	Empirical formula	MW	Yield, %	M. p. °C	Colour	Analysis (Calc.), Found			
						C	H	N	Metal
L	C ₁₈ H ₁₆ N ₂ O ₂	292.33	81	171	Dark brown	(73.95) 73.67	(5.52) 5.40	(9.58) 9.21	-
[Co(phen)(L)]Cl ₂	C ₃₂ H ₂₈ Cl ₂ CoN ₄ O ₂	630.43	70	232	Greenish blue	(60.97) 60.38	(4.48) 4.21	(8.89) 8.08	(9.35) 9.20
[Ni(phen)(L)]Cl ₂	C ₃₂ H ₂₈ Cl ₂ N ₄ NiO ₂	630.19	68	267	Greenish yellow	(60.99) 60.64	(4.48) 4.21	(8.89) 8.60	(9.31) 9.30
[Mn(phen)(L)]Cl ₂	C ₃₂ H ₂₈ Cl ₂ MnN ₄ O ₂	626.43	75	261	Pale brown	(61.35) 60.88	(4.51) 4.47	(8.94) 8.74	(8.77) 8.35
[Cu(phen)(L)]Cl ₂	C ₃₂ H ₂₈ Cl ₂ CuN ₄ O ₂	635.04	77	208	Green	(60.52) 60.19	(4.44) 4.32	(8.82) 8.56	(10.01) 9.80
[Hg(phen)(L)]Cl ₂	C ₃₂ H ₂₈ Cl ₂ HgN ₄ O ₂	772.09	82	221	Off -white	(49.78) 49.69	(3.66) 3.32	(7.26) 7.16	(25.98) 25.35

Table2. Infrared spectral data (cm⁻¹) for the ligand (L) and its complexes.

Compounds	$\nu(\text{C-H})_{\text{arom}}$	$\nu(\text{C-H})_{\text{aliph}}$	$\nu(\text{C=O})$	$\nu(\text{C=N})_{\text{imine}}$	$\nu(\text{C=C})$	M – N	M – O
L	3007	2906	1710	1639	1535	-	
[Co(phen)(L)]Cl ₂	3059	2920	1712	1624, 1581	1527	528	424
[Ni(phen)(L)]Cl ₂	3034	2920	1712	1623, 1582	1528	523	448
[Mn(phen)(L)]Cl ₂	3024	2922	1712	1621, 1580	1531	502	428
[Cu(phen)(L)]Cl ₂	3003	2935	1712	1672, 1666	1529	527	438
[Hg(phen)(L)]Cl ₂	3041	2937	1712	1622, 1586	1530	517	450

Synthesis of Schiff base ligand

The ligand (L) was synthesized, as given in Scheme 1, by the usual condensation reaction¹⁰ in which (0.27g, 2 mmol) of *o*-phthalaldehyde, dissolved in 10 mL of methanol, was added to solution contain (0.06 g, 1 mmol) of ethylenediamine dissolved in 10 mL of methanol with continuous stirring. Three drops of glacial acetic acid was added. After complete addition, the reaction mixture was heated under reflux for about 4 h. The volume of reaction mixture was reduced by slow evaporation at room temperature. Then isolated compound was purified by recrystallization from a hot of ethanol (10 mL), to get a pure product of ligand, Yield: 81 %, m. P. 171 °C. ¹H NMR (300 MHz, DMSO-*d*₆) δ = 2.479 (DMSO), 5.38 (2H, CH₂), 7.31-8.28 (m, 5H, C₆H₅), 10.38 (1H, HCO), 8.78-8.85 (m, 1H, HC=N). ¹³C NMR δ = 40.8 (DMSO), 56.70, 61.84 (CH₂), 101.41(=C-N), 128.50-141.13(C₆H₅), 160.05(C=O), 192.87 (C=N).

**Scheme 1.** Synthesis of ligand L.

General procedure of preparation of metal complexes

An aqueous solution (1 mmol) of the metal salts was added gradually with stirring to a methanolic KOH solution (0.29 g, 1 mmol) of the Schiff base. A methanolic solution of 1,10-phenanthroline (0.18 g, 1 mmol) was added to the mixture keeping the stoichiometric ratio of 1:1:1 in each case. The mixture was refluxed with constant stirring for about 2 h. The mixture was cooled to room temperature. The coloured product formed was filtered then recrystallized from ethanol.¹¹

Antimicrobial Screening

The ligand and its complexes were tested against bacteria. Antibacterial testing was done by (MIC) the paper disc method.¹¹ The bacterial applied are *Staphylococcus aureus*, *Bacillus cereus*, *Escherichia coli* and *Pseudomonas aeruginosa* and *Escherichia coli*. Cultures of screen bacteria were preserved in nutritive agar environments and sub-cultured in Petri dishes prior to screening at 10⁻³ mol L⁻¹ concentration.

Table 3. Diameter of zone of inhibition (mm).

The increase in the antimicrobial activity of the complexes may be due to the metal chelation. From comparative analysis as shown in the Table 3, it is absorbed that all the metal complexes are more potent biotical than the ligand.

Conclusion

The mixed complexes were obtained as coloured powdered materials and were characterized using FT-IR, electronic spectra, and magnetic measurements. The elemental analyses were in good agreement with the complexes. From the antimicrobial activity data, it is observed that the complexes exhibit higher activity than the free ligand. The increase in the antimicrobial activity of the complexes may be due to the metal chelation. From comparative analysis as shown in the Table 3 it is observed that all the metal complexes are more potent biotical than the free ligand.

Acknowledgment

We are thankful to Department of Chemistry, College of Education for Pure Sciences, Ibn-Al -Haitham, University of Baghdad for providing financial support.

References

- ¹Singh, D. P., Kumar, R., Mehani, R. and Verma, S. K. , *J. Serb. Chem. Soc.*, **2006**, *71*, 939.
- ²Deepa, K., Madhu, N. T., Radhakrishnan, P .K., *Met. Org. Chem.*, **2005**, *35*, 883.
- ³Chohan, Z. H., Pervez, H., Rauf, A., Khan, K. M. and Supuran, C. T., *J. Enzyme Inhib. Med. Chem.*, **2004**, *19*, 417.
- ⁴Karvembu, R. and Natarajan, K., *Polyhedron*, **2002**, *21*, 219
- ⁵Ali, S. A., Soliman, A. A., Aboaly, M. M. and Ramadan, R. M., *J. Coord. Chem.*, **2002**, *55*, 1161.
- ⁶Chatterjee, D., Mitra, A. and Roy, B. C., *J. Mol. Catal.*, **2000**, *17*, 161.
- ⁷Alaudeen, M., Abraham, A. and Radhakrishnan, P. K., *Sci. Chem. Sci.*, **1995**, *107(2)*, 123.
- ⁸Singh, L., Mohan, G., Parashar, R. K., Tripathi, S. P. and Sharma, R. C., *Curr. Sci.*, **1986**, *55*, 846.
- ⁹Cimerman, Z., Miljanic, S. and Galic, N., *Croatica Chemica. Acta.* **2000**, *73(1)*:81- 95.
- ¹⁰Zhen-Feng, C., Yan-Cheng, L., Li-Min, L., Heng-Shan, W., San-Hai Q., Bo-Long, W.,He-Dong, B., Bin, Y., Hoong-Kun, F., Hua-Gang, L., Hong, L. and Orvig, C., *Dalton. Trans.*, **2009**, *38(2)*, 262-272.
- ¹¹Zhen-Feng, C., Li, M., Li-Min, L., Yan-Cheng, L., Yan, P., Xue, H., Hong-Hong, W., Hua-Gang, L. and Hong, L., *J. Inorg. Biochem.*, **2011**, *105(2)*,171-180.
- ¹²Arai, E., Nishida, Y., Wasa, J., Urakawa, H. Z. L., *J. Cancer*, **2011**, 611.
- ¹³John, V. D. and Krishnankutty, K., *Appl. Organomet. Chem.*, **2006**, *20*, 477
- ¹⁴Khopde, S. M., Priyadarsini, K. P., Venketesan, P. and Rao, M. N. A., *Biophys..Chem.*, **1999**, 80-85.
- ¹⁵Duff, J. C. and Bills, E. J., *J. Chem. .Soc.*, **1932**, 1987
- ¹⁶Ferguso, L. N., *Chem. Rev.*, **1946**, *38*, 227–254.
- ¹⁷Bellamy, L. J., *The Infrared Spectra of Complex Molecules*, 3rd Ed., Methuen, London, **1966**.
- ¹⁸Nakamoto, K., *Infrared Spectra of Inorganic and Coordination Compounds*, 2nd Ed., Wiley Interscience, New York, **1970**.
- ¹⁹Puri, B. R., Sharma, L. R., and Kalia, K. C., *Principles of Inorganic Chemistry*, Milestone Publications, New Delhi, **2008**.
- ²⁰Robert, M. S., Francis, X .W. and David, J. K., *Spectrometric Identification of Organic Compounds*, John Wiley & Sons, 2005.
- ²¹Mahalakshmi N. and Rajavel, R., *Asian J. Biol. Pharm. Res.*, **2011**, *2(1)*, 525- 543.
- ²²Tolulope, M. F., Olorunfemi, O. O. and Isaac A., *J. Chem. Pharm. Res.*, **2014**, *6(6)*, 816-819.

Received: 14.04.2016.

Accepted: 25.09.2016.



CORPUSCULAR-WAVE PROCESSES IN QUANTUM TRANSITIONS

G. A. Korablev^[a] and N. G. Petrova^[b]

Keywords: Potential gradient, quantum transitions, corpuscular-wave dualism, geodesic angle.

Two principles of adding energy characteristics of structural interactions are fulfilled if the process flows either along the potential gradient or against it. Transforming these rules onto the corpuscular-wave dualism, we can assume that corpuscular interactions flow along the potential gradient (principle of adding reciprocals of energies), and wave processes – against the potential gradient (principle of algebraic addition of energies). Such approach is confirmed by the empiric equation, in which the act of quantum action is narrowed to the energy redistribution in the system “particle-wave”. It is demonstrated that the angular vector of rotational-translation motion of electrons at quantum transitions changes in compliance with the quantum number of the square tangent of this angle.

* Corresponding Authors

E-Mail: korablevga@mail.ru, chembio@sky.chph.ras.ru

[a] Department of Physics, Izhevsk State Agricultural Academy

[b] Department of Information Security and Communication of the Agency of Informatization and Communication of the Udmurt Republic

In particular, such supposition is confirmed by the formula of electron transport possibility (W_∞) due to the overlapping of wave functions 1 and 2 (in steady state) during electron-conformation interactions (eqn.1).

$$W_\infty = \frac{1}{2} \frac{W_1 W_2}{W_1 + W_2} \quad (1)$$

Introduction

The problem of quantum-wave dualism was mainly solved in the period of quantum mechanics development. Thus, the application of de Broglie equation allows defining the borders of such phenomena. But the predominating property depends on the process conditions. And it is quite complicated to find out which of them will operate in each particular case, although it is known that the wave pattern more often takes place at low energies, and corpuscular at high ones.

According to Max Born each process can be interpreted either from the corpuscular or wave point. However, it is very difficult to prove that whether one is dealing with particles or waves since all the characteristic properties of the process cannot be defined. Therefore, wave and corpuscular descriptions should be considered as two ways of considering one and the same objective process complementing each other.¹

Thus, these problematic issues of quantum-wave dualism need to be further investigated and discussed. In this paper the attempt is made to clarify them from the point of the notions of space-energy interactions.

Results and Discussion

Principles of adding energy characteristics of interactions

The analysis of kinetics of various physical and chemical processes shows that in many cases the reciprocals of velocities, kinetic or energy characteristics of the corresponding interactions are added.

Eqn. (1) is used for evaluating the characteristics of diffusion processes followed by non-radiating transport of electrons in proteins.²

From classical mechanics it is known that the relative motion of two particles with the interaction energy $U(r)$ takes place as the motion of material point with the reduced mass μ in the field of central force $U(r)$, and general translational motion as a free motion of material point with the mass (eqn. 2 and 3)

$$\frac{1}{\mu} = \frac{1}{m_1} + \frac{1}{m_2} \quad (2)$$

$$m = m_1 + m_2 \quad (3)$$

Such things take place in quantum mechanics as well.³

For dynamic thermodynamic systems, the first commencement of thermodynamics is as follows.

$$\delta E = d\left(U + \frac{mv^2}{2}\right) \pm \delta A \quad (4)$$

where δE is the amount of energy transferred to the system, element $d(U + mv^2/2)$ characterizes the changes in internal and kinetic energies of the system, $+\delta A$ is the work performed by the system and $-\delta A$ is the work performed with the system.

Table 1. Directedness of the interaction processes.

No.	Systems	Type of potential field	Process	U	r_2/r_1 x_2/x_1	U_2/U_1	Sign ΔU	Sign δA	Gradient
1	opposite electrical charges	electrostatic	attraction	$-k(q_1q_2/r)$	$r_2 < r_1$	$U_2 > U_1$	-	+	along the gradient
			repulsion	$-k(q_1q_2/r)$	$r_2 > r_1$	$U_2 < U_1$	+	-	against the gradient
2	similar electrical charges	electrostatic	attraction	$k(q_1q_2/r)$	$r_2 < r_1$	$U_2 > U_1$	+	-	against the gradient
			repulsion	$k(q_1q_2/r)$	$r_2 > r_1$	$U_2 < U_1$	-	+	along the gradient
3	elementary masses m_1 and m_2	gravitational	attraction	$-\gamma(m_1m_2/r)$	$r_2 < r_1$	$U_2 > U_1$	-	+	along the gradient
			repulsion	$-\gamma(m_1m_2/r)$	$r_2 > r_1$	$U_2 < U_1$	+	-	against the gradient
4	spring deformation	field of elastic forces	compression	$k(\Delta x^2/2)$	$x_2 < x_1$	$U_2 > U_1$	+	-	against the gradient
			extension	$k(\Delta x^2/2)$	$x_2 > x_1$	$U_2 > U_1$	+	-	against the gradient
5	photoeffect	electrostatic	repulsion	$k(q_1q_2/r)$	$r_2 > r_1$	$U_2 < U_1$	-	+	along the gradient

As the work value numerically equals the change in the potential energy, therefore,

$$+\delta A = -\Delta U \quad (5)$$

$$-\delta A = +\Delta U \quad (6)$$

It is probable that not only in thermodynamic but in many other processes in the dynamics of interaction of moving particles, not only the value of potential energy is critical, but its change as well. Therefore the following criteria should be fulfilled for two-particle interactions (eqn. 7),

$$\delta E = \left(\frac{m_1 v_1^2}{2} + \frac{m_2 v_2^2}{2} \right) \pm \Delta U \quad (7)$$

Here

$$\Delta U = U_2 - U_1 \quad (8)$$

where U_2 and U_1 are the potential energies of the system in final and initial states.

The character of the change in the potential energy value ΔU was analyzed by its sign for various potential fields and the results are given in table 1.

From the table it is seen that the values $-\Delta U$ and accordingly $+\delta A$ (positive work) correspond to the interactions taking place along the potential gradient, and ΔU and $-\delta A$ (negative work) occur during the interactions against the potential gradient.

The solution of two-particle task of the interaction of two material points with masses m_1 and m_2 , obtained under the condition of the absence of external forces, corresponds to the interactions flowing along the gradient, the positive work is performed by the system (similar to the attraction process in the gravitation field).

The solution of this equation via the reduced mass, μ , is the Lagrange equation for the relative motion of the isolated system of two interacting material points with masses m_1 and m_2 , which in coordinate x is as follows:

$$\mu \cdot x'' = -\frac{\partial U}{\partial x} \quad \frac{1}{\mu} = \frac{1}{m_1} + \frac{1}{m_2}$$

Here U is the mutual potential energy of material points and μ is reduced mass. At the same time, $x'' = a$ (feature of the system acceleration). For elementary portions of the interactions Δx can be represented as follows:

$$\frac{\partial U}{\partial x} \approx \frac{\Delta U}{\Delta x}$$

That is

$$\mu a \Delta x = -\Delta U.$$

Then

$$\frac{1}{1/(a\Delta x)} \frac{1}{(1/m_1 + 1/m_2)} \approx -\Delta U,$$

$$\frac{1}{(1/(m_1 a \Delta x) + 1/(m_2 a \Delta x))} \approx -\Delta U \quad (9)$$

$$\frac{1}{\Delta U} \approx \frac{1}{\Delta U_1} + \frac{1}{\Delta U_2} \quad (10)$$

where ΔU_1 and ΔU_2 are the potential energies of material points on the elementary portion of interactions and ΔU is the resulting potential energy of this mutual interactions.

Therefore, one can conclude that

1. In the systems in which the interactions proceed along the potential gradient (positive performance), the resulting potential energy is found to be based on the principle of addition of reciprocals of the corresponding energies of subsystems.⁴ Similarly, the reduced mass for the relative motion of two-particle system is calculated.

2. In the systems in which the interactions proceed against the potential gradient (negative performance), the algebraic addition of their masses as well as the corresponding energies of subsystems is performed (by the analogy with Hamiltonian).

From the equation (10) it is seen that the resulting energy characteristic of the system of two material points interaction is found based on the principle of addition of reciprocals of initial energies of interacting subsystems.

Electron with the mass m moving near the proton with the mass M is equivalent to the particle with the mass⁵ μ i.e.

$$\mu = \frac{mM}{m+M}$$

Therefore when modifying the eqn. (10), we can assume that the energy of atom valence orbitals (responsible for interatomic interactions) can be calculated⁶ by the principle of adding reciprocals of some initial energy components based on the following equations:

$$\frac{1}{q^2/r_i} + \frac{1}{W_i n_i} = \frac{1}{P_E} \quad (11)$$

$$\frac{1}{P_0} = \frac{1}{q^2} + \frac{1}{(Wrn)_i} \quad (12)$$

or

$$P_E = P_0/r_i \quad (13)$$

Here W_i is the electron orbital energy,⁷ r_i is the orbital radius of i -orbital,⁸ $q = Z^*/n^*$,⁹ n_i is the number of electrons of the given orbital, Z^* and n^* are the effective nucleus charge and effective main quantum number, and r is the bond dimensional characteristics.

For a free electron $P = P_E = Wr$, where $W = 0.510034$ MeV or 0.81872 J.

As the dimensional characteristic, we used the value of electron classic radius $r = 2,81794 \times 10^{-15}$ m and, therefore, $P_E = 2,30712 \times 10^{-28}$ J m.

Act of quantum action

The formulation of eqns. 10, 11 and 12 is not principally new. Already in 1924 the following equation was obtained based on Compton's effect

$$\frac{1}{hv'} = \frac{1}{hv} + \frac{1-\cos\theta}{mc^2} \quad (14)$$

Here hv' is the energy of scattered photon, hv is the energy of incident photon, mc^2 is the own energy of electron, θ is the scattering angle. At the same time, the energy of photons decreases by the value additionally obtained by the electron. In this way the act of quantum action takes place, resulting in the energy redistribution between the corpuscular and wave properties of the interacting systems.

It is even easier, if the action proceeds during the interaction of the pair of similar particles. During the interaction along the potential gradient (corpuscular mechanism) the resultant energy $W_k = W/2$. If this process goes against the gradient (wave movement), the total energy $W_w = 2W$. The ratio between them $W_w/W_k = 4$.

Electric current is the motion of electrons along the potential gradient. If we assume that the magnetic field generated by them is the wave process, the ratio between the electric and magnetic constants needs to contain this digit 4, which is confirmed in the following empirical equation:

$$h = \left(\frac{4+2\alpha}{2\pi}\right)^2 P_e \frac{\varepsilon}{\mu} \quad (15)$$

Here ε is the electric constant, μ is the magnetic constant, h is Plank's constant and α is fine structure constant, a parameter characterizing the interactions of quantum electron-positron and electromagnetic fields. Number π is determined by the ratio between the rotational motion (circle perimeter) and translational motion (length of diameter).

Size α can pay off on the equation:

$$\alpha = \frac{P_e}{E_P \lambda}, \quad (15a)$$

where E_P - energy of a proton and λ - compton wavelength. The percentage error of calculations in this equation is about 0.06 %.

The proportionality coefficient in the eqn. (15) has the dimension of velocity ($m s^{-1}$) for the ratio (F/Hn) , i.e. in such way the rate of energy redistribution in the system "particle-wave" is characterized.

Table 2. Energies of quantum transitions.

Atom	Transition	W_1 (eV)	W_2 (eV)	ΔW (J)	W_k (J)	λ (Å) *	$h\nu$ (J)
C(IV)	2s-2p	19.201	11.792	11.871	11.705	1549	12.824
N(V)	2s-2p	25.724	15.445	16.469	15.462	1238	16.046
O(VI)	2s-2p	33.859	17.195	26.699	18.267	1031	19.267
Al(III)	3s-3p	10.706	5.7130	7.9997	5.9886	1854	10.7145
Si(IV)	3s-3p	14.690	8.0848	10.583	8.3554	1393	14.260
C(III)	2s ² -2s2p	19.201·2	19.201+11.792	11.871	27.480	977	20.332
N(IV)	2s ² -2s2p	25.724·2	25.724+15.445	16.469	36.638	765	25.967
Si(III)	3s ² -3s3p	14.690·2	14.690+8.0848	10.583	20.557	1206	16.4715
Al(II)	3s ² -3s3p	10.706·2	10.706+5.7130	7.9997	14.889	1670	11.895

* Reference 11

Table 3. Quantization of the geometry of structural transitions

Atom	Transition	$\varphi = h\nu/W_k$	$\langle\varphi\rangle$	K	θ	$\langle\theta\rangle$	$\langle 4/3 \theta^\circ \rangle$	Functions of square tangent (k)
C(IV)	2s-2p	1.0956	60.9°	2	54.45°	60.02°	-	$tg^2\varphi_r = 2$
N(V)	2s-2p	1.0377		2	59.67°			
O(VI)	2s-2p	1.0547		2	65.93°			
Al(III)	3s-3p	1.7951	$\varphi_g^\circ + 45.47^\circ = 100.2^\circ$	3 = 2+1	45.45°	46.2°	61.6°	$tg^260^\circ = 3$
Si(IV)	3s-3p	1.7067		3 = 2+1	47.02°			
C(III)	2s ² -2s2p	0.7399	43.1°	1	31.97°	31.7°	42.27°	$tg^245^\circ = 1$
N(IV)	2s ² -2s2p	0.7087		1	35.38°			
Si(III)	3s ² -3s3p	0.8013		1	29.27°			
Al(II)	3s ² -3s3p	0.7589		1	30.17°			

Therefore, the act of quantum action expressed via Plank's constant is narrowed to the energy equilibrium-exchange redistribution between the corpuscular and wave processes.

Generalizing the formalism of eqns. (10 and 15) onto all other interactions flowing along the potential gradient, we can make the conclusion that corpuscular processes take place in these cases, and wave dualism corresponds to the interactions against the potential gradient.

Angle of electron winding

It is known that a particle can have three main motions: translational, rotational and oscillatory. But quantum mechanics does not consider the issue of electron trajectory as we can speak only of the possibility of its location in the given point in space.

But an electron also moves if this translational motion goes along the potential gradient, then it correspond to corpuscular process, and rotational motion to wave one. The correlation of these energy redistribution acts depends on the values of initial energy criteria of the subsystems. During quantum transitions these can be orbital bond energies of the corresponding levels.

Thus, the main parameters of quantum transitions are as follows:

1. Energy of electromagnetic wave of quantum transition follows Plank's equation, $E=h\nu$, where ν is the

electromagnetic wave frequency, in such a way that the oscillatory motion demonstrates itself in quantum transitions, since the electromagnetic wave itself is the process of distribution of the corresponding oscillations.

2. Difference of bond energies of electrons on different energy level of transition, $\Delta W = W_2 - W_1$.

3. Resultant energy of their corpuscular interaction:

$$\frac{1}{w_k} = \frac{1}{w_1} + \frac{1}{w_2} \quad (16)$$

Let us consider some important macroprocesses in this case. The silkworm winds the natural (organic) silk thread only at a definite rotation angle. In cosmonautics the cellulose-viscose thread is wound around the metal cylinder of the spaceship following the special technology, and, what is important, at the same winding angle as the silkworm. The spaceship becomes most durable, more technologically high-quality and lighter.¹⁰ We can also speak of other examples of such phenomenon.

This angle (mainly as applicable to organic systems) was called the geodesic angle: $\varphi_g = 54.73^\circ$ or $54^\circ44'$.

In a general case, the winding angle (θ) is the angle between the geodesic line and vector of rotational motion.

The geodesic line is the shortest distance between two points in a geometric figure of rotation. Besides, planets are also rotating around the sun along the geodesic line. For five primary planets the angle between the axis of rotation and orbit equals from 62° up to 66.5° . The earth θ apparently taking into account also the influence of moon is $66^\circ 33'$. The sun has the same value Θ . In astronomic terms: obliquity of the sun ecliptic and obliquity of the earth equator to the orbit are numerically the same and equal $22^\circ 27'$. Isn't it the reason of special efficiency of solar action on the earth biophysical processes?

Nitrogen, oxygen, hydrogen and, most important, carbon are the main elements of organic materials. Carbon is a specific element, capable of easier hybridization of atomic orbitals with the quantum transition 2s-2p. Therefore, when temperature and pressure rise, the conditions for such hybridization of carbon atoms are formed in organic materials, and this, apparently, takes place in the winding technique in spaceships. And in the silkworm, the same way as in many other natural processes, the corresponding fermentative reactions take place, on which we are still learning how to work.

To calculate θ and φ_g we use the formulation of Compton equation (14), modifying it as applicable to quantum transitions:

$$\frac{1}{h\nu} - \frac{1}{W_k K} = \frac{1 - \cos\theta}{\Delta W} \quad (17)$$

By this equation the difference of energies of wave and corpuscular processes numerically equals the difference of bond energies of electrons on the corresponding orbitals, but when implementing the addition principles (in this case – deduction) of reciprocals of these parameters and taking into account the quantum geometry of transitions. In accordance with the law of energy conservation, this is the process of its redistribution during the quantum action. Angle θ is the angular vector of electron movement, which is quantized by integer number (K) via the square tangent of this angle i.e. $\text{tg}^2\varphi_g = 2$, $\text{tg}^2 60^\circ = 3$ and $\text{tg}^2 45^\circ = 1$. The notion of gyromagnetic (magnetic-mechanical) ratio (γ) numerically equaled to the ratio of magnetic moment of the particle (electron or atom) to its mechanical moment is used in quantum mechanics. For atoms $\gamma = -g\mu_B$, where μ_B – Bohr magneton; g – Lande factor (g - factor). For orbital magnetic moment of the electron $g_L=1$, for spin magnetic moment of the electron $g_S=2.00233$. Their ratio $g_S/g_L \approx 2$ that in accord with the ratios of rotational and translational components of electronic winding in the equation $\text{tg}^2\varphi_g = 2$.

The calculations by the equation (17) are given in tables 2 and 3. At the same time, the values of the angle θ are mainly correlated with the value $\varphi = h\nu/W_k$ in compliance with Table 3.

The notions of breaking stress in the process of plastics stretching by its winding pitch are used in papers,^{10,12,113} σ_α is the axial σ_β is the circumferential stress, which are replaced by the value N_α , the axial effort and N_β , the circumferential

effort, which are proportional to the stresses. At the same time, the following equation is fulfilled.

$$\frac{\sigma_\beta}{\sigma_\alpha} = \frac{N_\beta}{N_\alpha} = \text{tg}^2\varphi_g = 2 \quad (18)$$

This condition allows obtaining the equally tensioned system of threads with the minimal item weight.¹²

The quantum functions of square tangent $k = 1, 2, 3$ numerically determine the ratios of two triangle legs, whose values characterize energy dependencies via axial and circumferential stresses in the system with quantum and wave processes.

From Table 3 it is seen that quantum transitions of 2s-2p type for carbon atom, as distinguished from all other elements, are not accompanied with the changes in geodesic angle and coefficient k. Obviously, this property predetermines the unique features of the winding geodesic angle influence on the biosystems stability. Besides, in all transitions (except for 2s-2p) the correlation $\varphi \approx 4/3$ is fulfilled, which proves that such coefficient mainly compensates structural features of more complex transitions.

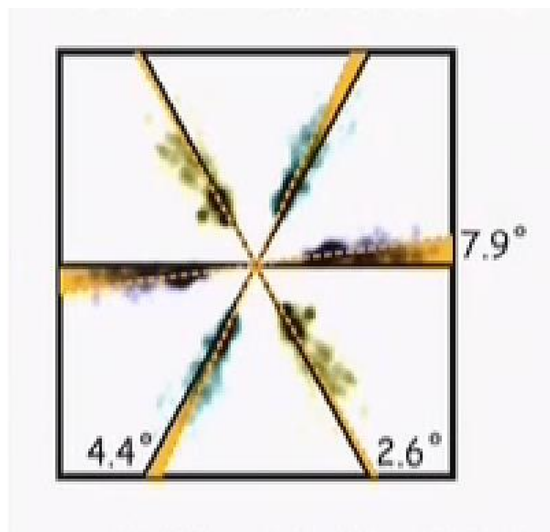


Figure 1. Statistic distribution of the cell number along the coordinate axes.

Some difference between the values of the angles φ and Θ or φ and $4/3\Theta$ is obviously determined by the effect of particle scattering around the main coordinate axes. Similarly, at the conformation of cellular structures the particles are statistically concentrated along the coordinate axes of hexagons (Figure 1) with the deviations by 2.6° ; 4.4° and 7.9° .¹⁴

The average number of such deviations equaled to 4.97 approximately corresponds to the difference $60^\circ - \varphi_g^\circ = 5.27^\circ$.

The dynamics of hexagonal formation of cellular systems is in compliance with the established¹⁵ condition of approximate equilibrium of spatial-energy characteristics of

the subsystems by all bond lines. This is also facilitated by the fact that biosystems with elements of the second period in their structure produce the winding angular vector (Θ) of 60° .

Conclusions

1. Two principles of adding energy characteristics of structural interactions can be transformed onto the processes of corpuscular-wave dualism.

2. It is assumed that in the process of rotational-translation motion of the electron the energies redistribute in the system “particle-wave”, which is demonstrated via the angular vector of such motion (winding angle).

References

- ¹Marison J. B., *General Physics with Biological Examples*, Vysshaya shkola, Moscow, **1986**, 623.
- ²Rubin A. B., *Biophysics*, Vol.1. *Theoretical Biophysics*, Vysshaya shkola, Moscow, **1987**, 319.
- ³Blokhintsev D. I., *Basics of Quantum Mechanics*, Vysshaya shkola, Moscow, **1961**, 512.
- ⁴Korablev G. A., Zaikov G. E., *Quantum and Wave Characteristics of Spatial Energy Interactions*, *Bioscience Methodologies in Physical Chemistry*, Apple Academic Press, Waretown, **2013**, 130-143.
- ⁵Eyring G., Walter J., Kimball G., *Quantum chemistry*, M., F. L., **1948**, 528.
- ⁶Korablev G. A., *Spatial-Energy Principles of Complex Structures Formation*, Brill Academic Publishers and VSP, Netherlands, **2005**, 426.
- ⁷Fischer C. F., *Atomic Data*, **1972**, 301-399.
- ⁸Waber J. T., Cromer D. T., *J. Chem. Phys.*, **1965**, *42* (12), 4116-4123.
- ⁹Clementi E., Raimondi D. L. *J. Chem. Phys.*, **1963**, *38*(11), 2686-2689; *J. Chem. Phys.*, **1967**, *47*, 1300-1307.
- ¹⁰Kodolov V. I., *Polymeric composites and technology of producing aircraft engines from them*, Izhevsk Mechanical Institute, **1992**, 200.
- ¹¹Allen K.U., *Astrophysical magnitudes*, Mir, Moscow, **1977**, 446.
- ¹²Ayushev T. Yu., *Geometric aspects of adaptive technology of producing structures by winding from fibrous composite materials*, BNC SO RAS Publishers, Ulan-Ude, **2005**, 212.
- ¹³Pidgainy Yu. M., Morozova V. M., Dudko V. A., *Mechanics of Polymers*, **1967**, 1096-1104.
- ¹⁴Moser, E., *Nobel lecture in Physiology*, 11.03.2015, TV channel Science”.
- ¹⁵Koablev G. A., Vasiliev Yu. G., Zaikov G. E., *Chem. Phys. Mesoscopy*, **2015**, *17*, 424-429

Received: 09.08.2016.

Accepted: 02.10.2016.



CRYSTAL STRUCTURE OF *N*-{(1*Z*)-3-oxo-1-(thiophen-2-yl)-3-[(2*E*)-2-(thiophen-2-ylmethylidene)-hydrazinyl]prop-1-en-2-yl}benzamide: *N,N*-dimethylformamide (1:1) solvate

Amit Kumar,^[a] K. N. Subbulakshmi,^[b,d] B. Narayana,^[b] B. K. Sarojini,^[c] László Kótai,^[e] Sumati Anthal^[a] and Rajni Kant^{[a]*}

Keywords: Hydrazine; Intermolecular hydrogen bond; Crystal structure; Direct methods.

N-{(1*Z*)-3-Oxo-1-(thiophen-2-yl)-3-[(2*E*)-2-(thiophen-2-ylmethylidene)hydrazinyl]prop-1-en-2-yl}benzamide:*N,N*-dimethylformamide (1:1) solvate, (C₁₉H₁₅N₃O₂S₂C₃H₇NO), crystallizes in the monoclinic space group C2/c with the following unit cell parameters: *a*= 21.111(3), *b*= 8.7685(8), *c*= 25.742(3) Å, β= 105.273(13)° and Z=8. The crystal structure was solved by direct methods and refined by full matrix least squares procedures to a final R value of 0.0962 for 2155 observed reflections. The crystal structure is stabilized by N–H⋯O and C–H⋯O hydrogen bonds. The DMF solvent gives rise to C10–H10⋯O3 intermolecular interaction.

* Corresponding Authors

Fax: +91 191 243 2051

E-Mail: rkant.ju@gmail.com

- [a] X-ray Crystallography Laboratory, Post-Graduate Department of Physics & Electronics,
 [b] Department of Chemistry, Mangalore University, Mangalagangothri-574199, D.K., Mangalore, India
 [c] Department of Industrial Chemistry, Mangalore University, Mangalagangothri- 574 199, D.K., Mangalore, India
 [d] Department of Chemistry, Shree Madhwa Vadiraja Institute of Technology and Management (VTU Belgaum), Vishwothama Nagar, Bantakal, Udupi-574115, Karnataka, India.
 [e] Institute of Materials and Environmental Chemistry, Research Centre for Natural Sciences, Hungarian Academy of Sciences, Budapest, Hungary

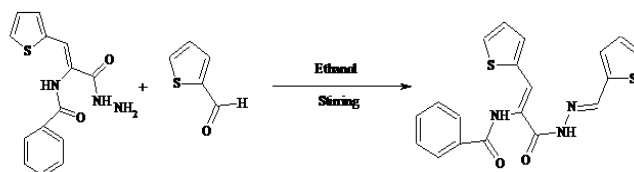
Introduction

Hydrazine derived from condensation of aldehyde with hydrazide have shown excellent biological activities such as, antimicrobial¹⁻², antifungal³, antitumor⁴⁻⁵, anti-inflammation⁶, analgesic⁷, antioxidant.⁸ Crystal structure of some Schiff bases *viz.*, 2-(1-phenylethylidene)hydrazinyl]-8-(trifluoromethyl)-quinoline, 2-[1-(3-bromophenyl)ethylidene]hydrazinyl]-8-(trifluoromethyl)-quinoline, 2-[8-(trifluoromethyl)quinolin-4-yl]-hydrazinylidene}ethyl]-phenol hydrate, and 2-[1-(naphthalen-2-yl)ethylidene]-hydrazinyl]-8-(trifluoromethyl)quinolone⁹, 2-phenyl-5-[(thiophen-2-yl)methylidene]-3-[(*E*)-(thiophen-2-yl)methylidene]amino}-3,5-dihydro-4*H*imidazol-4-one¹⁰, 1-(5-bromo-2-hydroxyphenyl)ethylidene]benzohydrazide¹¹, 1-(2-hydroxyphenyl)ethylidene]-3-ethoxybenzohydrazide¹², 2-fluoro-*N*'-[(2-hydroxy-naphthalen-1-yl)-methylidene]benzohydrazide¹³, (*E*)-3,4,5-trimethoxy-*N*'-[(6-methoxy-4-oxo-4*H*-chromen-3-yl)methylidene]benzohydrazide monohydrate¹⁴ have been reported. Structural information of '3-oxo-1-(thiophen-2-yl)-3-[(2*E*)-2-(thiophen-2-ylmethylidene)hydrazinyl]prop-1-en-2-yl}-benzamide is useful in developing the coordination properties of Schiff bases and to investigate new ligands.

Experimental

Synthesis

A mixture of 3-hydrazinyl-3-oxo-1-(thiophen-2-yl)prop-1-en-2-yl]benzamide (2.87 g, 0.01 mol) and thiophenaldehyde (1.12 g, 0.01 mol) in 20 ml ethanol were stirred 3-4 h.. The solid obtained was filtered washed with cold water, dried and recrystallized from ethanol. Single crystals were grown from methanol:1,4-dioxane(1:1) mixture by the slow evaporation method (M.P.435K-436K). The synthetic route for the compound is presented in Scheme 1.



Scheme 1. Synthesis of *N*-{(1*Z*)-3-oxo-1-(thiophen-2-yl)-3-[(2*E*)-2-(thiophen-2-ylmethylidene)hydrazinyl]prop-1-en-2-yl}benzamide:*N,N*-dimethylformamide (1:1) solvate

X-Ray structure determination

A crystal of dimensions 0.30x0.20x0.20 mm was used for data collection on X'calibur CCD area-detector single crystal X-ray diffractometer equipped with graphite monochromated MoK α radiation ($\lambda=0.71073$ Å). X-ray intensity data consisting of 9749 reflections were collected at 293(2) K and out of these reflections 4487 were found to be unique. The intensities were measured by ω -scan mode for θ ranging between 3.70 to 23.94°. A total number of 2155 reflections were treated as observed [$I > 2\sigma(I)$]. Data were corrected for Lorentz-polarization and absorption factors. The structure was solved by direct methods using

SHELXS97.¹⁵ All non-hydrogen atoms of the molecule were located in the best E-map. All the hydrogen atoms were geometrically fixed and allowed to ride on the corresponding non-H atoms with C-H= 0.93-0.96 Å, N-H= 0.86 Å and $U_{\text{iso}} = 1.2 U_{\text{eq}}(\text{C})$, except for the methyl groups where $U_{\text{iso}}(\text{H}) = 1.5 U_{\text{eq}}(\text{C})$. The final refinement cycles converged to an R-factor of 0.0962 ($wR(F2) = 0.2459$) for 2155 observed reflections. Residual electron density ranges from -0.739 to 0.796 $\text{e}\text{\AA}^{-3}$. Atomic scattering factors were taken from International Tables for X-ray Crystallography (1992, Vol. C, Tables 4.2.6.8 and 6.1.1.4). The crystallographic data are summarized in Table 1.

Table 1. Crystal data and other experimental details

CCDC Number	1494776
Crystal description	Plate shape
Crystal size	0.30 x 0.20 x 0.10 mm
Empirical formula	$\text{C}_{22}\text{H}_{22}\text{N}_4\text{O}_3\text{S}_2$
Formula weight	454.6
Radiation, wavelength	$\text{MoK}\alpha$, 0.71073 Å
Unit cell dimensions	$a = 21.111(3)$ Å, $b = 8.7685(8)$ Å, $c = 25.742(3)$ Å, $\alpha = 90.0^\circ$, $\beta = 105.273(13)^\circ$, $\gamma = 90.0^\circ$
Crystal system, space group	Monoclinic, $\text{C2}/c$
Unit cell volume	$4596.8(9)$ Å ³
No. of molecules per unit cell, Z	8
Absorption coefficient	0.262 mm^{-1}
$F(000)$	1904
θ range for entire data collection	$3.7090 < \theta < 23.9430$
Reflections collected / unique	9749/4487
Reflections observed $I > 2\sigma(I)$	2155
Range of indices	$h = -16$ to 26 , $k = -9$ to 10 , $l = -31$ to 31
No. of parameters refined	282
Final R-factor	0.0962
$wR(F2)$	0.2459
R_{int}	0.0351
R_σ	0.0713
Goodness-of-fit	1.019
$(\Delta/\sigma)_{\text{max}}$	0.001
Final residual electron density	$-0.739 < \Delta\rho > 0.796 \text{ e}\text{\AA}^{-3}$

Results and discussion

The molecule containing atomic labelling is shown in Figure 1 (ORTEP)¹⁶ and the packing diagram as generated using PLATON¹⁷ is shown in Figure 2. It consists of benzamide and two thiophene rings connected via methylenediazinyl. There exists an independent moiety of DMF molecule. The structural parameters, including bond distances and angles show a normal geometry.¹⁸ The benzene ring makes a dihedral angle of $76.14(2)^\circ$ with thiophene ring (A). The double bond $\text{C7}=\text{O1}$ and $\text{C13}=\text{O2}$ bond distance is confirmed by its respective distance of $1.227(5)$ Å and $1.226(5)$ Å, respectively. All the three rings are planar with maximum deviation of $0.0354(8)$ Å observed for C3 atom of the thiophene ring (A). The

conformations of the N-H and C=O bonds are *anti* with respect to each other. Benzamide ring is twisted with respect to thiophene ring (A) with a torsion angle ($\text{C5}-\text{C6}-\text{N3}-\text{C13}$) of $75.6(6)^\circ$. Methylene diazinyl chain is almost linear as indicated by the values of torsion angles $\text{C6}-\text{C7}-\text{N1}-\text{N2} = -178.6(4)^\circ$ and $\text{N1}-\text{N2}-\text{C8}-\text{C9} = -179.0(4)^\circ$.

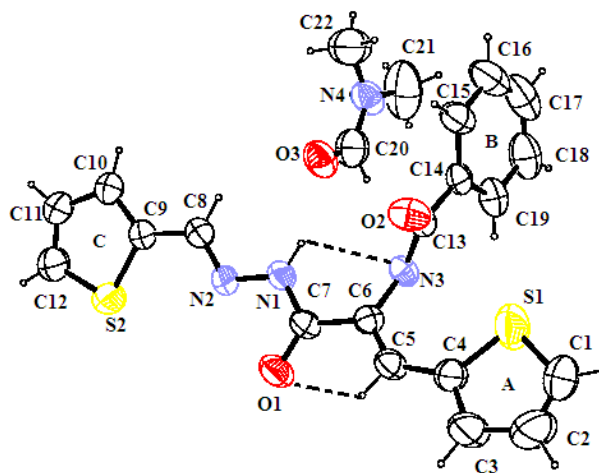


Figure 1. ORTEP view of the molecules with displacement ellipsoids drawn at 40 % probability level. H atoms are shown as small spheres of arbitrary radii.

Molecular packing in the unit cell is viewed down the b-axis is shown in Figure 2. There are two C-H \cdots O, N-H \cdots N and N-H \cdots O intramolecular hydrogen bonds (Table 3). C5-H5 \cdots O1 results in the formation of a virtual five-membered ring with S(5) graph-set motif.¹⁹ In the crystal structure, adjacent molecules are interconnected through N-H \cdots O and C-H \cdots O hydrogen bonds. DMF molecule is linked to molecule through C10-H10 \cdots O3 hydrogen bond.

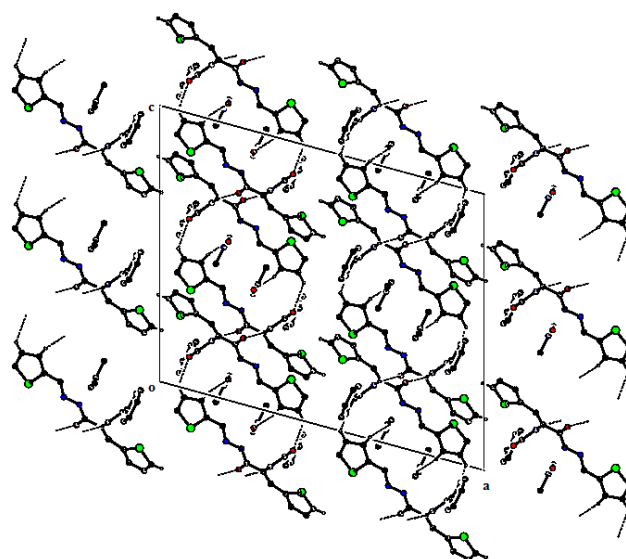


Figure 2. The crystal packing viewed down the b-axis.

Table 2. Selected bond lengths (Å), bond angles (°) and torsion angles(°) for non hydrogen atoms (e.s.d.'s are given in parentheses)

Bond distances		Bond angles		Torsion angles	
S1-C4	1.676(6)	C1-S1-C4	93.5(4)	S1-C4-C5-C6	-7.0(10)
N3-C6	1.415(6)	S1-C4-C5	127.8(4)	N2-N1-C7-C6	-178.6(4)
N1-N2	1.377(5)	N3-C6-C7	118.4(4)	O2-C13-C14-C19	29.9(7)
S2-C9	1.710(5)	C7-N1-N2	117.5(4)	N1-C7-C6-N3	16.2(6)
O2-C13	1.226(5)	O2-C13-C14	122.7(4)	C13-N3-C6-C5	75.6(6)
N2-C8	1.277(6)	O2-C13-N3	121.6 (4)	O1-C7-C6-C5	10.6(7)
O1-C7	1.227(5)	O1-C7-N1	122.4(5)	N1-C7-C6-C5	-167.0(5)
N2-C8	1.277(6)	O1-C7-C6	120.3(5)	N3-C6-C5-C4	-3.0(9)
N3-C13	1.360(5)	N3-C13-C14	115.7(4)	C4-S1-C1-C2	1.5(9)
S2-C9	1.710(5)	C8-N2-N1	117.3(4)	N2-C8-C9-S2	3.4(7)

Table 3. Geometry of intra and intermolecular hydrogen bonds

D-H...A	D-H, Å	H...A, Å	D...A, Å	∠[DH...A, °]
N1-H1...O3	0.86	2.08	2.897(6)	158
N1-H1...N3	0.86	2.47	2.799(5)	104
C5-H5...O1	0.93	2.32	2.736(6)	106
C8-H8...O3	0.93	2.49	3.246(6)	138
N3-H3...O1 ⁱ	0.86	1.99	2.782(5)	152
C10-H10...O3 ⁱⁱ	0.93	2.54	3.440(7)	162
C11-H11...O2 ⁱⁱ	0.93	2.51	3.198(8)	131

Symmetry code: (i) 1/2-x, -1/2+y, 1/2-z (ii) -x,y,1/2-z

Acknowledgement

RK is thankful to DST, New Delhi for funding under research project no: EMR/2014/000467.

References

- ¹El-Masry, A. H., Fahmy, H. H. and Abdelwahed. S. H. A., *Molecules.*, **2000**, *5*, 1429-1438.
- ²Pandey, S. N., Sriram, D., Nath, G. and De Clercq, E., *II Farmaco.* **1999**, *54*, 624-628.
- ³Singh, W. M. and Dash, B. C., *Pesticides.* **1988**, *22*, 33-37.
- ⁴Desai, S. B., Desai, P. B. and Desai, K. R. *Heterocycl. Commun.*, **2001**, *7*, 83-90.
- ⁵Misra, V. S., Singh, S., Agrwal, R. and Chaudhary, K. C., *J. Chem. Soc. Pak.* **1981**, *3*, 209-213.
- ⁶Todeschini, R., De Miranda, A. L. P., Da Silva, K. C. M., Pamini, S. C. and Barreiero, E. J., *Eur. J. Med. Chem.*, **1998**, *33*, 189-199.
- ⁷Sridar, S. K. and Ramesh, A., *Boil. Pharm. Bull.* **2001**, *24*, 1149-1152.
- ⁸Mamolo, M. G., Falagiaru, V., Zampieri, D., Vio, U., Banfi, E. and Scialino, G., *Farmaco. Sci.*, **2003**, *58*, 631-637.
- ⁹Jasinskia, J. P., Butcher, R. J., Mayekar, A. N., Yathirajan, H. S., Narayana, B. and Sarojini, B. K., *J. Mol. Struct.*, **2010**, *980*, 178-181.
- ¹⁰Subbulakshmi, K. N., Narayana, B., Hemmige, S. Y., Akkurt, M., Celik, O., Ersanli, C. C. and Glidewell, C., *Acta Cryst.*, **2015**, *C71*, 1-10.
- ¹¹Zheng, C. Z., Ji, Y., Chang, X. and Zhang, L., *Acta Cryst.*, **2008**, *E64*, o2487.
- ¹²Li, C. and Ban, H., *Acta Cryst.*, **2009**, *E65*, o876.
- ¹³Wang, D., Meng, X. and Ma, J., *Acta Cryst.*, **2012**, *E68*, 021.
- ¹⁴Ishikawa, Y. and Watanabe, K., *Acta Cryst.* **2014**, *E70*, o832.
- ¹⁵Sheldrick, G.M., *Acta Cryst.*, **2008**, *A64*, 112.
- ¹⁶Farrugia, L.J., *J. Appl. Cryst.*, **1997**, *30*, 565.
- ¹⁷Spek, A. L., *Acta Cryst.*, **2009**, *D65*, 148.
- ¹⁸Allen, F. H., Kennard, O., Watson, D.G., Brammer, L., Orpen, A.G. and Taylor, R., *J. Chem. Soc., Perkin Trans-II*, **1987**, S1.
- ¹⁹Bernstein, J., Davis, R. E., Shimoni, L. and Angew, N. L., *Chem. Int. Ed. Engl.*, **1995**, *34*, 1555.

Received: 22.09.2016.

Accepted: 02.10.2016.



SYNTHESIS AND ANTI-INFLAMMATORY ACTIVITY OF SOME NEW PYRAZOLO[3,4-*d*] PYRIMIDINES

Adel M. Kamal El-Dean^[a], Shawkat A. Abdel-Mohsen^{[a]*}, Yasser A. Elossaily^[a] and Istabrak I. Hussein^[a]

Keywords: Pyrazolo[3,4-*d*]pyrimidinone, 6-aryaminomethyl derivatives, sulfa drug, tetrazole, anti-inflammatory activity.

5-Amino-3-methyl-1-phenyl-1*H*-pyrazole-4-carbonitrile (**5**) was reacted with chloroacetyl chloride under fusion condition to afford two compounds, which identified as 6-chloromethylpyrazolo[3,4-*d*]pyrimidine (**3**) and 4-amino-5-chloropyrazolo[3,4-*b*]pyridine (**7**) in different ratios. Treatment of compound (**3**) with aromatic amines, gave the arylaminomethyl derivatives (**8a-c**). Compound (**3**) was reacted with sodium azide, phosphorous oxychloride, sulphanilamide to give new derivatives (**9**, **10**, and **14**). The 4-chloro derivative (**11**) underwent nucleophilic substitution using some reagent such as P₂S₅, sodium azide and hydrazine hydrate to furnish novel pyrazolo[3,4-*d*]pyrimidines (**12**, **13**, **15**, **16**, **17**). All synthesized compounds were characterized using elemental analysis and spectral techniques. The anti-inflammatory activity of all the newly synthesized compounds was evaluated using the carrageenan induced paw oedema test in rats using indomethacin as the reference drug.

* Corresponding Authors

Fax: +20882342708

E-Mail: shawk662001@yahoo.com

[a] Chemistry Department, Faculty of Science, Assiut University, Assiut, 71516, Egypt

Starting precursor, 5-amino-1-phenyl-1*H*-pyrazole-4-carbonitrile (**5**), was prepared using the reported procedure.²⁵

Synthesis of 6-chloromethyl-1-phenyl-1,5-dihydro-pyrazolo[3,4-*d*]pyrimidin-4-one (3**) and 4-amino-5-Chloro-1-phenyl-1,7-dihydro-pyrazolo[3,4-*b*]pyridin-6-one (**7**)**

A mixture of compound (**5**) (1 g, 5.4 mmol) and chloroacetyl chloride (0.75 mL, 6.6 mmol) was refluxed on water bath for 4 h. The reaction mixture was cooled and then heated with 15 mL of ethanol absolute for 5 min, the solid product was filtered, washed with hot ethanol, dried and recrystallized from DMF and identified as compound (**3**). The filtrate was then poured into ice cold water to give another solid, which was filtered off, dried and crystallized from dioxane and identified as compound (**7**).

Compound (**3**): Yield: 1.1 g (75.09 %), m.p. 272-274 °C. IR (cm⁻¹): 3150 (NH), 2988 (CH-aliphatic), 1672 (C=O). MS (*m/z* %): 260.41 (M⁺, 100). ¹HNMR (DMSO-*d*₆) δ = 12.75 (s, 1H, -NH), 8.50 (s, 1H, CH pyrazole), 8.25-7.45 (m, 5H, ArH), 4.36 (s, 2H, CH₂). Anal. Calcd. for C₁₂H₉ClN₄O (260.68): C, 55.29, H, 3.48, Cl, 13.60, N, 21.49 %. Found: C, 55.98, H, 3.26, Cl, 13.31, N, 21.18 %.

Compound (**7**): Yield: 0.35 g (75.12 %), m.p. 159-161 °C. IR (cm⁻¹): 3151, 3231 (NH, NH₂), 1679 (C=O). ¹HNMR (DMSO-*d*₆): δ = 11.48 (s, 2H, NH₂), 10.54 (s, 1H, -NH), 8.69 (s, 1H, CH pyrazole), 8.35-7.44 (m, 5 H, ArH and). Anal. Calcd. for C₁₂H₉ClN₄O (260.68): C, 55.29, H, 3.48, Cl, 13.60, N, 21.49%. Found: C, 55.63, H, 3.33, Cl, 13.73, N, 21.32 %.

General procedure for the synthesis of 6-arylaminoethyl-1-phenyl-pyrazolo[3,4-*d*]pyrimidin-4-(5*H*)-one (8a-c**)**

To a solution of compound (**3**) (2 g, 7.6 mmol) in dioxane (30 mL), a substituted aniline (7.8 mmol) was added. The reaction mixture was heated under reflux for 3-5 h. The

Introduction

Pyrazole derivatives are important intermediates¹⁻⁵ that possess biological and pharmacological activities.⁶⁻¹⁰ The chemistry of pyrimidine and fused pyrimidine derivatives has been of increasing interest, since molecules based on the pyrazolo[3,4-*d*] pyrimidine ring system exhibit a multitude of interesting pharmacological properties including purine analogues,¹¹⁻¹³ CNS depressant,¹⁴ neuroleptic,¹⁵ tuberculostatic,¹⁶ antibacterial and antifungal.¹⁷ Pyrazolo[3,4-*d*]pyrimidines were also identified as a general class of adenosine receptors.¹⁸ Furthermore, pyrazolo[3,4-*d*]pyrimidine derivatives were found to possess anti-inflammatory,¹⁹ antiviral,²⁰ and antitumor activities.²¹ As an extension of our studies on the synthesis of some new biologically active heterocyclic compounds,²²⁻²⁴ we now wish to report the synthesis of some new pyrazolo[3,4-*d*]pyrimidine derivatives to evaluate their anti-inflammatory activity by carrageenan paw edema method.

Experimental

Melting points are uncorrected and determined using a Gallenkamp melting point apparatus. The IR spectra were recorded on a Shimadzu 470 IR spectrometer (KBr) v max cm⁻¹. The ¹H and ¹³C NMR spectra were measured on a Varian EM-200 (1H: 400 MHz, 13C: 100 MHz) spectrometer with TMS as internal standard and DMSO-*d*₆ as a solvent and reported as δ ppm. Mass spectra were determined on a JEOL JMS-600 spectrometer. Elemental analyses (C, H, N, and S) were performed on an elemental analysis system GmbH VarioEL V2.3. The results were found to be in good agreement (±0.4 %) with the calculated value.

solvent was evaporated under reduced pressure and the residue was treated with water. The solid product was filtered off, washed with water, dried and recrystallized from ethanol.

6-Phenylaminomethyl-1-phenyl-pyrazolo[3,4-*d*]pyrimidin-4-(5*H*)-one (8a)

Yield: 1.60 g (66.13 %), m.p. 189–191 °C. IR (cm⁻¹): 3398, 3275 (NH), 2990 (CH-aliphatic), 1682 (C=O). MS (*m/z* %): 317.30 (M⁺, 100). ¹HNMR (DMSO-*d*₆) δ = 12.30 (s, H, NH), 8.35–7.11 (m, 11H, ArH and CH-pyrazole), 5.98 (s, 1H, NH), 4.30 (s, 2H, CH₂). Anal. Calcd. for C₁₈H₁₅N₅O (317.34): C, 68.13, H, 4.76, N, 22.07 %. Found: C, 67.87, H, 4.13, N, 21.91 %.

6-(4-Chlorophenylamino)methyl-1-phenyl-pyrazolo[3,4-*d*]pyrimidin-4-(5*H*)-one (8b)

Yield: 1.82 g (69.11 %), m.p. 229–231 °C. IR (cm⁻¹): 3350, 3189 (NH), 2950 (CH-aliphatic), 1677 (C=O). MS (*m/z* %): 350.98 (M⁺, 100). ¹HNMR (DMSO-*d*₆) δ = 12.35 (s, H, NH), 8.35–7.15 (m, 10H, ArH and CH-pyrazole), 6.09 (s, 1H, NH), 4.45 (s, 2H, CH₂). Anal. Calcd. for C₁₈H₁₄ClN₅O (351.79): C, 61.46, H, 4.01, Cl, 10.08, N, 10.91 %. Found: C, 61.32, H, 3.89, Cl, 9.92, N, 19.88 %.

6-(4-Tolylamino)methyl-1-phenyl-pyrazolo[3,4-*d*]pyrimidin-4-(5*H*)-one (8c)

Yield: 1.29 g (51.07 %), m.p. 191–193 °C. IR (cm⁻¹): 3330, 3170 (NH), 2955 (CH-aliphatic), 1690 (C=O). ¹HNMR (DMSO-*d*₆) δ = 11.25 (s, H, NH), 8.80 (s, 1H, CH-pyrazole), 8.30–7.33 (m, 9H, ArH), 6.11 (s, 1H, NH), 4.40 (s, 2H, CH₂). Anal. Calcd. for C₁₈H₁₄ClN₅O (331.38): C, 68.87, H, 5.17, N, 21.13 %. Found: C, 68.49, H, 5.03, N, 20.94 %.

6-(Azidomethyl)-1-phenyl-pyrazolo[3,4-*d*]pyrimidin-4-(5*H*)-one (9)

To a solution of compound (3) (1 g, 3.8 mmol) in DMF (20 mL), sodium azide (0.9 g, 14 mmol) was added. The reaction mixture was heated under reflux for 10 h. After cooling, 20 mL of cold water was added and extracted with diethyl ether (3x10 mL). The organic layers were combined, washed thoroughly with water (3x10 mL) and dried over anhydrous Na₂SO₄. The solvent was removed under reduced pressure, a yellowish orange crystals was obtained, which was recrystallized from dioxane-H₂O (1:1). Yield: 1.29 g (51.07 %), m.p. 191–193 °C. IR (cm⁻¹): 3290 (NH), 2990 (CH-aliphatic), 2235 (N₃), 1685 (C=O). MS (*m/z* %): 211.17 (M⁺-CH₂N₃⁺, 65). ¹HNMR (DMSO-*d*₆) δ = 11.95 (s, H, NH), 8.40 (s, 1H, CH-pyrazole), 8.25–7.23 (m, 5 H, ArH), 3.35 (s, 2H, CH₂). Anal. Calcd. for C₁₂H₉N₇O (267.25): C, 53.93, H, 3.39, N, 36.69 %. Found: C, 52.57, H, 3.18, N, 36.31 %.

4-Chloro-6-(chloromethyl)-1-phenyl-pyrazolo[3,4-*d*]pyrimidine (10)

A mixture of (3) (1 g, 3.8 mmol) and phosphorus oxychloride (2 mL, 22 mmol) was refluxed at 115 °C for 5h, cooled and poured onto ice water with stirring. The dark

purple powder was collected and recrystallized from acetone. Yield: 1.06 g (95.13 %), m.p. 110–112 °C. IR (cm⁻¹): 2990 (CH-aliphatic), MS (*m/z* %): 278.02 (M⁺, 100). ¹HNMR (DMSO-*d*₆) δ = 8.45 (s, 1H, CH-pyrazole), 8.15–7.42 (m, 5 H, ArH), 4.97 (s, 2H, CH₂). Anal. Calcd. for C₁₂H₈Cl₂N₄ (279.12): C, 51.64, H, 2.89, Cl, 25.40, N, 20.07 %. Found: C, 51.39, H, 3.12, Cl, 25.28, N, 20.41 %.

4-Chloro-N-[(4-chloro-1-phenyl-1*H*-pyrazolo[3,4-*d*]pyrimidin-6-yl)methyl]benzenamine (11)

Method A

A mixture of (10) (1.30 g, 5 mmol) and 4-chloroaniline (0.69 g, 5.20 mmol) in dioxane was refluxed for 5h, cooled and poured onto iced water with stirring. A light purple solid was collected and recrystallized from ethanol. Yield: 1.45 g (85.13 %), m.p. 195–197 °C. IR (cm⁻¹): 3354 (NH), 2995 (CH aliphatic), MS (*m/z* %): 369.00 (M⁺-H, 66.12). ¹HNMR (DMSO-*d*₆) δ = 8.60 (s, 1H, CH-pyrazole), 8.04–6.95 (m, 9H, ArH), 5.70 (s, 1H, NH), 3.95 (s, 2H, CH₂). Anal. Calcd. for C₁₈H₁₃Cl₂N₅ (370.24): C, 58.39, H, 3.54, Cl, 19.15, N, 18.92 %. Found: C, 58.68, H, 3.47, Cl, 19.56, N, 18.71 %.

Method B

A mixture of (8b) (0.35 g, 1 mmol) and phosphorus oxychloride (0.5 mL, 5.5 mmol) was refluxed at 115°C for 5h. The cooled reaction mixture was poured into water (20 mL). The solid product was filtered off, washed with water, dried and recrystallized from ethanol to give (10). It was identical with the product obtained by method A (m.p. and mixed m.p.). Yield: 0.26 g (72.31 %).

6-[(4-Chlorophenylamino)methyl]-N-(4-chlorophenyl)-1-phenyl-1*H*-pyrazolo[3,4-*d*]pyrimidin-4-amine (12)

A mixture of (10) (1.30 g, 5 mmol) and 4-chloroaniline (1.39 g, 10.40 mmol) in dioxane was refluxed for 10 h, cooled and poured onto iced water with stirring. A light brown solid was collected and recrystallized from ethanol-water (1:1). Yield: 1.42 g (66.24 %), m.p. 255–257 °C. IR (cm⁻¹): 3354, 3220 (NH), 2985 (CH aliphatic), MS (*m/z* %): 460.88 (M⁺-1, 59.11). ¹HNMR (DMSO-*d*₆) δ = 8.50 (s, 1H, CH-pyrazole), 8.21–7.05 (m, 13 H, ArH), 5.66 (s, 1H, NH), 3.55 (s, 2H, CH₂). Anal. Calcd. for C₂₄H₁₈Cl₂N₆ (461.35): C, 62.48, H, 3.93, Cl, 15.37, N, 18.22 %. Found: C, 62.83, H, 3.52, Cl, 15.61, N, 18.11 %.

6-[(4-Chlorophenylamino)methyl]-1-phenyl-1*H*-pyrazolo[3,4-*d*]pyrimidine-4(5*H*)-thione (13)

A mixture of (8b) (0.70 g, 2 mmol) and phosphorus pentasulfide (0.5 g, 2.30 mmol) in dry pyridine (10 mL) was refluxed for 12 h, cooled and poured into iced water, acidified to pH 4–5. A yellow powder was separated. The precipitate was filtered, washed thoroughly with water, dried and recrystallized from ethanol. Yield: 0.58 g (80.19 %), m.p. 161–163 °C. IR (cm⁻¹): 3330, 3286 (NH), 2916 (CH aliphatic), 1085 (C=S). ¹HNMR (DMSO-*d*₆) δ = 12.29 (s, 1H, NH), 8.45 (s, 1H, CH-pyrazole), 8.27–7.09 (m, 10 H, ArH), 4.70 (s, 2H, CH₂), 3.90 (s, 1H, NH). Anal. Calcd. for

C₁₈H₁₄ClN₅S (367.86): C, 58.77, H, 3.84, Cl, 9.64, N, 19.04, S, 8.72 %. Found: C, 59.12, H, 3.67, Cl, 9.43, N, 19.25, S, 8.48 %.

4-[[4-Oxo-1-phenyl-4,5-dihydro-1H-pyrazolo[3,4-*d*]pyrimidin-6-yl)methyl]amino]benzenesulfonamide (14)

A mixture of (3) (0.5 g, 1.9 mmol) and sulfanilamide (0.35 g, 2 mmol), in dry pyridine (10 mL), was refluxed for 3 h, cooled and poured into cold water with stirring, filtered off and the filtrate concentrated, cooled in a refrigerator, a light orange powder was obtained, which was recrystallized from dioxane. Yield: 0.48 g (64.27 %), m.p. 315–317 °C. IR (cm⁻¹): 3410, 3390, 3270 (NH, NH₂), 2972 (CH aliphatic), 1360, 1180 (S=O). MS (*m/z* %): 392.08 (M⁺-4H, 33.38). ¹HNMR (DMSO-*d*₆) δ = 13.15 (s, 1H, NH pyrimidine), 8.65 (s, 1H, CH-pyrazole), 9.20 (s, 1H, NH-SO₂), 8.45-7.29 (m, 9H, ArH), 6.11 (s, 1H, NH₂), 3.34 (s, 2H, CH₂). Anal. Calcd., for C₁₈H₁₆N₆O₃S (396.42): C, 54.54, H, 4.07, N, 21.20, S, 8.09 %. Found: C, 54.76, H, 4.29, N, 21.03, S, 8.19 %.

4-Hydrazino-N-[(4-chloro-1-phenyl-1H-pyrazolo[3,4-*d*]pyrimidin-6-yl)methyl]benzenamine (15)

A mixture of (11) (0.74 g, 2 mmol) and hydrazine hydrate (5 mL) in absolute ethanol (20 mL) was refluxed for 6 h. The reaction mixture was poured onto ice. The product was isolated and crystallized from acetic acid as reddish white needles. Yield: 0.49 g (68.31 %), m.p. 225–227 °C. IR (cm⁻¹): 3450, 3375, 3260 (NH, NH₂), 2997 (CH aliphatic). ¹HNMR (DMSO-*d*₆) δ = 12.75 (s, 1H, NH), 10.85 (s, 1H, NH), 8.50 (s, 1H, CH pyrazole), 8.27-7.11 (m, 9 H, ArH), 4.95 (s, 2H, NH₂), 3.80 (s, 2H, CH₂). Anal. Calcd. for C₁₈H₁₆ClN₇ (365.82): C, 59.10, H, 4.41, Cl, 9.69, N, 26.80 %. Found: C, 59.38, H, 4.19, Cl, 9.81, N, 26.62 %.

4-Azido-N-[(4-chloro-1-phenyl-1H-pyrazolo[3,4-*d*]pyrimidin-6-yl)methyl]benzenamine (16)

A mixture of (11) (0.74 g, 2 mmol) and sodium azide (0.13 g, 2 mmol) in DMF (20 mL) was stirred at room temperature overnight. The reaction mixture was extracted with CH₂Cl₂ (3x10 mL) and the organic layer was dried over anhydrous CaCl₂. The solvent was removed under reduced pressure to give a light brown solid and recrystallized from ethanol. Yield: 0.52 g (70.18 %), m.p. 118–120 °C. IR (cm⁻¹): 3250, (NH), 2980 (CH aliphatic), 2202 (N₃). ¹HNMR (DMSO-*d*₆) δ = 8.60 (s, 1H, CH-pyrazole), 8.15-7.15 (m, 9 H, ArH), 5.90 (s, 1H, NH), 3.78 (s, 2H, CH₂). Anal. Calcd., for C₁₈H₁₃ClN₈ (376.80): C, 57.38, H, 3.48, Cl, 9.41, N, 29.74 %. Found: C, 57.09, H, 3.82, Cl, 9.24, N, 29.93 %.

4-Chloro-N-[(7-phenyl-7H-pyrazolo[4,3-*e*]tetrazolo[1,5-*c*]pyrimidin-5-yl)methyl]aniline (17)

Method A

A mixture of (11) (0.37 g, 1 mmol) and sodium azide (0.06 g, 1 mmol) in acetic acid (10 mL) was refluxed for 8 h. The reaction mixture was cooled and diluted with water and extracted with CH₂Cl₂ (3x10 mL) and the oil layer dried over anhydrous Na₂SO₄. The solvent was removed under

reduced pressure to give a pale brown solid, which was recrystallized from dioxane. Yield: 0.25 g (66.10 %), m.p. 168–170 °C. IR (cm⁻¹): 3320, (NH), 2890 (CH aliphatic), 1281, 1136 (N=N=N). MS (*m/z* %): 348.59 (M⁺-N₂, 71.29). ¹HNMR (DMSO-*d*₆) δ = 8.67 (s, 1H, CH-pyrazole), 8.19-7.08 (m, 9 H, ArH), 6.12 (s, 1H, NH), 4.11 (s, 2H, CH₂). Anal. Calcd. for C₁₈H₁₃ClN₈ (376.80): C, 57.38, H, 3.48, Cl, 9.41, N, 29.74 %. Found: C, 57.55, H, 3.67, Cl, 9.73, N, 29.51 %.

Method B

A solution of sodium nitrite (0.07 g, 1 mmol) dissolved in the least amount of water was added drop wise to an ice-cold solution of compound (15) (0.36 g, 1 mmol) in acetic acid (10 mL) and kept in an ice bath at -5 °C. The reaction mixture was allowed to stand overnight at room temperature, then it was poured into water (100 mL). The precipitate that formed was filtered off and crystallized from dioxane to give (17). It was identical with the product obtained by method A (m.p. and mixed m.p.). Yield: 0.22 g (58.42 %).

Anti-inflammatory evaluation

Adult albino rats, weighing 150–200 g, were used. The animals were allowed food and water ad libitum, except during the experiment. They were housed in a room at 23±2 °C with a 12 h light/dark cycle. The animals were randomly allocated into groups of 6 animals each at the beginning of the experiment and were fasted for 24 h before the experiment with free access to water. All of the compounds and the reference drug were suspended in a 0.5 % carboxymethyl cellulose (CMC) solution. The standard drug indomethacin was administered orally at a dose of 20 μmol kg⁻¹. The tested compounds were administered orally at an equimolar oral dose relative to 20 μmol kg⁻¹ of indomethacin. The control group received a 0.5 % CMC solution. Into the sub-plantar region of the right hind paw of each rat, 0.1 mL of 1 % carrageenan solution in saline was injected subcutaneously, 1 h after the administration of the test compounds and standard drug. The right paw volume was measured using a digital plethysmometer (Model 7150, Ugo Basile, Varese, Italy), directly before and after 1, 2, 3 h, intervals after administration of the tested compounds. The percent oedema inhibition was calculated from the mean effect in the control and treated animals according to the following equation.

$$\text{Percent oedema inhibition} = (v_c - v_t/v_c) \times 100 \quad (1)$$

where

v_t represents the mean increase in paw volume in rats treated with tested compounds and

v_c represents the mean increase in paw volume in the control group of rats.

Potency was expressed as % oedema inhibition of the tested compounds relative to % oedema inhibition of indomethacin as depicted in Table 1. All the results are expressed as the mean±standard error of the mean (S.E.M.). Statistical evaluation was performed using A NOVA

Results and Discussions

The only synthesis report²² available for the key intermediate compound (**3**) was route A in Scheme 1, in which readily available compound (**1**) reacted²⁵ with chloroacetyl chloride to yield acylated product (**2**), which underwent subsequent ring closure to produce (**3**).

Table 1. Anti-inflammatory activity of some pyrazolo[3,4-*d*]pyrimidine derivatives using acute carrageenan-induced paw oedema in rats.

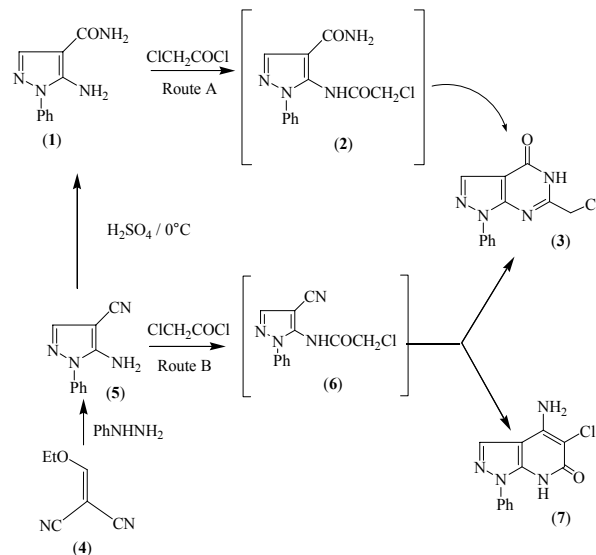
Compd	Oedema inhibition ^a			Potency
	1 h	2 h	3 h	
8a	12.2±1.4	16.7 ± 1.2	24.5±1.5	41.6
8b	32.2±1.0	44.1 ± 1.5	60.6 ±1.2	>100
8c	9.6 ±1.5	13.3 ± 1.3	19.2 ±1.5	32.6
9	12.3 ±1.1	19.6 ± 1.3	24.8 ±0.8	42.2
10	36.4±1.6	48.3± 1.1	63.2± 0.9	>100
11	33.8±1.4	42.3± 1.3	60.8±1.1	>100
12	22.6±1.3	27.2± 1.4	38.8± 1.4	65.9
13	37.2 ±1.0	46.1 ± 1.1	64.1± 1.5	>100
14	39.9 ±1.2	50.1 ± 1.3	68.9 ±1.2	>100
15	30.2 ±0.9	36.6 ± 1.1	39.1 ±1.1	66.4
16	27.3 ±1.4	29.2 ± 1.1	33.7 ±0.9	57.3
17	17.8 ±0.99	23.2 ± 1.1	29.3 ±1.1	49.8
Indo-methaci	31.5 ±1.2	40.2 ± 1.2	58.8 ±1.5	100.0

^aDose 20 μmol kg⁻¹, *n* = 6, Statistically significant from the indomethacin at *p*<0.05.

We were able to obtain the annulated products (**3**) and (**7**) following this literature method via route B in Scheme 1. Thus, when (**5**) was treated with chloroacetyl chloride and heating on steam bath for long time (Route B), two products (**3**) and (**7**) in 75 % and 25 % yield, respectively were isolated. The reaction mixture was separated by fractional crystallization, in which a crystalline solid, m.p. 272–274 °C (Lit, 270-272 °C)²² obtained from hot ethanol was characterized as (**3**) formed through Dimroth rearrangement mechanism. The second solid fraction m.p. 159–161 °C was obtained after cooling the filtrate and poured onto water, which was identified as (**7**). The structure of compound (**3**) was confirmed by the absence of the cyano group, and the presence of two bands at 3150 cm⁻¹ and at 1672 cm⁻¹ for both NH and C=O groups, respectively. Additionally, mass spectrum of compound **3** exhibited a molecular ion peak at 260.41 (M⁺, 100%), which is in agreement with the expected structure. (Scheme 1). The structure of (**7**) was elucidated using spectral and analytical analysis. Its ¹HNMR displayed two characteristic peaks at 11.48 and 10.54 ppm for both NH₂ and NH protons.

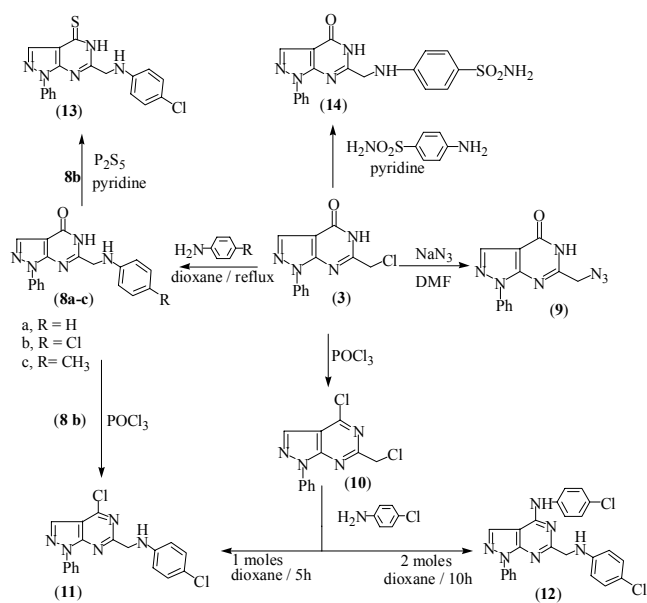
Pyrazolopyrimidine (**3**) underwent nucleophilic substitution reaction of chlorine atom with primary aromatic amines in dioxane to give (**8a-c**). Structure of compounds (**8a-c**) showed absorption bands in the range 3398-3170 cm⁻¹ for two NH groups and 1690-1677 cm⁻¹ for C=O group. Their ¹HNMR displayed the characteristic signals at 5.98-6.11 ppm for -NH, at 4.30-4.45 ppm for methylene protons CH₂ and at 12.30-11.25 ppm due to NH-pyrimidine. The mass spectrum of (**8a**) showed a molecular ion peak at 317.30 (M⁺, 100%), which is in agreement with the suggested structure. When compound (**3**) was heated with sodium azide in the presence of DMF, it afforded the

corresponding 6-azidomethyl derivative (**9**). The IR spectrum of (**9**) showed an absorption band at 2235 cm⁻¹ corresponding to N₃ function. Also, in the mass spectrum of (**9**), the molecular ion peak at *m/z* = 267.25 was not observed, but it showed a base peak at *m/z* = 211.17 due to loss of CH₂N₃⁺. Compound (**10**) was obtained by the chlorination of (**3**) using phosphorus oxychloride. The



Scheme 1. Synthesis of compounds (**3**) and (**7**).

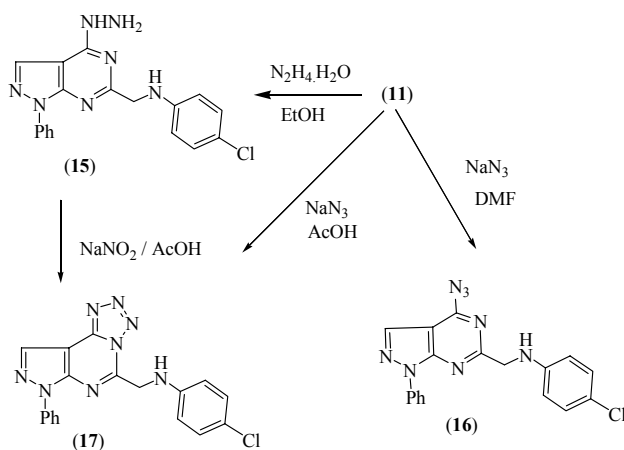
structure of (**10**) was confirmed by both analytical and spectral data. Thus, IR spectrum revealed the disappearance of absorption bands at 3150 and 1672 cm⁻¹ for NH and C=O. MS of (**10**) exhibited a molecular ion peak at 278.02 (M⁺, 100%), which is in agreement with the expected structure. Regioselective amination reactions of compound (**10**) using one and two equivalents of 4-chloroaniline in refluxing dioxane, indicated that, the reaction products depends on the molar ratios and the duration of reaction. Thus, refluxing of (**10**) with one mole for 5 h, afforded the product of the most replaceable sp³ chlorine atom, (**11**).



Scheme 2. Synthesis of compounds (**8** – **14**) from (**3**).

As a chemical evidence, the formation of compound (**11**) was also achieved through heating of a sample of (**8b**) with phosphorus oxychloride. On the other hand, treatment of (**10**) with two moles of 4-chloroaniline for 8 h, yielded the (**12**). The structures of (**11**) and (**12**) were deduced from their satisfactory spectral and analytical data, for example, the MS of compound (**11**) showed its correct parent ion peak at 369.0 (M^+ , 100 %) 1H NMR spectrum showed two characteristic peaks at 5.70 ppm for NH proton. The pyrazolopyrimidinone derivative (**8b**) was converted into the corresponding thione (**13**) by refluxing with P_2S_5 in dry pyridine. As an example for sulfa drugs, the derivative (**14**) was synthesized by refluxing of compound (**3**) with sulphanilamide in dry pyridine. The IR spectrum of of compound (**14**), showed absorption bands at 3410, 3390, 3270 and 1360 cm^{-1} due to NH, NH_2 and SO_2 groups (Scheme 2).

Finally, the behavior of compound (**11**) towards some nucleophilic reagent was investigated. Thus, treatment of (**11**) with hydrazine hydrate in boiling ethanol, furnished the corresponding 4-hyrazino derivative (**15**) in good yield. The structure of compound (**15**) was elucidated from its elemental and spectral data. The IR spectrum showed absorption bands at 3450, 3375 and 3260 cm^{-1} assignable to NH-NH₂ group. Also, Its 1H NMR spectrum showed the presence of the three NH protons at 12.75, 10.85 and 4.95 ppm. Furthermore, interaction of (**11**) with sodium azide in DMF as a basic solvent, furnished the 4-azido derivative (**16**), whereas upon heating in acetic acid, the pyrazolotetrazolopyrimidine derivative (**17**) was obtained via ring closure reaction with the N3-pyrimidine ring.²⁶ As a chemical evidence, the formation of compound (**17**) was achieved through heating of (**15**) with sodium nitrite in acetic acid at 0 °C. The structure of compounds (**16**) and (**17**) was confirmed using elemental and spectral data. The IR spectrum of compound **16** revealed absorption bands at 3250 and 2202 cm^{-1} for both NH and N_3 (azido) groups, respectively. The disappearance of the absorption band for N_3 group in compound (**17**), which displayed characteristic new absorption bands at 1281, 1136 for N-N=N (tetrazole ring). In the MS of (**17**), the molecular ion peak at $m/z = 376.80$ was not observed, but it showed a base peak at $m/z = 348.59$ due to loss of N_2^+ , reinforcing the formation of (**17**) (Scheme 3).



Scheme 3. Synthesis of compounds (**15** – **17**) from (**11**).

Anti-inflammatory activity

The anti-inflammatory activity of the synthesized compounds was determined by the acute carrageenan induced paw oedema standard method in rats.²⁷ From the obtained results (Table 1), it has been observed that several newly prepared compounds (**8b**, **10**, **11** and **13**) revealed better anti-inflammatory properties (60.6–64.1 % inhibition of oedema) as compared to that by indomethacin (58.8 % inhibition). In addition, substitution in compound (**3**) with 4-aminobenzenesulphonamide group resulting in (**14**), which is the most effective anti-inflammatory agent, revealing better activity (68.9 % inhibition) than that of indomethacin. However, comparing the activity of 6-arylaminomethyl-1-phenyl-pyrazolo[3,4-d]pyrimidin-4-(5H)-ones (**8a-c**), it was observed that that substitution with an electron-withdrawing group, chloro, in phenyl (**8b**) (60.6 % inhibition), seems more favorable for constructing an anti-inflammatory active agent than the case of substitution with an electron-donating group CH_3 , as exhibited in (**8c**) (19.2 % inhibition). Meanwhile, upon chlorination of compound (**3**), the obtained 4-chloro derivative (**10**) showed a significant increase in the anti-inflammatory (63.2 % inhibition). However, replacement of the chlorine atom of compound (**10**) in position 6 by 4-chloroaminophenyl group derivative (**11**) possessed higher activity (60.8 % inhibition) than the di-substituted isomer (**12**) (38.8 % inhibition). Finally, (**13**) exhibited more anti-inflammatory activity (64.1 % inhibition) than its ketone analogue (**8b**), comparable to that of indomethacin (58.8 % inhibition). Among the synthesized compounds (**15-17**), no significant difference was perceived in the activity and they showed weak to moderate activity (49.8 - 66.4 % inhibition).

Conclusion

The objective of the present study was to synthesize, characterize and investigate the anti-inflammatory activity of some new pyrazolo[4,3-d]pyrimidine derivatives. The starting compound 6-chloromethyl-1-phenyl-1,5-dihydro-pyrazolo[3,4-d]pyrimidin-4-one (**3**) was used to synthesize the target compounds. Compounds (**8b**, **10**, **11**, **13** and **14**) showed the most anti-inflammatory activity when compared to that of indomethacin.

Acknowledgments

The authors are grateful to Prof. Dr. Ahmed Moharem, Professor of Botany and Microbiology department and the director of Mycology center and colleagues of Faculty of Medicine, Assiut University for their kind help in performing the pharmacological screening. **Conflict of Interest:** The authors declare no conflict of interest.

References

- Sharma, P., Rane, N., Gurrarn, V. K., *Bioorg. Med. Chem. Lett.*, **2004**, *14*, 4185.
- Huang, C. Q., Wilcoxon, K. M., Grigoriadis, M. D., McCarthy, J. R., Chen, C., *Bioorg. Med. Chem. Lett.*, **2004**, *14*, 3943.

- ³ Dhavale, D. D., Matin, M. M., Sharma, T., Sabharwal, S. G., *Bioorg. Med. Chem.*, **2004**, *12*, 4039.
- ⁴ West, T. P., *Microbiol. Res.* **2004**, *29*, 159.
- ⁵ Devesa, I., Alcaraz, M. J., Riguera, R., Ferrandiz, M. L., Eue. J. *pharmacol.*, **2004**, *488*, 255.
- ⁶ Taylor, E. C., Hartke, K. S., *J. Am. Chem. Soc.*, **1959**, *81*, 2456.
- ⁷ Rutavichyus, A. I., Valyulene, S. P., Mozolis, V. V., *J. Org. Chem. USSR.*, **1987**, 1083.
- ⁸ Singh, S. P., *Heterocycles*, **1990**, *31*, 855.
- ⁹ Anderson, E. L., Lasey, J. E., Greene, I., C., Lafferty, J. L., Reiff, H. E., *J. Med. Chem.*, **1964**, *7*, 259.
- ¹⁰ Mohant, S. K., Sriaahar, R., Padmanavan, S. Y., Mittra, A. A., *Indian J. Chem.*, **1977**, *15b*, 146.
- ¹¹ Schenone, S., Bruno, O., Radi, M., Botta, M., *Mini-Rev. Org. Chem.*, **2009**, *6*, 220.
- ¹² Al-Afleq, E. I., Abubshait, S. A., *Molecules*, **2001**, *6*, 621.
- ¹³ Salaheldin, A. M., Oliveira, C. L., Rodrigues, M., *Synth. Commun.*, **2009**, *39*, 1186.
- ¹⁴ Abdou, M. I., Saleh, A. M., Zohdi, H. F., *Molecules* **2004**, *9*, 109.
- ¹⁵ Filler, R., *Chem., Technol.*, **1974**, *4*, 752.
- ¹⁶ Kirkpatrick, W. E., Okabe, T., Hillyard, I. W., Robins, R. K., Dren, A. T., Novinson, T., *J. Med. Chem.* **1997**, *20(3)*, 386.
- ¹⁷ Holla, B. S., Mahalinga, M., Karthikeyan, M. S., Akberali, P. M., Shetty, N. S., *Bioorg. Med. Chem.*, **2006**, *14*, 2040.
- ¹⁸ Davies, L. P., Chow, S. C., Skerritt, J. H., Brown, D. J., Johnston, G. A. R., *Life Sci.*, **1984**, *34*, 211.
- ¹⁹ Rama, K. K., Krishna, K. K., Renuka, S., Ravindra, K., *J. Chem. Pharm. Res.*, **2011**, *3(4)*, 848.
- ²⁰ Gawin, R., De-Clercq, E., Naesens, L., Stawinska, M. K., *Bioorg. Med. Chem.*, **2008**, *16(18)*, 8379.
- ²¹ Kim, D. C., Lee, Y. R., Yang, B. S., Shin, K. J., Kim, D. J., Chung, B. Y., Yoo, K.H., *Eur. J. Med. Chem.* **2003**, *38*, 525.
- ²² Elkhawaga, A. M., Kamal-El-Dean, A. M., Radwan, S., M., Ahmed, A. A., *Bull. Korean Che. Soc.*, **2009**, *30*, 561.
- ²³ Talaat, I. E., Shawkat, A. A., *Molecules*, **2012**, *17*, 14464.
- ²⁴ Shawkat, A. A., Talaat, I. E., Hussein, S. E., *Chem. Pharm. Bull.* **2016**, *64*, 476.
- ²⁵ Cheng, C. C., Robins, R. K., *J. Org. Chem.*, **1956**, *21*, 1240.
- ²⁶ Saleh, A. B. Ahmed, A. F., Abdel-Galil, E. A., Emam, M. F., Atef, K., *Molecule*, **2013**, *18*, 15051.
- ²⁷ Winter, C. A., Risly, E. A., Nuss, G. W., *Proc. Soc. Exp. Biol. Med.*, **1962**, *111*, 544.

Received: 17.09.2016.

Accepted: 04.10.2016.



CORRECTION OF A DATA ANALYSIS EQUATION RELATING TO TWO-SUBSTRATE ENZYME CATALYZED REACTIONS

V. I. Krupyanko^[a]

Keywords: Correction of equation; data analysis of two (A + B) substrate reactions.

Symmetric anti-directivity in the course of change in the ratios between K_A and K_B in the equation $v = VAB/(K_A K_B + K_A B + K_B A + AB)$ is suggested to be potential for applying when this equation is used to treat data on the mechanism of enzymatic action involving two (A + B) substrates.

Corresponding Authors

Tel: (495) 925 74 48

Fax: (495) 956 33 70

E-Mail: krupyanko@ibpm.pushchino.ru; pH76@mail.ru

[a] G.K. Skryabin Institute of Biochemistry and Physiology of Microorganisms, Russian Academy of Sciences, 142290, Pushchino, Moscow region, Pr. Nauki 5, Russia.

Introduction

An appreciation of Eqn. 1 and number of its variations

$$v = \frac{VAB}{K_A K_B + K_A B + K_B A + AB} \quad (1)$$

where

v – initial reaction rate,

V – maximum reaction rate,

A – concentration of the first substrate,

B – concentration of the second substrate,

K_A – the Michaelis constant of the first substrate,

K_B – the Michaelis constant of the second substrate

are frequently used at data analysis of enzyme inhibition and activation of the two-substrate (A + B) enzyme catalyzed reactions in the conditions, when the proceeding of cleavage of the first A substrate (at excessive concentration of the 2nd substrate (B >> A) is studied and vice versa, when the first substrate (A >> B) is taken in excess or (A = B)).¹⁻¹⁴

The estimation of the Michaelis K_m constants and V_m maximum reaction rates by the 1st (and the 2nd) substrate is made by the Eqn. 2.^{1,7,9,11,14}

$$v = \frac{V}{\frac{K_A}{A} + 1} \quad (2)$$

The same approach is used to study the kinetics of the reaction proceeding in the presence of enzyme inhibitors (i) or activators (a).⁵

Thus, the values of parameters V and K_A acquire the sense of the effective K'_A and V' constants and maximum reaction rates determined with the attempt to calculate the respective K_i and K_a constants of enzyme inhibition and activation by the Eqn. (1) or its numerous modifications.¹⁻¹⁴

Analysis of Eqn. (1) and its modifications shows that they are applicable only in the cases of (i) two monoparametrical associative (type IV_i , by the parametrical classification Table 1, line 4),¹⁵ (ii) the same enzyme competitive inhibition (according to the traditional terminology),^{16,17} (iii) catalytic (Table 1, line 3)¹⁸⁻²⁴ or (iv) the same enzyme non-competitive inhibition.^{16,17}

Other attempts to modify Eqn. (1) aimed to calculate the constants of mixed (K'_A)^{10,11,12} and non-competitive enzyme inhibition^{10,11,16} may lead to unacceptable values of such constants for practical use.

As for the attempts to use Eqn. (1) and its modifications for calculation of data on enzyme activation, the results may turn out the opposite, i.e. data treatment of enzyme activation is performed within enzyme inhibition using the terminology of inhibited enzyme catalyzed reactions and by taking into account the respective K_i constants of enzyme inhibition.^{1-7, 14}

The difficulties in use of the Eqn. (1) and its modifications are in the fact that these modifications do not take into account the symmetric anti-directivity of effects of enzyme activation to effects of enzyme inhibition so evident at the level of changes in initial rates of these enzyme catalyzed reactions.

$$v_i < v_0; \quad v_a > v_0 \quad (3)$$

The following approach is used for calculation of the K_{IV_i} constants of associative enzyme inhibition of type IV_i (Table 1, line 4) by authors in most cases.

(a) the Eqn. (1) is simplified to Eqn. (4)

$$v_i = \frac{VA}{K_A \left(1 + \frac{i}{K_{is}}\right) + A} \quad (4)$$

where K_A parameter acquires the sense of K_m^0 , the Michaelis constant, and the K_{is} parameter i.e., the constant of competitive enzyme inhibition.

(b) For calculation of the K_{III} constant of catalytic (type III_i) (Table 1, line 3) or non-competitive enzyme inhibition^{16,17} the following modification of the equation (1) is used^{1,2,9,14}

$$v_i = \frac{VA}{K_A \left(1 + \frac{i}{K_{is}}\right) + A \left(1 + \frac{i}{K_{ii}}\right)} \quad (5)$$

where K_A is Michaelis constant (K_m^0) and K_{is} and K_{ii} parameters acquire the sense of the K_i constant of non-competitive enzyme inhibition.

Use of the Eqns. (4) and (5) after simple transformations, when the symbol K_{is} slope constant of enzyme inhibition (Eqn. 4) acquires the sense of the K_{IVi} constant of competitive (i.e. associative enzyme inhibition, Table 1, line 4) and the symbols K_{is} slope constants and K_{ii} intercept constants of enzyme inhibition (which is the same i.e. $K_{is} = K_{ii}$, because the $(K'_m V^0 / K_m^0 V'; i)$ coordinates of slopes at $K'_m = K_m^0$ are simplified to the coordinates of intercepts $(1/V'; i)$ ²³ acquire the symbol of the K_{III} constant of catalytic (Table 1, line 3) or non-competitive^{16,17} enzyme inhibition.

After substitution of the K_{is} parameter in Eqn. (4) by K_{IVi} and re-grouping of denominator Eqn. (5) with transfer of the co-multiplier

$$1 + \frac{i}{K_{III}} = 1 + \frac{i}{K_{is}} = 1 + \frac{i}{K_{ii}}$$

in the denominator at V , a possibility opens up to take into account symmetric anti-directivity of effects of enzyme activation to effects of enzyme inhibition, because then Eqn. (4) is simplified to Eqn. (6) and Eqn. (5) to Eqn. (7).

$$v_{IVi} = \frac{V^0}{1 + \frac{K_m^0}{S} \left(1 + \frac{i}{K_{IVi}}\right)} \quad (6)$$

$$v_{IIIi} = \frac{V^0 \left(\frac{1}{1 + \frac{i}{K_{III}}} \right)}{1 + \frac{K_m^0}{S}} \quad (7)$$

These equations are widely used and for a long time in enzyme kinetics for calculation of the constants K_{IVi} and K_{III} of competitive and non-competitive enzyme inhibition, respectively.^{16,17}

To enhance the possibility of applying the approach described in Eqns. (1–5) for data treatment of enzyme activation, it is necessary to write Eqns. 6 and 7 in the form of Eqns. 8 - 10.

$$v_{IVi} = \frac{V^0}{1 + \frac{K_m^0}{S} \cdot F} \quad (8)$$

$$v_{IIIi} = \frac{V^0 \left(\frac{1}{F}\right)}{1 + \frac{K_m^0}{S}} \quad (9)$$

$$F = 1 + \frac{e}{K_e} \quad (10)$$

where F is the factor (always positive) of multiplicity of increase of the kinetic parameters K_m^0 and V^0 of initial (uninhibited $i = 0$ and non-activated $a = 0$) reaction determined in the presence of effectors (e): $i, a, B \gg A$ and etc.

By comparison of the dependence between the position of factor F in Eqns. (8) and (9) and the position of lines IV and III relative to line 0 of initial uninhibited and non-activated enzyme catalyzed reaction (Table 1, Figure 3 and 4) it is easy to see that if the presence of the 3rd component ($i, a, B \gg A$ and etc.) in the reacting system leads to increase of the K_m^0 reaction parameter ($K'_m > K_m^0$) (Table 1, Figure 4, line IV) then the F factor will be in numerator at K_m^0 , (Table 1, Eqn. 4a) thus, demonstrating increase of this parameter by $1+e/K_e$ times (Eqn. 6 in the text or Eqn. 4a, in Table 1), to demonstrate a decrease of the V^0 parameter ($V' < V^0$), as one might expect, the F factor will be in denominator at V^0 , showing the fact of decrease of this parameter by $1+e/K_e$ times (Eqn. 7 in the text), (Eqn. 3a in Table 1). It is analogous to other equations of Table 1.

We can summarize all the above discussion concerning Eqns. (1 – 10) in the form of two rules.

(1) The necessity of taking into account the symmetric anti-directivity in the course of change of ratios between (K_A and K_B) parameters in Eqn. (1) when this equation is used to calculate v_i and v_a of the initial velocities of the enzyme catalyzed reactions inhibition and activation and

2) To validate the applicability of the above rule using the practical examples.

Experimental

We studied the influence of 5-fluorouracil (5-Fur) on initial rates of p-nitrophenylphosphate (pNPP) cleavage in the reaction catalyzed by porcine alkaline phosphatase (E.C. 3.1.3.1). The reagents obtained from Sigma (USA) were employed. The plots of a course of pNPP cleavage were recorded by a CF-4 DR two-beam spectrophotometer (Optica Milano, Italy). Reactions were performed in 0.05 M Tris-HCl buffer (pH 9.0) at ionic strength 0.1 using NaCl of high purity at constant mixing¹⁵ in a thermostat (37 °C) by monitoring the increase of absorbance ($+\Delta A_{400}$) of solution containing the substrate, enzyme and activator against the solution of the same composition but without the enzyme. The concentration of pNPP was changed from 0.294×10^{-4} – 0.98×10^{-4} M, the concentration of porcine alkaline phosphatase was $2.1 \mu\text{g mL}^{-1}$.

The initial reaction rates (v) were defined by the angle of slope of tangents to initial segments of curves of a course of enzyme catalyzed reactions in not less than five parallel experiments. The kinetic parameters K_m and V parameters were calculated by plots in the (v^{-1} ; S^{-1}) coordinates of Lineweaver-Burk using the program Sigma Plot, version 2000 (USA). Root-mean-square deviation of determination: $v = \pm 2.5\%$, K_m and $V = \pm 7.5\%$, $K_{va} = \pm 10\%$.

Results and Discussion

Determination of the intersection points of straight lines.

The results show (Figure 1) that a course of change of initial rates of activated enzyme catalyzed reactions (v_a) obtained in the presence of 5-Fur (his symbol a_v) goes above the plot drawn in the absence of ($a_v = 0$) activator, i.e. it is an activated enzymatic reaction ($v_a > v_0$). Increment of the ordinates between the points ($\Delta v = v_a - v_0$) at increasing concentration of the substrate cleaved enlarges – obviously, line 1 at further increase in substrate concentration will intersect line 0, i.e. enzyme activated will be replaced by enzyme inhibition ($v_a < v_0$). What type of enzyme activation is there in the range of used substrate concentrations? The experimental data (Figure 1) are enough to determine the values of (K'_m , K^0_m , V' , V^0) parameters to employ any computing program as for example, given in literature.²¹ According to the ratio of the parameters, $K'_m < K^0_m$, $V' < V^0$, $a_v > 0$, one can establish (as seen from Table 1, line 11) that this enzyme catalyzed reaction corresponds to type (V'_a) of enzyme activation, hence, the equation (11a) of Table 1 can be used for calculation of v_{va} rates of this enzyme catalyzed reaction.

However, it is more convenient to plot the dependence of v_{va} and v_0 parameters of Figure 1 in the coordinates of Lineweaver-Burk (Figure 2), which results in the same values of $K^0_m = 5.45 \times 10^{-5}$ M, $V^0 = 9.363 \mu\text{mol} \cdot \text{min}^{-1} \mu\text{g protein}^{-1}$ parameters of initial reaction and $K'_m = 3.47 \times 10^{-5}$ M, $V' = 8.803 \mu\text{mol} \cdot \text{min}^{-1} \mu\text{g protein}^{-1}$, which can also be obtained using the parameters of Figure 1 and 2.

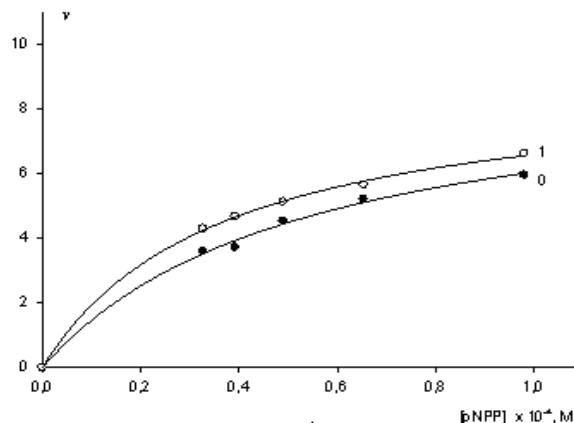


Figure 1. Plots of activating effect of 5-Fur on initial rates of pNPP cleavage catalyzed by porcine alkaline phosphatase represented in the (v ; S) coordinates. Note: line 1 – the concentration of activator 0.001 M, line 0 – the activator is absent; $v \mu\text{mol} \cdot \text{min}^{-1} \mu\text{g protein}^{-1}$

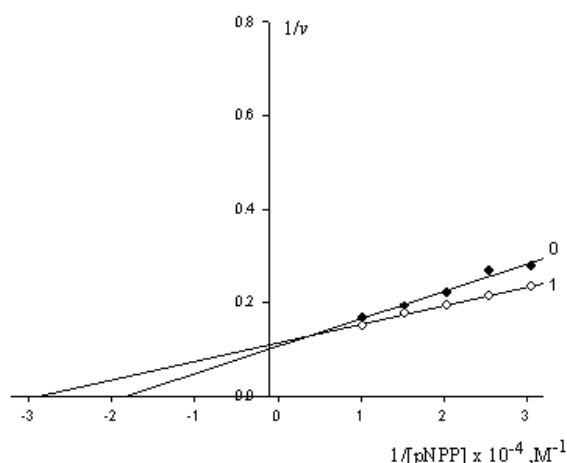


Figure 2. Plots of activating effect of 5-Fur on initial rates (v) of pNPP cleavage catalyzed by porcine alkaline phosphatase represented in the (v^{-1} ; S^{-1}) coordinates. Note: line 1 – the concentration of activator 0.001 M, line 0 – the activator is absent; $v \mu\text{mol} \cdot \text{min}^{-1} \mu\text{g enzyme}^{-1}$

It is seen from Table 1 (Figure 11) that when the position of the experimental line V of activated reaction (Figure 2 of the text and figure 11 of Table 1) goes below the line 0 of initial reaction in the 1st quadrant of the coordinates of Lineweaver-Burk plot and crosses it at a point located to the left of a scale of reverse concentrations of substrate cleaved, but to the right of the ordinate axis. This point of the coordinates can be approximately determined from the plot in Figure 2, using the projections of the point on the coordinate axes. For more exact determination of the coordinates one needs to use a general solution of Eqns. 11a and 8a of Table 1 in (v^{-1} ; S^{-1}) coordinates.

$$\frac{1}{v'} = \frac{K'_m}{V'} \cdot \frac{1}{S} + \frac{1}{V'} \quad (11)$$

and

$$= \frac{1}{v_0} = \frac{K_m^0}{V^0} \cdot \frac{1}{S} + \frac{1}{V^0} \quad (12)$$

where: K'_m and V' are concrete values of parameters of Eqn. (11).

By making equal the right parts of Eqns. (11) and (12) one gets Eqn. (13)

$$\frac{1}{S_{\text{int}}} = \frac{V' - V^0}{K'_m V^0 - K_m^0 V'} \quad (13)$$

and

$$\frac{1}{v_{\text{int}}} = \frac{K_m^0 - K'_m}{K_m^0 V' - K'_m V^0} \quad (14)$$

By substituting the values of all necessary parameters obtained earlier (Figure 2 in text) in the deduced equations, it can be established that the plots of this figure intersect in the point with the coordinates $1/S_{\text{int}}$ and $1/v_{\text{int}}$ at $0.375 \cdot 10^4 \text{ M}^{-1}$ and $0.128 \mu\text{mol}^{-1} \cdot \text{min} \cdot \mu\text{g protein}$, respectively.

To deduce equations for calculation of the coordinates of the intersection point of Figure 1, one must act analogously, i.e. by making equal the right parts of Eqn. (8a) and Eqn. (11a) (Table 1) and re-writing them to the form of Eqn. (15).

$$v' = \frac{V'}{1 + \frac{K'_m}{S}} \quad (15)$$

It can be established that curvilinear plots of figure 1 shall intersect in a point with the coordinates:

$$S_{\text{int}} = \frac{K'_m V^0 - K_m^0 V'}{V' - V^0} \quad (16)$$

and

$$v_{\text{int}} = \frac{K_m^0 V' - K'_m V^0}{K_m^0 - K'_m} \quad (17)$$

By having substituted the values of necessary parameters (Figure 1 or 2) in Eqns. (16) and (17), one can show that plots of this figure shall intersect in a point with the coordinates S_{int} and v_{int} at $2.67 \cdot 10^{-4} \text{ M}$ and $7.813 \mu\text{mol} \cdot \text{min}^{-1} \mu\text{g protein}^{-1}$ respectively. This would be much more difficult to establish by using non-linear regression of curves 1 and 0 (Figure 1).

Analysis of the parallelism positions of plots of a course of change in initial reaction rates in the $(v^{-1}; S^{-1})$ coordinates.

In experimental practice a necessity often arises to state the presence of parallelism of lines at data treatment of the non-trivial I_i and I_a types of enzyme inhibition and activation (Figures 2 and 14, Table 1).

As an example, let us use the results of a study of the inhibitory effect of increasing concentrations of isopropanol on initial rates of pNPP cleavage catalyzed by eel alkaline phosphatase (EC 3.1.3.1). Enzyme is a Sigma (USA) product. A range of pNPP concentration used and a technique of recording the initial rates of substrate cleavage have been given above. The concentration of enzyme was $2.46 \mu\text{g mL}^{-1}$. The results are shown in Figure 3.

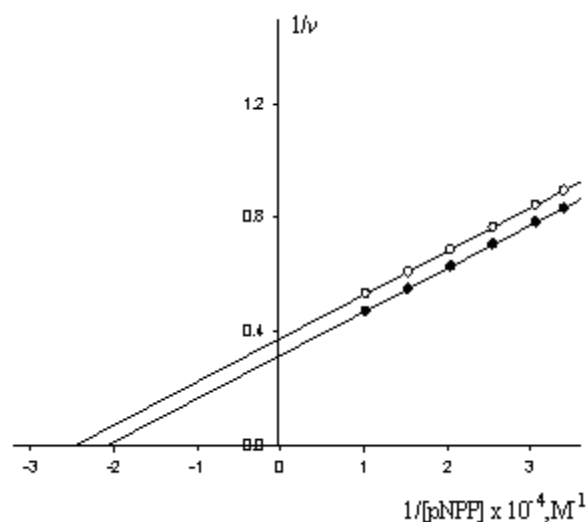
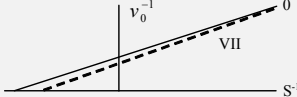
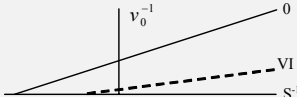
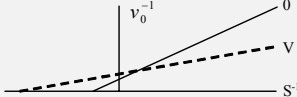
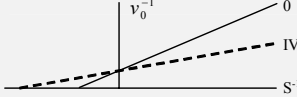
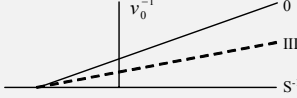
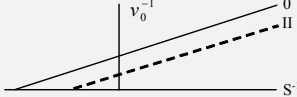
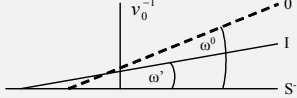


Figure 3. Plot of inhibitory effect of i-PrOH on initial rates of pNPP cleavage by eel alkaline phosphatase represented in the $(v^{-1}; S^{-1})$ coordinates. Note: line 1 – the concentration of inhibitor 0.0005 M , line 0 – the inhibitor is absent; $v \mu\text{mol} \cdot \text{min}^{-1} \mu\text{g protein}^{-1}$ and $K_m^0 = 4.824 \cdot 10^{-5} \text{ M}$ of pNPP cleavage in the presence of 0.0005 M inhibitor change as follows: $V' = 2.66 \mu\text{mol} \cdot \text{min}^{-1} \mu\text{g protein}^{-1}$ and $K'_m = 4.071 \cdot 10^{-5} \text{ M}$, which characterizes the I_i type ($K'_m < K_m^0$, $V' < V^0$, $i > 0$) of unassociative enzyme inhibition (Table 1, line 2).

The similarity of the slope angles of plots 1 and 0, $K'_m/V' = 1.530$ conventional units (c. u.) and $K_m^0/V^0 = 1.526$ c.u. (conventional unit) respectively is quite satisfactory, considering the deviations in values of K'_m , K_m^0 , V' and V^0 .

Table 1. Equations for calculation of the v_i and v_a initial rates of enzyme catalyzed reactions

No	Effect	Type of effect	Correlation between the K'_m and V' parameters	Plots in the $(v_0^{-1}; S^{-1})$ coordinates	Equations for calculation of v_i and v_a (see continuation.)
1	Inhibition ($i > 0$)	I_i	$K'_m > K_m^0; V' < V^0$		$v_{Ii} =$ (Eq. 1a)
2		II_i	$K'_m < K_m^0; V' < V^0$ $\text{tg}\omega' = \text{tg}\omega^0$		$v_{IIi} =$ (Eq. 2a)
3		III_i	$K'_m = K_m^0; V' < V^0$		$v_{IIIi} =$ (Eq. 3a)
4		IV_i	$K'_m > K_m^0; V' = V^0$		$v_{IVi} =$ (Eq. 4a)
5		V_i	$K'_m > K_m^0; V' > V^0$		$v_{Vi} =$ (Eq. 5a)
6		VI_i	$K'_m < K_m^0; V' < V^0$ $\text{tg}\omega' > \text{tg}\omega^0$		$v_{VIi} =$ (Eq. 6a)
7		VII_i	$K'_m < K_m^0; V' < V^0$ $\text{tg}\omega' < \text{tg}\omega^0$		$v_{VIIi} =$ (Eq. 7a)
8	No effect	I_0	$K'_m = K_m^0; V' = V^0$		$v_0 =$ (Eq. 8a)

9	Activation ($a > 0$)	VII_a	$K'_m > K_m^0; V' > V^0$ $\text{tg}\omega' > \text{tg}\omega^0$		$v_{VIIa} = (\text{Eq. 9a})$
10		VI_a	$K'_m > K_m^0; V' > V^0$ $\text{tg}\omega' < \text{tg}\omega^0$		$v_{VIa} = (\text{Eq. 10a})$
11		V_a	$K'_m < K_m^0; V' < V^0$		$v_{Va} = (\text{Eq. 11a})$
12		IV_a	$K'_m < K_m^0; V' = V^0$		$v_{IVa} = (\text{Eq. 12a})$
13		III_a	$K'_m = K_m^0; V' > V^0$		$v_{IIIa} = (\text{Eq. 13a})$
14		II_a	$K'_m > K_m^0; V' > V^0$ $\text{tg}\omega' = \text{tg}\omega^0$		$v_{IIa} = (\text{Eq. 14a})$
15		I_a	$K'_m < K_m^0; V' > V^0$		$v_{Ia} = (\text{Eq. 15a})$

*The symbol of a plots in Figs. 1 – 15 corresponds to the type of reaction under study. For example: line 0 characterizes the position of initial (nonactivated) enzymatic reaction, line I – the position of a plot representing the I_a type of activated enzymatic reaction (Fig. 15a) etc.

№ 1. (type I_i , biparametrically coordinated inhibition)

$$v_{II} = \frac{V^0 \cdot \frac{1}{\left(1 + \frac{i}{K_{yi}}\right)}}{1 + \frac{K_m^0}{S} \cdot \left(1 + \frac{i}{K_{xi}}\right)} = \frac{V^0 \cdot \frac{1}{\left(1 + \frac{i}{K_{IIIi}}\right)}}{1 + \frac{K_m^0}{S} \cdot \left(1 + \frac{i}{K_{IVi}}\right)} \quad (1a)$$

№ 2. (type II_i, unassociative inhibition)

$$v_{IIi} = \frac{V^0 \cdot \frac{1}{\left(1 + \frac{i}{K_{yi}}\right)}}{1 + \frac{K_m^0}{S} \cdot \frac{1}{\left(1 + \frac{i}{K_{xa}}\right)}} = \frac{V^0 \cdot \frac{1}{\left(1 + \frac{i}{K_{IIIi}}\right)}}{1 + \frac{K_m^0}{S} \cdot \frac{1}{\left(1 + \frac{i}{K_{IVa}}\right)}} \quad (2a)$$

№ 3. (type III_i, catalytic inhibition)

$$v_{IIIi} = \frac{V^0 \cdot \frac{1}{\left(1 + \frac{i}{K_{yi}}\right)}}{1 + \frac{K_m^0}{S}} = \frac{V^0 \cdot \frac{1}{\left(1 + \frac{i}{K_{IIIi}}\right)}}{1 + \frac{K_m^0}{S}} \quad (3a)$$

№ 4. (type IV_i, associative inhibition)

$$v_{IVi} = \frac{V^0}{1 + \frac{K_m^0}{S} \cdot \left(1 + \frac{i}{K_{xi}}\right)} = \frac{V^0}{1 + \frac{K_m^0}{S} \cdot \left(1 + \frac{i}{K_{IVi}}\right)} \quad (4a)$$

№ 5. (type V_i, pseudoinhibition)

$$v_{Vi} = \frac{V^0 \cdot \left(1 + \frac{i}{K_{ya}}\right)}{1 + \frac{K_m^0}{S} \cdot \left(1 + \frac{i}{K_{xi}}\right)} = \frac{V^0 \cdot \left(1 + \frac{i}{K_{IIIa}}\right)}{1 + \frac{K_m^0}{S} \cdot \left(1 + \frac{i}{K_{IVi}}\right)} \quad (5a)$$

№ 6. (type VI_i, discoordinated inhibition)

$$v_{VIi} = \frac{V^0 \cdot \frac{1}{\left(1 + \frac{i}{K_{yi}}\right)}}{1 + \frac{K_m^0}{S} \cdot \frac{1}{\left(1 + \frac{i}{K_{xa}}\right)}} = \frac{V^0 \cdot \frac{1}{\left(1 + \frac{i}{K_{IIIi}}\right)}}{1 + \frac{K_m^0}{S} \cdot \frac{1}{\left(1 + \frac{i}{K_{IVa}}\right)}} \quad (6a)$$

№ 7. (type VII_i, transient inhibition)

$$v_{VII_i} = \frac{V^0 \cdot \frac{1}{\left(1 + \frac{i}{K_{yi}}\right)}}{1 + \frac{K_m^0}{S} \cdot \frac{1}{\left(1 + \frac{i}{K_{xa}}\right)}} = \frac{V^0 \cdot \frac{1}{\left(1 + \frac{i}{K_{III_i}}\right)}}{1 + \frac{K_m^0}{S} \cdot \frac{1}{\left(1 + \frac{i}{K_{IVa}}\right)}} \quad (7a)$$

№ 8. Initial (uninhibited and nonactivated) reaction

$$v_0 = \frac{V^0}{1 + \frac{K_m^0}{S}} \quad (8a)$$

№ 9. (type VII_a, transient activation)

$$v_{VII_a} = \frac{V^0 \cdot \left(1 + \frac{a}{K_{ya}}\right)}{1 + \frac{K_m^0}{S} \cdot \left(1 + \frac{a}{K_{xi}}\right)} = \frac{V^0 \cdot \left(1 + \frac{a}{K_{IIIa}}\right)}{1 + \frac{K_m^0}{S} \cdot \left(1 + \frac{a}{K_{IVi}}\right)} \quad (9a)$$

№ 10. (type VI_a, discoordinated activation)

$$v_{VI_a} = \frac{V^0 \cdot \left(1 + \frac{a}{K_{ya}}\right)}{1 + \frac{K_m^0}{S} \cdot \left(1 + \frac{a}{K_{xi}}\right)} = \frac{V^0 \cdot \left(1 + \frac{a}{K_{IIIa}}\right)}{1 + \frac{K_m^0}{S} \cdot \left(1 + \frac{a}{K_{IVi}}\right)} \quad (10a)$$

№ 11. (type V_a, pseudoactivation)

$$v_{Va} = \frac{V^0 \cdot \frac{1}{\left(1 + \frac{a}{K_{ya}}\right)}}{1 + \frac{K_m^0}{S} \cdot \frac{1}{\left(1 + \frac{a}{K_{xa}}\right)}} = \frac{V^0 \cdot \frac{1}{\left(1 + \frac{a}{K_{III_i}}\right)}}{1 + \frac{K_m^0}{S} \cdot \frac{1}{\left(1 + \frac{a}{K_{IVa}}\right)}} \quad (11a)$$

№ 12. (type IV_a, associative activation)

$$v_{IVa} = \frac{V^0}{1 + \frac{K_m^0}{S} \cdot \frac{1}{\left(1 + \frac{a}{K_{xa}}\right)}} = \frac{V^0}{1 + \frac{K_m^0}{S} \cdot \frac{1}{\left(1 + \frac{a}{K_{IVa}}\right)}} \quad (12a)$$

№ 13. (type III_a, catalytic activation)

$$v_{IIIa} = \frac{V^0 \cdot \left(1 + \frac{a}{K_{ya}}\right)}{1 + \frac{K_m^0}{S}} = \frac{V^0 \cdot \left(1 + \frac{a}{K_{IIIa}}\right)}{1 + \frac{K_m^0}{S}} \quad (13a)$$

№ 14. (type II_a, unassociative activation)

$$v_{IIa} = \frac{V^0 \cdot \left(1 + \frac{a}{K_{ya}}\right)}{1 + \frac{K_m^0}{S} \cdot \left(1 + \frac{a}{K_{xi}}\right)} = \frac{V^0 \cdot \left(1 + \frac{a}{K_{IIa}}\right)}{1 + \frac{K_m^0}{S} \cdot \left(1 + \frac{a}{K_{IVi}}\right)} \quad (14a)$$

№ 15. (type I_a, biparametrically coordinated activation)

$$v_{Ia} = \frac{V^0 \cdot \left(1 + \frac{a}{K_{ya}}\right)}{1 + \frac{K_m^0}{S} \cdot \frac{1}{\left(1 + \frac{a}{K_{xa}}\right)}} = \frac{V^0 \cdot \left(1 + \frac{a}{K_{IIIa}}\right)}{1 + \frac{K_m^0}{S} \cdot \frac{1}{\left(1 + \frac{a}{K_{IVa}}\right)}} \quad (15a)$$

There is another possibility to characterize parallelism of such plots (Figure 3). Data analysis shows that a system of linear Eqns. (2a) and (8a) will not have a general solution if the determinant of this system is equal to zero, and it may

$$\begin{vmatrix} \frac{K_m^0}{V^0} & -1 \\ \frac{K_m'}{V'} & -1 \end{vmatrix} = 0 \quad (18)$$

occur in the case of parallelism of the positions of respective lines (like the lines of Figure 3). Substituting the experimental data of Figure 3 in Eqn. (18) yields a value of 0.004 c.u. for the determinant ($K_m'/V' - K_m^0/V^0$), which is a satisfactory feature of parallelism of these lines.

Examples of data of the III and IIa types of biparametrically dis-coordinated enzyme inhibition and activation¹⁵ are rather often found in practical enzymology, 10–14 but the technique employed to determine parallelism of the positions of lines of the like type (see Eqns. 11 and 12) by estimating the value of the determinant is not used for data treatment in studies of analogous types of enzyme

activation and inhibition. Probably, it may be explained by the absence of Eqns. 2a and 14a of Table 1 for calculation of initial reaction rates of such types of enzyme inhibition and activation in practical enzymology.

References

- ¹Bhatnagar, A., Das, B., Gavva, S. R., Cook, P. F., Srivastava, S. K., *Arch. Bioch. Biophys.*, **1988**, 261(1), 264.
- ²Hara, A., Nakayama, T., Nakagawa M., Inoue Y., Tanabe H., Sawada H., *J. Biochem.* **1987**, 102(6), 1585.
- ³Garbers D. L., *Biochim. Biophys Acta*, **1978**, 523(1), 82.
- ⁴Kato, N., Sahn, H., Wagner, F., *Biochim. Biophys. Acta*, **1979**, 566(1), 12.
- ⁵Rose, Z. B., Grove, D. S., Seal, S. N., *J. Biol. Chem.*, **1986**, 261(24), 10996.
- ⁶Monasterio, O., Cardenas, M. L., *Biochem. J.*, **2003**, 371(1), 29.
- ⁷Bheemanai, S., Chandrashekar, S., Nagaraja, V., Rao, D. N., *J. Biol. Chem.*, **2003**, 277(35); 31499.
- ⁸Petit, C. M., Koretke, K. K., *Biochem. J.*, **2002**, 363(3), 825.
- ⁹Lin Y., Alguindigie S. S., Volkman J., Nicholas K. M., West A. N., Cook P. F., *Biochemistry*, **2007**, 46(3), 890.
- ¹⁰Dinh, M., Grunberger, D., Ho, S., Tsing, Y., Shaw D., Lee, S., Barnett, J., Hill J., *J. Biol. Chem.*, **2007**, 282(12), 8768.
- ¹¹Papp, E., Tse, J. K. Y., Ho, H., Wang, S., Shaw, D., Lee, S., Barnett, J., Swinney, D. C., Bradshaw M. J., *Biochemistry*, **2007**, 46(51), 15103.
- ¹²Shimizu, Y., Sakuraba, H., Doi, K., Ohshima, T., *Arch. Bioch. Biophys.*, **2008**, 470(2), 102.
- ¹³Bhat, J. Y., Shastri, B. G., Balaram, H., *Biochem. J.*, **2008**, 409(1), 263.
- ¹⁴Czekster, C. M., *Biochemistry*, **2011**, 50(3), 376.
- ¹⁵Krupyanko, V. I., *A Vector Method of Representation of Enzymic Reactions*, Moscow. Nauka, **1990**, 146, (in Russian).
- ¹⁶Webb, L., *Enzyme and metabolic inhibitors*. Moscow :Mir Publisher, **1966**, 862, (in Russian).
- ¹⁷Dixon, M., Webb, E. C., *Enzymes*, Moscow, Mir Publisher, **1982**, 2, 481, (in Russian).
- ¹⁸Krupyanko, V. I., *Process. Biochem.*, **2004**, 39(7), 805.
- ¹⁹Krupyanko, V. I., *J. Biochem. Mol. Toxicol.*, **2009**, 23(2), 101.
- ²⁰Krupyanko, V. I. *J. Biochem. Mol. Toxicol.*, **2009**, 23(2), 97.
- ²¹Krupyanko, V. I., *J. Biol. Sci.*, **2007**, 7(3), 506.
- ²²Krupyanko, V. I., *Eur. Chem. Bull.*, **2014**, 3(6), 582.
- ²³Krupyanko, V. I., *Eur. Chem. Bull.*, **2014**, 3(8), 815.
- ²⁴Krupyanko, V. I., *Eur. Chem. Bull.*, **2015**, 4(3), 142.

Received 12.02.2016.

Accepted: 09.10.2016.